NASA Contractor Report 3809

A Review of Some Reynolds Number Effects Related to Bodies at High Angles of Attack

Edward C. Polhamus

GRANT NAG1-261
AUGUST 1984

NASA

NASA Contractor Report 3809

A Review of Some Reynolds Number Effects Related to Bodies at High Angles of Attack

Edward C. Polhamus
Virginia Associated Research Campus
Newport News, Virginia

Prepared for
Langley Research Center
under Grant NAG1-261

National Aeronautics
and Space Administration
Scientific and Technical Information Branch

1984

TABLE OF CONTENTS

TABLE OF CONTENTS

A REVIEW OF SOME REYNOLDS NUMBER EFFECTS RELATED TO BODIES AT HIGH ANGLES OF ATTACK

by

Edward C. Polhamus
Virginia Associated Research Campus, Newport News, VA.

SUMMARY

This paper presents a review of some effects of Reynolds number on selected aerodynamic characteristics of two- and three-dimensional bodies of various cross sections relavant to aircraft and missile fuselages at high angles of attack at subsonic and transonic speeds. Emphasis is placed on the Reynolds number ranges above the subcritical and angles of attack where lee-side vortex flow or unsteady wake type flows predominate. Lists of references, arranged in subject categories, are presented with emphasis on those which include data over a reasonable Reynolds number range, but also including some selected papers providing background information and prediction methods. Selected Reynolds number data representative of various aerodynamic flows around bodies are presented and analyzed and some effects of these flows on aerodynamic phenomena related to static longitudinal and directional chacteristics, spin damping, and out-of-plane side forces are discussed. Finally, some suggestions for high Reynolds number research in the new National Transonic Facility on bodies at high angles of attack are offered.

INTRODUCTION

The aerodynamic design of of modern aerospace vehicles is often critically dependent on the accuracy with which full scale viscous flow characteristics can be predicted. One of the areas that is particularly sensitive to Reynolds number effects is the high angle of attack characteristics of both aircraft and missiles. The current strong interest in providing expanded maneuver performance capbilities while maintaining satisfactory handling qualities and avoiding spin entry has increased the importance of high angle of attack aerodynamics and the need for full scale Reynolds number simulation.

Current operational wind tunnels used for vehicle development fall short of simulating full scale Reynolds numbers by at least an order-of-magnitude for the many compressible flow conditions involved, thereby requiring large theoretical or empirical extrapolations which are often of questionable accuracy. This is particularly true for the high angle of attack conditions involving complicated separated flows with strong vortex interactions. This was one of the reasons for the decision to construct the National Transonic Facility (NTF) at the Langley Research Center. This high Reynolds number wind tunnel, based on the cryogenic pressure tunnel concept developed at Langley, is currently nearing operational status.

As an aid to utilizing the capabilities of the National Transonic Facility in the most effective manner, it appears desirable to document the most pertinent Reynolds number studies available in the literature and analyze selected data of particular interest in relation to the anticipated research and development programs to be carried out in the NTF. Such documents should be of value in developing meaningful Reynolds number oriented research programs for the NTF, and thus make best use of the cryogenic pressurized tunnel concept, which can isolate certain parameters and provide new and improved simulation.

The purpose of this paper, therefore, is to document one aspect of the high angle of attack aerodynamics described above; that of Reynolds number dependent flows related to the aerodynamics of bodies such as missiles and the fuselages of aircraft and spacecraft.

The paper concentrates on the review and analysis of those data that cover a reasonable Reynolds number range and points out areas where extensions of such data using the capabilities of high Reynolds number

tunnels such as the NTF will be of particular value. Extensive reference lists are provided and divided into various categories as an aid to those wishing to make further use of the available literature on Reynolds number effects on bodies. While papers describing various prediction methods are listed, no evaluation of their relative accuracies is attempted. Some papers which came to the author's attention after the text was completed are listed as "some additional papers."

The discussion and reference lists are, in general, limited to the subsonic and transonic speed regimes.

1. FORCES ON CYLINDERS IN NORMAL FLOW

Many of the Reynolds number dependent viscous flow phenomena encountered by missiles and aircraft fuselages at high angles of attack can be related, at least qualitatively, to the flow about two dimensional cylinders in normal flow having the same or similar cross-sectional shapes. This qualitative similarity of the flows also extends into the compressible flow region.

Because of this relationship between two-dimensional and three-dimensional flows about fuselage-type bodies and the fewer number of parameters involved in the two-dimensional case, it has been selected as the initial section of the present analysis.

1.1 Circular Cylinders

In this section, the available data regarding the major effects of Reynolds number on the aerodynamic flow characteristics for circular cylinders immersed in a flow normal to the cylinder axis will be analyzed. Some of the general papers which provide good fundamental descriptions of the flow details are listed as references 1.1 through 1.5. Papers containing the experimental data to be utilized in this review are listed as references 1.6 through 1.44. For convenience, the reference list is divided by subjects; and within each subject they are, in general, listed in chronological order for historical interest.

Since the emphasis in this paper is on the higher Reynolds numbers above the critical range, no attempt is made to cite the many low Reynolds number studies. For those interested in this range, Morkovin (reference 1.3) provides a rather extensive list of papers.

1.1.1 Smooth surface cylinders

The various Reynolds number ranges to be discussed are identified in figure 1.1 and related to the separation, vortex shedding characteristics, and relative drag levels of smooth circular cylinders in incompressible flow.

The "subcritical" range is defined as that range below a Reynolds number, based on cylinder diameter, of $R_D=2x10^5$. In this range, laminar separation occurs on the front at a separation angle, θ_S, of approximately 80^o resulting in a wide wake and a high drag coefficient. In this range, the vortex shedding in the wake, while not of the classical "Karman" type, can be characterized as having a dominant periodicity. This range is followed by the "critical" range in which the laminar separation is followed by a turbulent reattachment enclosing a laminar bubble. The turbulent flow then separates further aft, at about $\theta=130^o$, at a Reynolds number of about $4x10^5$, resulting in a narrowing of the wake and a large reduction in drag. In this range, the wake is unstructured with no dominant periodicity, and the vortex shedding frequencies become of the "wide-band random" type.

The "supercritical" Reynolds number range, as defined here, extends from about $R=4x10^5$ to about $R=6x10^6$. In this range, transition moves upstream, forward of the laminar separation point and eventually to the vicinity of the forward stagnation point with the separation point moving forward from about 130^o to 115^o, and there is a corresponding increase in drag coefficient. In the upper part of the supercritical region, the vortex shedding shifts to a "narrow-band random" pattern and the drag starts to level off.

In the range above $R=6x10^6$, the vortex wake flow becomes at least "quasi-periodic" and some evidence of a drag reduction has been observed. In this paper, the term "hypercritical" is adopted for this range.

It will be noted that the term "hypercritical" departs from historical precedence. The term "transcritical" has been accepted through usage for this region, although some controversy has appeared in the literature associated with its somewhat inconsistent connotation in describing the Reynolds number beyond the "supercritical" range. With the expected increase in high Reynolds number research in both two-dimensional and three-dimensional flows as a result of the availability of new high Reynolds number wind tunnels, consideration of adoption of a new term appears timely. In attempting to accomplish this in the past, some researchers have combined the

"critical" and "supercritical" regions and substituted the term "transcritical" followed then by "supercritical." While this provides a somewhat more logical terminology, the loss of the term "critical" describing the region where the separation characteristics are changing very rapidly and the shifting of the term "supercritical" from the region which it has defined for many decades appears undesirable. Therefore, since "transcritical" is a relatively new term whose use has been somewhat restricted due to the rather limited research in this region, this paper drops its use, substituting "hypercritical" and retains the well-established terms in the lower regimes. With the anticipated increase in two-dimensional and three-dimensional research in the "hypercritical" range, a consistent adoption of this term should soon eliminate the confusion that may result initially.

Many correlations have been made of the effect of Reynolds number on the drag of circular cylinders in incompressible flow. However these correlations invariably have shown extremely wide bands of uncertainty, particularly in the higher Reynolds number ranges (see reference 1.5 for example). While the effects of surface condition, compressibility, end conditions, etc., are sometimes cited as possible causes; no concerted attempt has been made to isolate these effects, and therefore, such an attempt will be made here.

The data selected from the literature search to establish the low speed drag coefficient for two-dimensional smooth circular cylinders is presented in figure 1.2 as a function of Reynolds number based on free stream conditions and the cylinder diameter. To ensure that effects of compressibility are insignificant, the data used has been limited to that obtained at Mach numbers less than 0.15. Comparisons of the drag variation with Reynolds number for cylinders of various diameters where the Reynolds number variations were obtained by velocity changes (references 1.9, 1.10, and 1.14), indicated that measurable compressibility effects began in the range of Mach number from 0.18 to 0.20 with the value of 0.15 being selected as a conservative upper limit for esentially incompressible flow.

To establish the level of drag coefficient at subcritical Reynolds numbers, data from the classical experiment performed by Wieselsberger at Gottingen (reference 1.6) is used. Wieselsberger tested 9 cylinders having diameters ranging from 0.05 to 300mm to cover the range of Reynolds numbers from 0.2 to 800,000. However, for the range of interest here only the data obtained with the 80mm (3.15 in) diameter cylinder is presented in figure

1.2. It will be noted that in addition to establishing the constant drag level for the subcritical range, his data establishes the beginning of the critical range. Although Wieselsberger also tested a 300mm cylinder to cover the full critical Reynolds number range, the data is not used here in view of possible end-plate boundary-layer and blockage effects associated with this extremely large diameter cylinder of relatively short length.

To establish the remainder of the critical Reynolds number range, the 4" diameter cylinder data of Stack (reference 1.8), the 8.34" diameter of Polhamus (reference 1.10), and the 12" diameter of Delany and Sorensen (reference 1.9) are added to that of Wieselsberger. (It should be noted that in the subcritical range, the two data points from reference 1.10 are low due, in all probability, to inaccuracy associated with the very low dynamic pressures). In the critical range, good agreement exists between all of the data, and it appears that the variation is accurately established.

Although Stack obtained data in the upper critical range, the Mach number exceeded the 0.15 limit selected for the correlation. The Delany and Sorensen data in the lower critical range has been eliminated due to the effects of leakage at the wall pointed out by the authors. Their data in the upper critical and supercritical ranges is tentatively assumed valid in view of the greatly reduced end effects of three-dimensional cylinders in this Reynolds number range (see references 1.42 and 1.44).

In the lower supercritical range, the data of Delaney and Sorensen, and Polhamus are presented in figure 1.2 and reasonably good agreement is observed. It should be noted that the data at higher supercritical Reynolds number presented in references 1.9 and 1.10 have been eliminated to avoid exceeding the Mach number limitation described earlier. The minimum drag coefficient, which occurs in the low supercritical range, is about 0.25 and is in good agreement with the flight test data published by Stephens (reference 1.7).

Data from other sources in this range have been omitted for the following reasons. The data of Humphreys (reference 1.11) is not utilized since the critical Reynolds number is low, indicating the probability of too high a stream turbulence level. In addition, only one data point below a Mach number of 0.15 and with the ends sealed was obtained in the supercritical range. The data of Jones et. al. (reference 1.15) in the lower supercritical range were obtained in freon at a tunnel stagnation pressure of

1/10 atmosphere and the resulting low dynamic pressure caused low measurement accuracy (which was confirmed by the senior author).

In the higher supercritical and hypercritical range of Reynolds number, it appears from the literature survey that only the data of Jones, et. al. (reference 1.15) satisfied the low Mach number and smooth surface condition requirements. Additional data sources often used in attempting to define the drag variation in the upper supercritical and hypercritical Reynolds number range are those of Roshko (reference 1.20) and Schmidt (reference 1.13). However, in the present study Roshko's data, because of the surface condition of the cylinder, is included with the rough cylinder data rather than the smooth cylinder data. The Schmidt data was not utilized since it was obtained with a three-dimensional cylinder. Care must exercised in analyzing Schmidt's data due to the large variation in Mach number for a given Reynolds number. Results from the study by James et. al. (reference 1.27) did not meet the Mach number criteria.

In the study by Jones et. al., a 36" cylinder was tested in air for the upper supercritical Reynolds number range, and in freon to extend the data into the hypercritical range. These data, taken from table I of reference 1.15, illustrates the increase in drag in the upper supercritical region as the transition point moves to the front face, resulting in a wider wake with less pressure recovery. The turbulent boundary layer can better withstand the adverse pressure gradient and the turbulent separation point remains aft of the laminar separation point. Above a Reynolds number of about 6×10^6, in the so-called hypercritical Reynolds number range, the drag remains essentially constant as the transition point moves well forward on the front face of the cylinder and the separation point becomes relatively insensitive to Reynolds number. It is anticipated with further increases in Reynolds number that some decrease in drag will occur as fully turbulent flow is reached and the turbulent boundary layer begins to thin. A reduction of friction drag would be expected as well as an aft movement of the turbulent separation point. Tests in the new high Reynolds number wind tunnels would be useful in this regard.

From the above analysis, it appears that much of the data scatter in the supercritical and hypercritical Reynolds number ranges shown in previous summary papers can be identified as the effects of compressibility and surface condition, and that figure 1.2 represents a reasonably accurate drag variation for smooth circular cylinders in incompressible flow for Reynolds

numbers from the subcritical through the supercritical range. As pointed out, additional data is required to define the variation in the hypercritical Reynolds number range.

1.1.2 Effects of surface roughness

The effect of surface roughness on the drag of circular cylinders normal to an incompressible flow is illustrated in figure 1.3. Since the primary interest in this paper is in the supercritical and hypercritical Reynolds number range, the data from the well-known early study carried out at lower Reynolds numbers by Fage and Warsap (reference 1.18) is not presented. In figure 1.3, the smooth cylinder "baseline" curve is taken from the correlation of figure 1.2, discussed in the previous section, in which the surface roughnesses selected appeared to be the lowest available and essentially "aerodynamically" smooth. It is recognized, however, that some small level of roughness drag may be present in the baseline curve, particularly in the hypercritical Reynolds number range. The roughness level for the various Reynolds number ranges is indicated for the baseline curve in terms of effective sand-grain height.

The sources of data for rough cylinders at Mach numbers equal to or less than 0.15 which exceed the critical Reynolds number of the smooth cylinder are Roshko (reference 1.20), Achenbach (reference 1.21), Schulz and Hayn (reference 1.22), and Szechenyi (reference 1.24 and 1.25).

The cylinder used by Roshko was an 18" diameter seamless black steel pipe which, after being cleaned by sandblasting, had a surface roughness of "about 200×10^{-6} inches" resulting in a non-dimensional sand-grain roughness parameter, r/D, of about 10^{-5}. Achenbach used glued spheres and applied a factor of 0.55 (obtained by curve fitting with the Fage and Warsap data in the critical range) to the sphere diameters to obtain equivalent sand-grain roughness (r_s/D) values of 110×10^{-5}, 450×10^{-5}, and 900×10^{-5}. Szechenyi's cylinders were roughened with calibrated spherical glass beads, and for the purpose of this paper, the factor of 0.55 used by Achenbach has been applied to convert Szechenyi's data to an equivalent sand-grain roughness. It is recognized that such conversions are questionable and that the factor may not be independent of Reynolds number. However, since sand-grain roughness is more closely related to surfaces encounted on actual aircraft, the factor of 0.55 is used as a "tentative" conversion, subject to further investigation.

In addition, the effects of tunnel turbulence variations, differences in roughness structure, etc., makes the definition somewhat qualitative at best. However, it is thought that the data as presented illustrates the relationship between roughness and Reynolds number with regard to drag.

Since the drag curves obtained by Achenbach are well defined by closely spaced data points, only his final curves are presented. In connection with the data from Szechenyi, it should be noted that some inaccuracy may have been encountered in transcribing and coverting the data from figure 3 of reference 1.25.

Achenbach's data is for relatively large roughness grain size and is in general good agreement with the early Fage and Warsap data with regard to the classical effect of roughness. This classical effect is to promote an earlier transition to a turbulent boundary layer, and thus a reduced pressure drag. This reduction is less than that obtained on smooth cylinders in the critical range and is followed by a more rapid increase in the supercritical range. It has been suggested by Batham (reference 1.23) that the higher value of minimum drag is due to the roughness dispersing the turbulent bursts and leaving the boundary layer less capable of withstanding the adverse pressure gradient. Achenbach's study extends the data on highly rough cylinders into the upper supercritical Reynolds number range and illustrates the leveling off of the drag in this region as a value approaching that for the subcritical smooth cylinder. This is the result of the transition point moving close to the stagnation point so that separation occurs near the minimum pressure point similar to the subcritical laminar separation case. For large values of roughness, the drag becomes essentially indepedent of r/D.

For smaller size roughness, the data of Szechenyi appears to indicate that below the supercritical Reynolds number range, roughness levels less than $r/D=8\times10^{-5}$ probably do not produce any measurable effect on the drag. As the boundary layer thins in the supercritical range, however, the roughness level of $r/D=8\times10^{-5}$ begins to produce a measurable drag increment for R_D values greater than about 10^6. This trend appears to be substantiated by Roshko's data in the upper supercritical and hypercritical range where an appreciable drag increment due to roughness is observed for a roughness parameter of only 1.1×10^{-5}.

The dashed lines used in figure 1.3 to connect the low roughness data to the smooth cylinder curve are entirely conjectural but are presented to illustrate the possible onset of roughness effects above the critical Reynolds number.

With regard to the drag of rough cylinders in the hypercritical Reynolds number range, it is of interest that data was obtained in this high Reynolds number range as early as 1929 by Dryden and Hill and published in a seldom cited paper (reference 1.19). They obtained data, in natural winds, on a power plant chimney constructed of brick. But due to three-dimensional effects and undetermined equivalent sand type roughness, no attempt is made here to include the data in figure 1.3.

From the results of figure 1.3, it appears desirable to establish the onset of roughness effects in the Reynolds number range above 10^7. This may require a smooth reference test with surface finish of higher polish than tested previously.

Additional data on the effects of surface conditions in compressible flow would also be of value particularly in the subsonic range and at Reynolds numbers above 10^6. Data obtained at lower Reynolds numbers suggest that for compressible flow at subcritical Mach numbers, surface roughness may reduce the drag even in the supercritical Reynolds number range (see references 1.22 and 1.27). For supercritical Mach numbers, with shock-induced separation on the forward face, Macha (references 1.36 and 1.37) has indicated drag reductions due to surface roughness for Mach numbers up to 0.9 over the Reynolds number range for which data is available.

1.1.3 Effects of compressibility

As mentioned earlier, measurable effects of compressibility are encountered at Mach numbers well below the critical Mach number which, depending upon the boundary layer condition, occurs in the range of 0.40. This is not surprising since at a Mach number as low as 0.25, the minimum pressure coefficient is more negative than the incompressible value by nearly 9% according to the Karman-Tsien equation (reference 1.30). This increases the magnitude ot the adverse pressure gradient thereby moving the separation point forward and reducing the pressure in the separated region. Figure 1.4 summarizes the existing smooth cylinder data for Mach numbers in the range from essentially incompressible to 0.50 which is slightly in excess of the

critical. For applications related to the subject of this paper, Mach numbers normal to the cylinder axis up to 0.5 are usually sufficient. If information for higher Mach numbers is required, data can be found in references 1.33, 1.34, 1.36, and 1.37, although the data is limited to Reynolds numbers below 10^6.

In figure 1.4, the line representing the incompressible variation of circular cylinder drag coefficient with Reynolds number is from figure 1.2 and represents Mach numbers equal to or less than 0.15. In the subcritical Reynolds number range where the incompressible laminar separation point occurs on the front face. the effects of compressibility for Mach numbers up to 0.5 are relatively small and appear to be well established by the data of Stack (reference 1.31) and Gowen and Perkins (reference 1.34). However, in the higher Reynolds number range of interest for this paper, the trends with Mach number can only be partially established.

From the data obtained by Stack (reference 1.31) and Schulz and Hayn (reference 1.14) on cylinders of various diameters, it is fairly well established that at least below the critical Mach number, compressibility shifts the critical Reynolds number range to considerably higher Reynolds numbers as seen in figure 1.4. It is presumed that this effect is associated with a delay in the formation of boundary layer turbulence due to the increased magnitude of the favorable pressure gradient on the forward face, and an increase in the adverse gradient aft of the minimum pressure point. That the changes in pressure gradients can be appreciable is seen in the fact that the minimum pressure coefficient is more negative by nearly 24% at a Mach number of 0.40 according to calculations by the inviscid full-potential transonic theory described in reference 1.39. These changes in pressure gradient affect not only the separation point and wake width but also result in a more negative pressure at the separation point, and therefore, in the wake. This results in an increased drag over the entire Reynolds number range.

The only applicable data on compressibility effects in the upper supercritical and lower hypercritical Reynolds number range appears to be that obtained by Jones et. al. (Table II of reference 1.35), and their data is shown in figure 1.4 for constant Mach numbers of 0.25, 0.35, and 0.40. For the Mach number of 0.25 both the air and freon data is presented, but for the other two Mach numbers the freon data has been omitted in view of possible real gas effects which tend to cause departures from air results in

the higher local Mach number conditions (see references 1.40 and 1.41). In this regard, it is of interest to note that the rather unusual peaky type variation of c_d with Reynolds number for M=0.35 and M=0.40 shown in figure 12 of reference 1.35 would essentially disappear if the air and freon data were separated and if the 1/10 atmosphere freon data (with its low accuracy) was eliminated. Since the freon data represents the highest Reynolds number data available, the degree to which it represents results in air might be worthy of further study.

Although the data is rather sparce, it appears from figure 1.4 that the effect of compressibility at subcritical Mach numbers is a minimum at low supercritical Reynolds numbers and increases considerably in the hypercritical range as the boundary layer becomes thinner.

Based on the data of figure 1.4 it is apparent, that except for the data of reference 1.35 in the lower hypercritical range, very little penetration has been made into the Mach-Reynolds number envelope above a Reynolds number of about 5×10^6. The new cryogenic wind tunnels provide a source for the needed data.

1.1.4 Effects of fineness ratio

Although fineness ratio (length-to-diameter ratio, L/D) effects involve three-dimensional flows, the cylinders (at $\alpha=90^o$) with "squared-off" ends will be covered here while the conventional nose shapes appropriate to fuselages will be treated in a subsequent section on three-dimensional bodies.

The flow around the ends of cylinders of finite length has a pronounced effect on the drag. Possible sources of the drag changes include various combinations of venting from the end region into the near wake (which increases the pressure in the separated region) reduced velocities and Reynolds numbers near the ends, and separation at the sharp corners of the "squared-off" tips. The primary sources of data for the effect of fineness ratio are the experimental investigations of Wieselsberger (reference 1.42) and McKinney (reference 1.44). Both investigations show a very large reduction in drag, at subcritical Reynolds numbers, as the fineness ratio is reduced which is attributed primarily to the aforementioned venting into the near wake.

To investigate the influence of Reynolds number, Wieselsberger tested one finite length cylinder through the critical range, and McKinney investigated a large number of fineness ratios over a wide range of Reynolds numbers. Reynolds number variations for two fineness ratios selected from these studies are shown in figure 1.5 in terms of the drag proportionality factor, η, (ratio of finite length cylinder drag coefficient to that for an infinite length cylinder) in the critical Reynolds number range (the flagged symbol is from Wieselsberger and is used to extrapolate McKinney's data to the subcritical level). The results indicate that increases with Reynolds number and approaches a value of 1.0 at the end of the critical range. This is apparently associated with a reduction of venting into the near wake for the low drag conditions where the wake is narrow and the pressure recovery rather high. McKinney has shown that under these conditions, lower fineness ratios can generate drag coefficients which are higher than the two-dimensional case (η>1.0) due, at least in part, to the increased importance of the flow separation around the "squared-off" ends (see reference 1.44).

That portion of McKinney's supercritical data which was obtained at Mach numbers less than 0.15 is also shown in figure 1.5 and illustrates the reduction of η as the turbulent separation point moves forward widening the wake and reducing the pressure recovery, and thereby again allowing pressurization due to end effects.

The only data found in the upper supercritical Reynolds number range is that obtained by Dryden and Hill on a 10-foot diameter cylinder in natural winds (reference 1.19). The factor for this data was determined by comparing the three-dimensional data extracted from the natural wind data with the two-dimensional correlation from wind tunnel data presented in figure 1.2. Because of uncertainties regarding the turbulence level, velocity distribution and surface condition for the natural wind tests the extracted factor is shown as a band. Despite these uncertainties, the values of are such that they reinforce the expectation that drag reductions due to finite length continue into the upper supercritical range.

The reader is referred to reference 1.44 for the effects of Reynolds number on the drag of finite length cylinders with hemispherical ends or noncircular cross sections.

1.1.5 Lifting cylinders

An investigation of the effects of Reynolds number on the aerodynamic characteristics of two-dimensional lifting cylinders of circular cross section in incompressible flow has been carried out by Lockwood and McKinney (reference 1.11) and some of their results are shown in figure 1.6. This lift was generated by a spoiler type flap, and both the flap projection, h, and orientation angle, δ, were investigated. For the data shown, the flap projection was 6% of the cylinder diameter.

In figure 1.6, the lift coefficient, c_ℓ, is presented as a function of Reynolds number, R_D, for various flap orientation angles, δ. The flap acts as a spoiler and tends to fix the separation line on the lower surface of the cylinder. The resulting wake deflection and lift force depends on the location of the upper surface separaton line. The results shown in figure 1.6 illustrate the large increase in lift coefficient in the critical Reynolds number range for $\delta=90^o$ from the free stream velocity vector) associated with the rearward movement of the turbulent separation line on the side opposite the flap resulting in large negative pressures which are augmented by the induced circulation. It will be noted that the maximum lift coefficient, which occurs in the upper critical Reynolds number range, approaches a value of 1.6, which is about 2.5 times the drag coefficient.

As the Reynolds number increases in the supercritical range, the lift decreases due to the forward movement of the turbulent separation line. The loss of lift resulting generally from positioning the flap either fore or aft of the 90^o position is also shown. For detailed pressure measurements and other flap projections, the reader is referred to reference 1.11.

Although the above study was made to investigate the application of the lifting cylinder concept for the recovery of expended cylindrical rocket boosters, the results are also related to the use of slender nose strakes on three-dimensional fuselages at moderate and high angles of attack. For example, similar Reynolds number dependency might also be expected with retractable nose strakes used to develop side forces at high angles of attack to augment declining directional control. The potential hazard of developing such controls in the wind tunnel at subcritical Reynolds numbers is apparent.

A somewhat more familiar application of slender nose strakes is that of providing directional stability at high angles of attack to offset the loss

of vertical tail effectiveness. In this application, the high crossflow velocity at the windward strake relative to that on the leeward strake results in an increased vortex strength and a net vortex induced side force that augments the directional stability. The magnitude of the forces generated can be influenced by Reynolds number through its effect on the natural separation location and the velocity at the strake location. (Limited data on two-dimensional cylinders with two flaps 180^{o} apart that is related to the above strake application is also contained in the Lockwood and McKinney study.)

1.2 Non-Circular Cylinders

For a variety of practical reasons, the cross-sectional shapes of aircraft fuselages often deviate from a circle. For modern combat aircraft with relatively long fuselage forebodies ahead of the wing and having the requirement to maneuver to high angles of attack, the crossflow characteristics of their non-circulator forebodies often play an important role in the aerodynamic characteristics of the aircraft. This is particularly true with regard to such handling qualities as directional stability, nose slice, spin damping, pitch-up, etc.

Shortly after the development of Allen's crossflow theory (see section 4), it became apparent that data on two-dimensional cylinders of various non-circular cross-sections was needed in order to apply the method to non-circular shapes. Although some data was available, it was generally limited to subcritical Reynolds numbers. This prompted the two-dimensional cylinder drag study carried out by Delany and Sorensen (reference 1.45) that covered a variety of shapes over a range of Reynolds numbers. Their tests were made at zero flow incidence angle, and therefore, limited primarily to applications related to the longitudinal aerodynamics of three-dimensional bodies.

Later, a low speed study by Letko and Williams (reference 1.46) illustrated the strong effect of fuselage cross-sectional shape on the directional stability of aircraft type configurations at moderate and high angles of attack. The study of cross-sectional shape on aircraft stability was soon extended to additional shapes and to higher speeds by other researchers (see references 1.47 through 1.50). The large effects encountered and the fact that the separated flows involved would be Reynolds number dependent prompted the two-dimensional non-circular cylinder studies

by Polhamus et. al. (reference 1.51 and 1.52) and Lockwood (reference 1.53) in which the effect of flow incidence was varied and the forces parallel and perpendicular to the wind were measured. These data, which covered subcritical, critical, and supercritical Reynolds number conditions, allowed application of the crossflow theory for the tested geometries to combined angles of attack and sideslip and to combinations of spin rates and sink speeds.

The purpose of this section on non-circular cylinders is to present some representative examples of the important Reynolds number effects encountered along with a brief discussion of the implication, particularly with regard to future aerodynamic research. The reader is referred to references 1.45 and 1.51 through 1.53 for the complete data presentations and discussions.

1.2.1 Zero flow incidence angle

The variation of drag coefficient with Reynolds number for some selected two-dimensional cylinders of various non-circular cross-sectional shapes at zero flow incidence is presented in figure 1.7 through 1.10. Since all of the shapes presented are flat on the windward face, the Reynolds number has been based on the maximum width of the cylinder normal to the free stream direction since it is a somewhat more meaningful length for these shapes with regard to boundary layer development as the windward corners are approached.

Figure 1.7 summarizes the low subsonic speed data from references 1.45, 1.51, and 1.52 for square cross-sections having various values of the non-dimensional corner radius, r/w, where r is the radius and w is the width of the cylinder. The results illustrate the large effect of corner radius both on the level of the drag and on the Reynolds number for transition from subcritical to supercritical flow. For the smallest radius, r/w=.021, separation occurs on the windward corners, due to the strong adverse gradient, and the drag is essentially the same as that for a flat plate. Some drag reduction might be expected, even for this small radius, at some Reynolds number beyond the limit of the test data, and the extrapolation shown is based on the correlation presented in figure 9 of reference 1.51, which represents a conjectured trend. The reduction of drag in the subcritical Reynolds number range, as the radii are increased, appears to be associated primarily with some recovery of the suction pressure loops on the windward corners due to the reduced adverse pressure gradients. The earlier

occurrence of the critical Reynolds number range and the reduction in supercritical drag level also is associated with the reduction in adverse pressure gradients. A more detailed analysis can be made with the aid of the measured pressures for an r/w of 0.245 presented in Table I of reference 1.52 and by comparisons with inviscid theoretical results, such as presented in reference 1.54.

The fact that the drag variation for the square cylinder does not monotonically approach that for the circular cylinder as the corner radius increases is due to the fact that the square has four suction pressure loops compared to two for the circle. This and the fact that the drag of the diamond-shaped cylinders do approach the circle monotonically is discussed in reference 1.51. For a summary of the effects of Reynolds number on a series of diamond-shaped cylinders having various corner radii, the reader is referred to figure 9(b) of reference 1.51.

An example of the effect of compressibility on the drag coefficient of a square cylinder is presented in figure 1.8, which was obtained from some unpublished measurements made in the Langley High Speed 7-by-10 Foot Tunnel on a semispan model having an effective fineness ratio of 16 and an r/w of 0.245.

Figure 1.9 illustrates the drag reduction, for given corner radii, associated with increases in the cylinder depth in the stream direction. This drag reduction is due primarily to improved flow reattachment downstream of the windward corners.

The effect of corner radius on basic triangular cross-sections is presented in figure 1.10. In order to provide the probable lower bound over a wide Reynolds number range, the case for an r/w value of .500 (circle) is reproduced from figure 1.2.

Although a considerable amount of data exists for non-circular cylinders at zero flow incidence, it is primarily limited to incompressible flow and Reynolds numbers less than 2×10^6. Research needs to be extended into the compressible flow regime and to higher Reynolds numbers.

1.2.2 Effect of flow incidence

In references 1.51 through 1.53, non-circular cylinders were tested over a wide range of flow incidence angles and Reynolds numbers to identify the types of viscous dependent crossflows that might be expected on non-circular

forebodies at high angles of attack in sideslip. In general, the results indicated that large changes in cross wind or side force coefficient, c_y', are encountered that can have an important bearing on aircraft directional stability at high angles of attack and on spin damping.

Some examples of the effects of cross-sectional shape obtained are presented in figures 1.11 through 1.14, where the side force coefficient is shown as a function of Reynolds number, R_w, for a constant flow incidence angle, ϕ. A value of ϕ of 10^o has been selected for these examples, and the reader is referred to references 1.51 through 1.53 for the results of other flow incidence angles and other cross-sectional shapes.

The critical effect that Reynolds number can have on the side force generated by square cylinders with round corners is illustrated in figure 1.11. Side force data for corner radii of 8% and 24.5% of the cylinder width are presented along with pressure distribution data for the 24.5% radius cylinder. Of course, for pure inviscid flow with no "Kutta condition" imposed, no side force would be developed. For the viscous flow case, however, large side forces can be developed which generally change sign with Reynolds number, as illustrated by the data for the 24.5% radius cylinder. In the lower Reynolds number range, a postive (towards the wind) side force is developed followed by a transition to a negative side force beginning at a Reynolds number, R_w, of about 0.5×10^6. The flow mechanism generating these forces can be seen from the subcritical and supercritical pressure distributions shown in the sketches. These pressure distributions were taken from the experimental results of reference 1.52 and are compared with the inviscid theory of reference 1.54. For the case shown, the terms "subcritical" and "supercritical" refer only to the flow conditions around the front leeward corner (left side in the sketch). The pressure distribution obtained at a Reynolds number of 0.3×10^6 indicates laminar separation at the front leeward corner due to the strong adverse pressure gradient, with only a fraction of the theoretical suction loop being achieved; attached flow being developed around a sizable portion of the front windward corner, as a result of the reduced adverse gradient; and turbulent separation on the rear windward corner. The positive side force results from the combination of the near-theoretical suction pressures on the front windward corner, the partial suction pressure development around the rear windward corner, and the loss in suction pressures on the leeward corners. As the Reynolds number increases, the pressure loop development

essentially reverses as attached flow develops on the front leeward corner, with turbulent separation on the rear leeward corner. In addition, a circulation is established which reduces the suction pressure loop on the front windward corner and increases the magnitude of the front leeward suction pressure loop beyond that for the inviscid theory without circulation. As a result of these flow changes, a large negative side force is developed. This force is nearly equal to $2\pi\sin\phi$, the normal force generated by a flat plate in potential flow at a flow incidence angle, ϕ, and a Kutta condition at the trailing edge.

The results shown for the smaller (8%) radius square cylinder shown in figure 1.11 illustrate the higher level of Reynolds number required to produce attached flow around the front leeward corner as a result of the steeper adverse gradient associated with the smaller corner radius.

The significance of the forces developed with regard to fuselage forebodies are that a positive side force translates into a restoring moment with regard to directional stability at high angles of attack and translates into a propelling moment during a flat spin. With the side force changing sign at supercritical Reynolds numbers, it is very important that full-scale Reynolds number conditions be accurately simulated when investigating high angle of attack directional stability and spin characteristics. This was discussed in detail in reference 1.51 and led to the current procedures used in spin tunnel testing. A more complete discussion of the effects of Reynolds number on directional stability and spin damping will be presented in section 4.2.

According to figure 1.11 (using the 24.5% radius cylinder as an example), additional critical Reynolds numbers might be expected both below and above that shown. For example, at lower Reynolds numbers separation would be expected to occur well forward on both front corners and a side force value closer to zero would probably occur. At Reynolds numbers above the highest shown in figure 1.11, the suction loops around the rear corners might be expected to develop, first on the windward corner and then on the leeward corner. With these flow changes and the resulting circulation changes, additional variations in side force might be expected to occur. Such multiple critical Reynolds number effects would have important implications in relation to directional stability and spin damping.

The capabilities of the new high Reynolds number cryogenic wind tunnels offer a means of exploring these possible multiple critical Reynolds number effects, and this will be discussed more in section 4.

While a complete summary of the available two-dimensional data on non-circular cross sections is beyond the scope of this paper, a few more examples of the effects of Reynolds number on side force are presented in figures 1.12 through 1.14. Figure 1.12 illustrates the difference in force characteristics generated by a rectangular cross section having rounded corners and a cross section with a similar shape on the windward half but an elliptical shape on the leeward half (referred to as a triangular shape). The rectangular cylinder characteristics are similar to those of the previously discussed square cylinder. However, because of its steeper adverse pressure gradients, the triangular cylinder encounters the critical Reynolds number on both corners within the test range and at higher Reynolds numbers than for the rectangle. No additional large Reynolds number effects would be expected for the triangular cylinder, while additional effects smilar to those discussed relative to the square cylinder would be expected for the rectangular cylinder.

Figure 1.13 illustrates the effect of corner radius for two basically triangular type cross sections taken from the results of references 1.51 and 1.53. The shift of the positive side force loop to a higher Reynolds number for the cylinder having the smaller corner radii is due, of course, to the more severe adverse pressure gradients.

An illustration of the critical nature of slight departures from a circular cross section on the side force developed in the critical number range is presented in figure 1.14. This data was taken from the study carried out by Lockwood (reference 1.53) on a parametric series which transitioned between the circular cylinder and cylinder E of figure 1.12. For the complete series results over a wide range of flow incidence angles, the reader is referred to reference 1.53.

1.3 References

General

1.1 Goldstein, Sydney: Modern Developments in Fluid Dynamics. Oxford, The Clarendon Press, vol. 2, sec. 195, 1938, pp. 439-440.

1.2 Schlichting, Herman: Boundary Layer Theory. McGraw-Hill Book Company, New York. 6th Edition, 1968.

1.3 Morkovin, M.V.: Flow around circular cylinder - a kaleidoscope of challenging fluid phenomena. A.S.M.E. symposium on fully separated flows. Philadelphia, 1964.

1.4 Sarpkaya, Turgut: Separated Flow about Lifting Bodies and Impulsive Flow about Cylinders. AIAA Journal, Vol. 4, No. 3, March 1966.

1.5 Shih, W.C.L.: High Reynolds Number Cylinder Flow Workshop: Physical Research, Inc., Rept. PRI-LA-81-003, August 1981.

Low Speed

1.6 Wieselberger, C.: Neuere Feststellungen über die Gesetze des Flüssigkeits und Luftwiderstandes. Phys. Zeitschrift, Vol. 22, pp. 321-328, 1921. (Translation available as "New Data on the Laws of Fluid Resistance," NACA TN 84, 1922).

1.7 Stephens, A.V.: Drag of Circular Cylinders in Flight. R. & M. No. 1892, British A.R.C., 1940.

1.8 Stack, John: Compressibility Effects in Aeronautical Engineering. NACA ACR, 1941.

1.9 Delaney, Noel K. and Sorensen, Norman E.: Low-Speed Drag of Cylinders of Various Shapes. NACA TN 3038, 1953.

1.10 Polhamus, Edward C.: Effect of Flow Incidence and Reynolds Number on Low-Speed Aerodynamic Characteristics of Several Non-circular Cylinders with Applications to Directional Stability and Spinning. NASA TR R-29, 1959.

1.11 Lockwood, Vernard E. and McKinney, L. W.: Effect of Reynolds Number on the Force and Pressure Distribution of a Two-Dimensional Lifting Circular Cylinder. NASA TN D-455, 1960.

1.12 Humphreys, John S.: On a circular cylinder in steady wind at transition Reynolds numbers. Journal of Fluid Mechanics, vol. 9, 1960., p. 603.

1.13 Schmidt, Louis V.: Fluctuating Force Measurements Upon a Circular Cylinder at Reynolds Numbers up to 5×10^6. NASA TM X-57,779, 1966.

1.14 Schulz, G., Hayn, F.: Widerstandsmessungen an Systemteilen von Rohrkonstructionen, DVL 1-NK-I-68-34 (1968).

1.15 Jones, George W., Jr.; Cincotta, Joseph J.; and Walter, Robert W.: Aerodynamic Forces on a Stationary and Oscillating Circular Cylinder at High Reynolds Numbers. NASA TR R-300, 1969.

1.16 Van Nunen, J.W.G.: Pressure and Forces on a Circular Cylinder in a Crossflow at High Reynolds Number, Proceedings, Symposium on Flow-Induced Structural Vibrations, Karlsruhe, Germany, 1972.

1.17 Murthy, V.S. and Rose, W.C.: Surface Shear Stress Measurements on Circular Cylinder in Crossflow at Near-Critical Reynolds Numbers. NASA TM 78,454, January 1978.

Surface Roughness

1.18 Fage, A. and Warsap, J.H.: The effects of turbulence and surface roughness on the drag of a circular cylinder. ARC, R & M No. 1283, 1929.

1.19 Dryden, H.L. and Hill, G.C.: Wind Pressure on Circular Cylinders and Chimneys. Bureau of Standards Journal of Research, Vol. 5, pp. 653-693, 1930.

1.20 Roshko, Anatol: Experiments on the Flow Past a Circular Cylinder at Very High Reynolds Numbers. J. Fluid Mech., Vol. 10, pt. 3, May 1961, pp. 345-356.

1.21 Achenbach, E.: Distribution of local pressure and skin friction around a circular cylinder in crossflow up to $Re=5x10^6$. Journal of Fluid Mechanics, Vol. 34, part IV, 1968, pp. 625-639.

1.22 Schulz, G., Hayn, P.: Widerstandsmessungen an Systemteilen von Rohrkonstructionen, DVL L-NK-I-68-34 (1968).

1.23 Batham, J.P.: Pressure distributions on circular cylinders at critical Reynolds numbers. Journal of Fluid Mechanics, Vol. 57, 1973, pp. 209-228.

1.24 Szechenyi, Edmond: Simulation de nombres de Reynolds éleves sur un cylindre en soufflerie. ONERA T.P. No. 1391, 1974.

1.25 Szechenyi, Edmond: Supercritical Reynolds Number Simulation for Two-Dimensional Flow over Circular Cylinders. Journal of Fluid Mechanics, Vol. 7, 1975, Pt. III, pp. 529-540.

1.26 Achenbach, Elmar: Influence of Surface Roughness on the Crossflow Around a Circular Cylinder. Journal of Fluid Mechanics, Vol. 46, 1971., Pt. II, pp. 321-335.

1.27 James, W.D.; Paris, S.W.; and Malcolm, G.N.: A Study of Viscous Crossflow Effects on Circular Cylinders at High Reynolds Numbers, AIAA Paper 79-1477, Williamsburg, VA, July 1979.

1.28 James, W.D.; Paris, S.W.; and Malcolm, G.N.: Study of Viscous Crossflow Effects on Circular Cylinders at High Reynolds Numbers. AIAA Journal, December 1980, pp. 1066-1072.

1.29 Buresti, Guido: The Effect of Surface Roughness on the Flow Regime around Circular Cylinders. Journal of Wind Engineering and Industrial Aerodynamics. 8(1981)105-115.

Effects of Compressibility

1.30 Tsien, Hsue-Shen: Two-Dimensional Subsonic Flow of Compressible Fluids. Journal Aero. Sci., Vol. 6, No. 10, August 1939, pp. 399-407.

1.31 Stack, John: Compressibility Effects in Aeronautical Engineering. NACA ACR, 1941.

1.32 Matt, H.: Hochgeschwindigkeitsmessungen an Rund - und Profilstangen verschiedener Durchmesser. Lilienthal - Gesellschaft für Luftfahrtforschung, Berlin, Bericht 156, October 1942. (Translation available as "High Speed Measurements on Cylindrical and Shaped Rods of Various Diameters" MAP Volkenrode, Reports and Translations No. 368, January 1946).

1.33 Welsh, Clement J.: The Drag of Finite-Length Cylinders Determined from Flight Tests at High Reynolds Numbers for a Mach Number Range from 0.5 to 1.3. NACA TN 2941, 1953.

1.34 Gowen, Forrest E. and Perkins, Edward W.: Drag of Circular Cylinders for a Wide Range of Reynolds Numbers and Mach Numbers. NACA TN 2960, 1953.

1.35 Jones, George W., Jr.; Cincotta, Joseph J.; and Walker, Robert W.: Aerodynamic Forces on a Stationary and Oscillating Circular Cylinder at High Reynolds Numbers. NASA TR R-300, 1969.

1.36 Macha, J.M.: A Wind Tunnel Investigation of Circular and Straked Cylinders in Transonic Crossflow. TAMU rep. 3319-76-01, Texas A & M Res. Found., College Station, TX, November 1976 (Also available as NASA-CR-149372).

1.37 Macha, J.M.: Drag of Circular Cylinders at Transonic Mach Numbers. J. Aircraft, Vol. 14, No. 6, June 1977, pp. 605-607.

1.38 Murthy, V.S. and Rose, W.C.: Form Drag, Skin Friction, and Vortex Shedding Frequencies for Subsonic and Transonic Crossflows on Circular Cylinder. AIAA Paper 77-687, Albuquerque, NM, June 27-29, 1977.

1.39 Green, Lawrence L. and South, Jerry C., Jr.: Conservative Full-Potential Calculations for Axisymmetric Transonic Flow. AIAA Paper No. 81-1204, 1981.

1.40 von Doenhoff, A.E. and Braslow, A.L.: Studies of the Use of Freon-12 as a Wind Tunnel Testing Medium. NACA TN 3000, 1953.

1.41 Posniak, O.M.: Investigation into the use of FREON 12 as a Working Medium in a High-Speed Wind Tunnel. College of Aeronautics, Cranfield, England. Note 72, 1957.

Effects of Fineness Ratio

1.42 Wieselsberger, C.: Der Widerstand von Zylindern. Ergb. Aerod. Versuchsanstalt zu Göttingen, Lfg. II, R. Oldenbourg (Munich), 1923, pp. 23-28.

1.43 Welsh, Clement J.: The Drag of Finite-Length Cylinders Determined from Flight Tests at High Reynolds Numbers for a Mach Number Range from 0.5 to 1.3. NACA TN 2941, 1953.

1.44 McKinney, Linwood W.: Effects of Fineness Ratio and Reynolds Number on the Low-Speed Crosswind Drag Characteristics of Circular and Modified-Square Cylinders. NASA TN D-540, 1960.

Non-Circular Cross Sections

1.45 Delaney, Noel L. and Sorensen, Norman E.: Low-Speed Drag of Cylinders of Various Shapes. NACA TN 3038, 1953.

1.46 Letko, William and Williams, James L.: Experimental Investigation at Low Speed of Effects of Fuselage Cross Section on Static Longitudinal and Lateral Stability Characteristics of Models having 0^{o} and 45^{o} Sweptback Surfaces. NACA TN 3551, 1955.

1.47 King, Thomas J., Jr.: Wind Tunnel Investigation at High Subsonic Speeds of Some Effects of Fuselage Cross Section Shape and Wing Height on the Static Longitudinal and Lateral Stability Characteristics of a Model Having a 45^{o} Swept Wing. NACA RM L55J25, 1956.

1.48 Malvestuto, Frank S., Jr. and Alford, William J., Jr.: Effects of Wing-Body Geometry on Lateral-Flow Angularities at Subsonic Speeds. NACA RM L55L22b, 1956.

1.49 Polhamus, Edward C.: Some Factors Affecting the Variation of Pitching Moment with Sideslip of Aircraft Configurations. NACA RM L55E20b, 1955.

1.50 Polhamus, Edward C. and Hallisy, Joseph M., Jr.: Effect of Airplane Configuration on Static Stability at Subsonic and Transonic Speeds. NACA RM L56A09a, 1956.

1.51 Polhamus, Edward C.: Effect of Flow Incidence and Reynolds Number on Low-Speed Aerodynamic Characteristics of Several Non-circular Cylinders with Applications to Directional Stability and Spinning, NASA TR R-29, 1959. (Supersedes NACA TN 4176).

1.52 Polhamus, Edward C.; Geller, Edward W.; and Grunwald, Kalman J.: Pressure and Force Characteristics of Non-circular Cylinders as Affected by Reynolds Number with a Method Included for Determining the Potential Flow about Arbitrary Shapes. NASA TR R-46, 1959.

1.53 Lockwood, Vernard E.: Effects of Reynolds Number and Flow Incidence on the Force Characteristics of a Family of Flat-Front Cylinders. NASA TN D-3932, 1967.

1.54 Ashley, Sophia Kokkinos: Inviscid Two-Dimensional Vortex-Panel Method for Calculating the Pressure Distribution over Non-circular Cylinders at Various Flow Incidence Angles. A thesis submitted to the faculty of Old Dominion University, August 1978.

Some additional papers

1.55 Nakamura, Y. and Tomonari, Y.: The effects of surface roughness on the flow past circular cylinders at high Reynolds numbers. Journal of Fluid Mechanics (1982), Vol. 123, pp. 363-378.

1.56 Salas, D.: Recent Developments in Transonic Euler Flow over a Circular Cylinder. NASA TM 83282, 1982.

1.57 Obasaju, E.D.: An Investigation of the Effects of Incidence on the Flow Around a Square Section Cylinder. The Aeronautical Quarterly, November 1983.

1.58 Kawamura, T.; Bunkyo, H.; and Kuwahara, K.: Computation of High Reynolds Number Flow Around a Circular Cylinder with Surface Roughness. AIAA 84-0340, January 1984.

2. FORCES ON CIRCULAR CYLINDERS IN OBLIQUE FLOW

Inasmuch as the flow at angle of attack or sideslip about a three-dimensional body of revolution having a cylindrical afterbody of circular cross section is related in several respects to that about a cylinder of infinite length in oblique flow, a brief review of the infinite cylinder characteristics is presented in the following sections.

The reader will note that in the interest of historical clarity, the description of the early studies of oblique cylinders will maintain the references to sweep and yaw of interest at that time. However, in the discussions of applications more directly related to the subject of this paper, the angle of attack, α, is used to define the oblique angle.

2.1 Independence Principle

Spurred by the growing interest in swept wings as a means of delaying the onset of compressibility effects, theoretical studies of the boundary layer development on yawed plates and infinite cylinders were begun during the mid 1940's as an initial step towards the development of a completely three-dimensional viscous flow theory. Studies of laminar boundary layers by Prandtl (reference 2.2) and Struminsky (reference 2.8), using the Navier-Stokes equations, illustrated that the boundary layer characteristics in attached laminar flow are independent of the spanwise velocity component. This finding, coupled with the earlier discovery that the inviscid flow velocity perturbations due to thickness are also unaffected by the spanwise velocity component, set the stage for the important research that followed.

Jones (reference 2.3), in discussing what Prandtl's work meant in terms of the boundary layer separation on yawed cylinders, coined the term "independence principle." Jones concluded that, for the laminar flow case at least, the flow around the cylinder should depend on conditions in the cross-flow plane only. In particular, he concluded that (a) the distance to the separation point in the crossflow plane should be independent of yaw angle; (b) the critical Reynolds number based on cylinder diameter and crossflow velocity should also not change with yaw angle (however, the critical Reynolds number based on cylinder diameter and freestream velocity should increase, by $1/\cos\beta$, with increasing yaw angle); (c) the "drag" force normal to the cylinder axis should be reduced by $\cos^2\beta$ as the yaw angle increased,

since the dynamic pressure in the crossflow plane would be reduced by that amount. Essentially, these same conclusions were reached independently by Sears (reference 2.4). Other early researchers in this area were Wild (reference 2.5) and Cooke (reference 2.6).

2.2 Experimental Results

The later experimental studies with yawed cylinders indicated that, while the independence principle generally applied in the low Reynolds number range where there was laminar separation which is relatively independent of Reynolds number, it did not apply at the higher Reynolds numbers where there was turbulent separation. The most complete experimental study of flow around yawed circular cylinders was that by Bursnall and Loftin (reference 2.7), which covered both critical and supercritical flow conditions. Their study showed that the critical Reynolds number, rather than being delayed to a higher freestream velocity as the independence principle indicated it should, actually occurred at lower freestream velocities as the yaw angle increased. From this study and that of Smith et. al. (reference 2.13), it appears that the transition from laminar to turbulent flow in the near wake and forward to the laminar separation point is indeed affected by the axial flow component. This results from the effect of the axial component in diverting the streamlines to a path more parallel to the freestream direction than normal to the axis. With the boundary state being related more to the "effective" Reynolds number along the streamline, Bursnall and Loftin indicated that the critical Reyolds number is nearly independent of yaw angle if it is based on chord lengths and velocities in the freestream direction rather than on those in the crossflow direction. Several methods have been proposed for approximating the "effective" Reynolds number related to the streamline path (see references 2.14 through 2.16, for example); among these it appears that Esch's factor (reference 2.15) collapses the Bursnall and Loftin data somewhat better than do the others and will be reviewed below. In the following, the oblique angle will be defined as angle of attack, α, in keeping with the subject of this paper.

The Esch factor approximates the angle-of-attack effects on streamline length by use of the ellipse formed by the intersection of the surface and the plane parallel to the freestream that cuts through the cylinder at an angle, α, with respect to its axis. By use of this concept, an "effective"

Reynolds number, R_{eff}, can be related to that based on diameter, R_D, as follows:

$$R_{eff} = R_D \, K_\alpha$$

$$\text{where } K_\alpha = \left[0.983/\sin\alpha + 0.311 + 0.287 \sin\alpha \right] \div \left[1.581 \right]$$

In the above formulation, K_α is equal to the ratio of the circumferential length in the plane parallel to the stream (ellipse), as described above, to that in the crossflow plane (circle). The resulting change in effective Reynolds number is roughly proportional to the actual change in streamline length (to the separation line) with angle of attack. A table of K_α values are given below:

α	K_α	α	K_α
10^o	3.81	40^o	1.28
15^o	2.65	45^o	1.21
20^o	2.08	50^o	1.15
25^o	1.75	60^o	1.07
30^o	1.53	80^o	1.01
35^o	1.38	90^o	1.00

In an attempt to evaluate the independence principle for similar boundary layer and separation conditions, the Bursnall and Loftin data is presented as a function of R_{eff} in figure 2.1. For the purpose of this paper, the angle of yaw has been converted to angle of attack and the drag coefficient defined as normal force coefficient (based on freestream dynamic pressure and body diameter) in order to be more readily associated with the

discussion of three-dimensional bodies at angle of attack to be presented in subsequent sections. In order to establish the degree to which the normal force coefficient based on normal velocity is independent of angle of attack, the parameter $c_n/\sin^2\alpha$ is plotted as a function of the effective Reynolds number, R_{eff}, for the various angles of attack, α. The results indicate that the critical effective Reynolds number does not vary greatly with angle of attack, implying that this method is reasonably accurate in predicting the effect of angle of attack on boundary layer transition.

The rapid decrease of normal force with increasing Reynolds number combined with some degree of inaccuracy in the method of estimating R_{eff} makes it difficult to analyze, with any degree of certainty, the normal force data of figure 2.1 in the critical range. However, in the supercritical range, where the effect of Reynolds number is greatly reduced, it is clearly evident that the independence principle does not hold. In this range, the results indicate that while the values of $c_n/\sin^2\alpha$ are about the same at the high angles, 75° and 90°, as would be expected by the independence principle, the values increase considerably as the angle of attack decreases. The corresponding pressure distribution for $\alpha=90^\circ$, 60°, and 30° at a value of R_e of approximately 4.5×10^5 are presented in figure 2.2. From these pressure distributions, it appears that as the angle of attack, α, is reduced, the laminar separation bubble disappears and stable lee-side vortices are formed as might be expected from the impulsive flow analogy (reference 2.17) for these finite length cylinders. These vortices produce a large normal force, analogous to the vortex lift of slender wings, and restrict the aft movement of the separation line with angle of attack.

Subsequent to the Bursnall and Loftin study, Trimble carried out a similar study of oblique circular cylinders in which he extended the investigation to lower angles of attack. Trimble's results, published by Glenny (reference 2.10), are presented in figure 2.3 in the same format as figure 2.1. Although, as mentioned above, data in the critical Reynolds number range are difficult to analyze, it is evident that the critical Reynolds number is somewhat lower than that of figure 1.2 and the Bursnall and Loftin data, possibly due to a higher wind tunnel turbulence factor.

In the supercritical range, of primary interest in this paper, the Trimble data is very informative. First, it will be observed that for the $\alpha=30^\circ$ case, representing the upper Trimble case and the lower Bursnall and

Loftin case, the agreement between the two experiments is exceptionally good (compare figures 2.1 and 2.3). At the lower angles of attack, 25° and 20°, Trimble's data shows essentially the same values of $c_n/\sin^2\alpha$, implying that the flow patterns are similar and the normal force value is dictated by the normal component of dynamic pressure. Trimble's measurements made at $\alpha=5^{\circ}$ are not presented in figure 2.3 since when there is a very high axial component of velocity, the Esch factor does not apply. However, it is of interest that for $\alpha=5^{\circ}$, those data points which are obviously in the supercritical region, the values of $c_n/\sin^2\alpha$ are in excellent agreement with those for $\alpha=20^{\circ}$ and $\alpha=25^{\circ}$ (see figure 7 of reference 2.10).

A summary of the types of flow encountered in the various angle of attack regimes is presented in figure 2.4 for both subcritical and supercritical conditions. For the subcritical condition, data measured by Relf and Powell (reference 2.1) are used inasmuch as it appears to be the only data which is definitely in the subcritical range over the complete angle of attack range. The data of Relf and Powell has sometimes been used to demonstrate the applicability of the "independence principle" over the complete range of angle of attack. However, as pointed out by Smith et. al. (reference 2.13), a careful examination of this subcritical data also indicates an increase in $c_n/\sin^2\alpha$ as the angle of attack is decreased as seen in figure 2.4. This variation with angle of attack appears consistent with the impulsive flow analogy which, from Sarpkaya's data (reference 2.17), predicts that for this cylinder fineness ratio of 80, the peak value of $c_n/\sin^2\alpha$ would be about 1.29 and would occur at an angle of attack of about 6° in subcritical flow. These low angles of attack correspond to early times in the impulsively started flow about a cylinder normal to the flow when only the two starting vortices are present prior to the wake flow generated by the cylinder.

For supercritical Reynolds numbers, the type of flow has a more pronounced effect on the variation of $c_n/\sin^2\alpha$ with angle of attack, as shown by the bottom curve of figure 2.4 for a Reynolds number of 4.5×10^6. At angles of attack between 70° and 90°, the force and pressure data of Bursnall and Loftin indicate, as might be expected, that essentially the same flow characteristics exist, with regard to the laminar bubble with its turbulent reattachment and separation leading to the characteristic unsteady and unstructured wake flow with no dominant vortex shedding frequency. Under

these conditions, the pressure forces are proportional to the normal component of the dynamic pressure, and $c_n/\sin^2\alpha$ is, therefore, independent of angle of attack in this range.

An analogous situation exists in the low angle of attack range where the combined data of Trimble and of Bursnall and Loftin indicate that in the angle of attack range from about 5° to about 40°, $c_n/\sin^2\alpha$ is again independent of angle of attack but that its value is considerably greater than for the high angle of attack range. As discussed previously, this lower angle of attack range is characterized by a steady, well-organized vortex flow which restricts the rearward movement of the separation line and results in a large, vortex-induced increase in normal force.

In the intermediate angle of attack range of about 40° to 70° where the flow might be described as "quasi-steady", there is a transition from the steady, well-ordered vortex flow to the unsteady, unstructured wake type flow. In this transition region, the parameter $c_n/\sin^2\alpha$ is, of course, no longer constant.

Unfortunately, there is no data in the higher supercritical and hypercritical Reynolds number range which is the range of primary interest with regard to full scale aircraft and missile applications. A possible consequence of hypercritical Reynolds number conditions can be speculated by returning to Trimble's results in figure 2.3. It is seen that for the 20° and 25° angles of attack, the values of $c_n/\sin^2\alpha$ are essentially the same and relatively constant with Reynolds number to the highest value investigated, a trend which might be expected to continue due to the predominance and stability of the vortex flow. On the other hand, the extreme angle of attack case represented by the results for the cylinder normal to the stream ($\alpha=90^\circ$), reproduced from figure 1.2, shows an increase in the normal force parameter in the middle supercritical range. In this range, the turbulent separation line has moved forward to a more stable position, and the wake is more structured and is characterized by the return of a dominant vortex shedding frequency (see section 3). The drag has increased as a result of the forward movement of the turbulent separation and approaches the value of the normal force parameter at the low angles of attack. In view of the above effects, it is conceivable that in the hypercritical Reynolds number range, the normal force parameter $c_n/\sin^2\alpha$ may be relatively independent of angle of attack over the entire range.

The above possibilities should be explored with the Reynolds number capability of the new cryogenic high Reynolds number tunnels, at least for three dimensional bodies, as will be discussed in section 4.

Additional information relative to oblique circular cylinders can be found in references cited in section 3.

2.3 References

2.1 Relf, E.H. and Powell, C.H.: Tests on Smooth and Stranded Wires Inclined to the Wind Direction and a Comparison of the Results on Stranded Wires in Air and Water, British ARC, R and M, No. 307, 1916.

2.2 Prandtl, L.: On Boundary Layers in Three-Dimensional Flow. Reports and Translations No. 64, File No. B.I.G.S. 84, M.A.P. Volkenrode May 1, 1946.

2.3 Jones, R.T.: Effects of Sweepback on Boundary Layer and Separation, NACA TN No. 1402, July 1947.

2.4 Sears, W.R.: The Boundary Layer of Yawed Cylinders, Journal of the Aeronautical Sciences, Vol. 15, No. 1, p. 49, January 1948.

2.5 Wild, J.M.: The Boundary Layer of Yawed Infinite Wings, Journal of Aeronautical Science, Vol. 15, 1949, p. 41.

2.6 Cooke, J.C.: The Boundary Layer of a Class of Infinite Yawed Cylinders, Proceeding Cambridge Philosophical Society, Vol. 46, 1950, p. 645.

2.7 Bursnall, William J. and Loftin, Laurence K., Jr.: Experimental Investigation of the Pressure Distribution about a Yawed Circular Cylinder in the Critical Reynolds Number Range. NACA TN 2463, 1951.

2.8 Struminsky, V.V.: Skolzhenie Kryla v Vyazkom i Szhimaemom Gaze, Doklady Akademii Nauk, USSR, T. LIV., No. 9, 1946, pp. 769-772. (English translation available as: Sideslip in a viscous compressible gas. NACA TM 1276, 1951).

2.9 Moore, F.K.: Yawed Infinite Cylinders & Related Problems - Independence Principle Solutions. Advances in Applied Mechanics, Vol. 4, pp. 181-187. Book published by Academic Press, Inc., 1956.

2.10 Glenny, D.E.: A Review of Flow Around Circular Cylinders, Stranded Cylinders, and Struts Inclined to the Flow Directions, Australian Department of Supply, Mechanical Engineering Note 284, October 1966.

2.11 Fiechter, M.: Uber Wirbelsysteme an schlanken Rotationskorpern und thren Einfluss auf die aerodynamischen Beiwerte. Duetsch-Franzosisches Forschungs-Institut Saint-Louis, Report 10/66, 1966.

2.12 Fletcher, C.A.J.: Investigation of the Magnus Characteristics of a Spinning Inclined Ogive - Cylinder Body at M=0.2. Australian Weapons Research Establishment, Technical Note HSA 159, 1970.

2.13 Smith, R.A.; Moon, Woo, Taik; and Kao, T.W.: Experiments on Flow about a Yawed Circular Cylinder. Journal of Basic Engineering, December 1972.

2.14 Clark, W.H.: Body Vortex Formation on Missiles in Incompressible Flows. AIAA Paper No. 77-1154, 1977.

2.15 Esch, Helmut: The Influence of Reynolds Number on the Normal-Force Characters of Slender Cylindrical Bodies. ESA TT-170, 1975.

2.16 Reding, Peter J. and Ericsson, Lars E.: Maximum Side Forces and Associated Yawing Moments on Slender Bodies. AIAA Paper 79-1647, 1979.

2.17 Sarpkaya, T.: Separated Flow about Lifting Bodies and Impulsive Flow about Cylinders. AIAA Journal, Vol. 4, No. 3, March 1966. pp. 414-420.

2.18 Schwabe, M.: Pressure Distribution in Nonuniform Two-Dimensional Flow. NACA TM 1039, January 1943.

3. VORTEX SHEDDING FROM TWO-DIMENSIONAL CYLINDERS

The wakes behind bluff bodies normal to the wind, such as the two-dimensional cylinders discussed in section 1, are characterized by shed vorticity of various frequencies which give rise to oscillating forces, particularly in a plane perpendicular to the wind. In aerospace engineering, these oscillating forces are of importance in such areas as aeroacoustic radiation, buffeting associated with protuberances, and oscillating loads on launch vehicles induced by surface winds.

Although this paper does not deal with oscillating forces, a knowledge of the two-dimensional vortex-shedding frequency is helpful in understanding some of the steady asymmetric vortex flow characteristics of slender three-dimensional bodies at large angles of attack (to be discussed in section 5). A brief review of the experimental studies regarding the influence of Reynolds number on vortex shedding beind two-dimensional bluff bodies will, therefore, be given in this section.

The reference list presented at the end of the section is divided into subject areas and in chronological order for the convenience of those readers wishing to make a more thorough study. Therefore, the citations in the text do not follow in numerical order.

Although the Aeolian tones produced by the action of the wind across wires, tree branches, etc. have been observed since antiquity, the first scientific research on this subject in modern times was published by Strouhal in 1878 (reference 3.1). Strouhal demonstrated that the Aeolian tones were independent of the length and tension of the wires, and depended on the diameter, D, and relative wind speed, V, only. He established the relation between these parameters which led to the now well-known "Strouhal number", S, the non-dimensional frequency parameter given by:

$$S = \frac{nD}{V}$$

where n is the frequency of vortex shedding from one side of the cylinder.

At essentially the same time, Raleigh concluded that the production of the tones was connected with the instability of the vortex sheets. He performed experiments which verified his suspicion that the wind induced vibrations of the Aeolian harp were not in the wind direction but

perpendicular to it and reported the results in 1879 (reference 3.2). Shortly thereafter, he concluded that the Strouhal number is dependent on the Reynolds number (reference 3.3), a fact that was to be clearly demonstrated by the research of Relf, published in 1921, and of Relf and Simmons published in 1924 (references 3.24 and 3.25). While their research adequately covered the subcritical Reynolds number range and provided a brief excursion into the critical range where they noted that dominant periodicity ceases, it was some twenty years later before significant research began in the higher Reynolds number regimes - research that is still ongoing but only slowly defining the detailed content and effects of the vortex wakes.

3.1 Circular Cylinders in Normal Flow

3.1.1 Vortex shedding data

The effects of Reynolds number on the vortex shedding frequency associated with two-dimensional circular cylinders normal to the stream at low speeds are summarized in figures 3.1 and 3.2 in terms of the Strouhal number, $\frac{nD}{V}$ versus Reynolds number based on diameter. In the interest of clarity and analysis, figure 3.1 presents only the results obtained from time histories of either lift fluctuations or surface pressure fluctuations, while figure 3.2 presents only those obtained from wake velocity fluctuations. The main features of the vortex shedding characteristics can be conveniently described with the aid of figure 3.1. From power spectral density analysis, the vortex wake character can be divided into various regimes depending upon the Reynolds number. In the well-known subcritical Reynolds number regime, a well-defined dominant periodicity exists at a Strouhal number of about 0.19, a value that has been obtained by many investigators from both local and wake measurements (the band of a large number of pressure fluctuations measurements made by Drescher (reference 3.31) being representative). In the critical Reynolds number range, where the laminar bubble with turbulent reattachment and separation is formed, the wake becomes narrow, and three-dimensional effects begin to appear in the separated shear layer due at least in part to the critical nature of the bubble stability. In this range, the dominant periodicity ceases to exist, and the fluctuations can be described

as wide-band random. By the time the supercritical region is reached ($R=4x10^5$), the frequencies have been observed to vary between two somewhat dominant values: a low value about equal to the subcritical Strouhal frequency, and a high value of the order of twice the subcritical frequency. This region, defined in the figure by the data of Loiseau and Szechenyi (references 3.40 and 3.41) extends through the supercritical Reynolds number regime with only a slight decrease in the high frequency value and a slight increase in the low frequency value with increasing Reynolds number.

From an analysis of local pressure spectra, Loiseau and Szechenyi conclude that the high frequency lift fluctuation mentioned above does not represent an increase in vortex shedding frequency but is the result of double-frequency pressures on the far leeward surface of the cylinder induced by the alternate shedding. They propose that as a result of the randomness of shedding in this Reynolds number range, a lift force at the double-frequency can be generated. However, in light of high frequency fluctuations observed in the near wake by other researchers and the implications of the narrowing of the wake deduced from the "universal wake Strouhal frequency" concept to be discussed later, it would appear to this author that high frequency shedding can occur in the critical and supercritical Reynolds number range.

In view of the wide-band nature of the wake fluctuations in this Reynolds number range, the Strouhal number becomes somewhat academic for the two-dimensional cylinder in normal flow. However, the establishment of the general trend in high frequency shedding with Reynolds number may be of value in analyzing the cyclic shedding along three-dimensional bodies of revolution in the angle of attack range where there is a stable and well-organized wake. This three-dimensional flow is related to an impulsively started flow about a cylinder at early times, prior to the generation of the unstructured wake. It is, therefore, felt that the high level of Strouhal frequency observed may, in fact, be representative of the vortex shedding along three-dimensional bodies of revolution in the critical and supercritical Reynolds number ranges. This will be discussed further in section 5 in relation to out-of-plane forces generated by three-dimensional bodies.

Returning to the two-dimensional cylinders, Jones et. al. (reference 3.38) found that in the upper supercritical range, from a Reynolds number of about $3x10^6$ to $6x10^6$, where the wake has again widened, the oscillation

spectra is of the narrow-band random type with a single peak (at a Strouhal number of about 0.22.) occurring at a Reynolds number of about $3x10^6$. They found a fairly rapid increase in Strouhal frequency as the Reynolds number was increased further, with a Strouhal frequency of about 0.28 being reached at a Reynolds number of about $6x10^6$. Above this Reynolds number, they found a "quasi-periodic" vortex shedding condition with a value of the Strouhal frequency parameter of about 0.30 being reached at a Reynolds number of about $8x10^6$. (The flagged symbols for the Jones et. al. data represent those measurement made in freon.) In this paper, the end of the supercritical Reynolds number range is taken to be $6x10^6$ corresponding to the beginning of the "quasi-periodic" vortex shedding region and the region above the supercritical is termed "hypercritical."

Although higher Reynolds number data obtained at higher Mach numbers indiciates that a "plateau" may have been reached, additional data is needed to establish the characteristics in the hypercritical range. This indication of the reappearance of periodic vortex shedding in the hypercritical range is consistent with the earlier study by Roshoko (reference 3.15) using wake measurements. With regard to the reappearance of periodic vortex shedding, another important contribution of the study by Jones et. al. is the convincing evidence from both surface flow pictures and pressure measurements that at the highest Reynolds number, three-dimensionality in the separating shear layer has in general been eliminated, and the flow is again essentially two-dimensional.

The general characteristics observed in figure 3.1, which is based on force characteristics, are essentially duplicated in figure 3.2 which is based on wake velocity fluctuation measurements. Each set of data in figure 3.2 was obtained by means of a hot wire probe located at the distances, X, aft of the rear of the cylinder. The same regions of fluctuation characteristics observed in figure 3.1 are found in the wake frequency data of figure 3.2. Differences observed in the onset of the frequency rise in the critical range may be associated with tunnel turbulence or differences in model surface condition. With regard to surface condition and the high Reynolds number data obtained by Roshko (reference 3.15), the reader is reminded that the drag analyses (section 1.1) indicated that the sandblasted surface had apparently contributed a measurable drag increment because of the thin boundary layer in the hypercritical range. It also should be noted that the Delany and Sorensen supercritical data presented in figure 3.2 have been

limited to that obtained at or below M=0.20, because some of the reductions in the Strouhal frequency parameter found in their study at the higher Reynolds numbers could be the result of a compressibility effect observed in their drag data (see section 1.1.1).

With regard to the high wake frequencies measured in the critical and supercritical range, it is recognized that controversy exists concerning the interpretation as in the case of the lift fluctuations described earlier. For example, Ericsson and Redding (reference 3.23), in questioning the high values of Strouhal number measured by Delany and Sorensen, speculate that they were associated with fluctuation in the wake formation region ahead of the shed vortex street because the measurements were made at positions less than two diameters downstream of the trailing edge. They cite the wake measurements of Modi and Dikshit (reference 3.22) and conclude from the measured vortex street geometries that the frequency could be more than twice as high at one diameter downstream than at 3.5 diameters downstream. It appears, however, that Ericcson and Redding did not account for the increase in vortex velocity with distance downstream found in reference 3.22, a factor which tends to result in a relatively constant frequency. In addition, it must be remembered that the Modi and Dikshit study was carried out at subcritical speeds where essentially all investigations have identified the same value of the Strouhal frequency regardless of the measuring station. Clarification of the vortex-street stability criterion could be of help in understanding the phenomena in the critical and supercritical range and this will be touched on in the following brief review of the universal wake Strouhal frequency studies.

3.1.2 Universal wake Strouhal frequency

While primarily of academic interest for two-dimensional circular cylinders normal to the flow because of the "broad-band" nature of the fluctuations in the wake, identification of the vortex shedding frequency in the critical and supercritical Reynolds number ranges may, as mentioned earlier, be of help in predicting the vortex shedding characteristics of three-dimensional bodies of revolution in the moderate and high angle of attack range. In these Reynolds number ranges, some additional insight might be derived from application of the "universal wake Strouhal frequency" concept.

Von Karman (reference 3.4) investigated the stability of the alternating vortex filaments shed from the sides of two-dimensional bluff bodies and found that for straight parallel paths only one arrangement was stable; that being the case where the distance between the two rows is 0.28 times the distance between successive vortices in the same row. Because of this "Von Karman street" characteristic several researchers have attempted to derive a universal Strouhal number, based on various wake characteristics, that would relate the vortex shedding frequencies of various bluff bodies. The earliest study appears to be that of Fage and Johansen (reference 3.7) who, by using measured wake widths and free stream velocity, found essentially the same wake Strouhal number for cylinders having rectangular (flat plate), circular, and wedge shaped cross sections. The most widely used universal wake Strouhal number is that developed by Roshko (reference 3.11) who, recognizing that the Fage and Johansen formulation held only for bodies having nearly the same wake velocities, developed a universal wake Strouhal number based on the

$$S^* = \frac{nd'}{V_s} = 0.164,$$

Von Karman vortex street stability criteria, where n is the vortex shedding frequency, d' is the distance between the free streamlines (shear layers) in the wake downstream of the coupling region and V_S is the velocity along the free streamline at the separation point. Solving for the frequency one gets

$$n = \frac{0.164 V_s}{d'},$$

which relates the vortex shedding frequency to the velocity and width of the wake. For the Strouhal frequency based on cylinder diameter, d, and for free stream velocity, V,

$$S = 0.164 \frac{d}{d'} \quad \frac{V_s}{V}$$

By theoretically relating d/d' and V_S/V to measured drag and base pressure, Roshko was able to predict measured shedding frequencies reasonably well in the subcritical Reynolds number range.

From this model of the wake vortex street, one might expect that the large reduction of d' in the critical and supercritical Reynolds number range due to the aft movement of the separation line might result in a higher Strouhal frequency, S. This, of course, assumes that the reduced velocities at the separation point do not completely compensate for the wake width reduction.

The most recent formulation of a universal Strouhal number appears to be that developed by Bearman (reference 3.20) which utilizes Kronauer's proposed criterion for vortex street stability (reference 3.17). Kronauer's criterion states that for a given vortex velocity the vortex street adjusts itself into the configuration giving minimum drag. Using this criterion, Bearman defined a new universal-wake Strouhal number and developed a method of predicting the standard body Strouhal number by use of on measured base pressure and drag.

Inasmuch as experimental wake studies exist that appear to cast some doubt on the universal nature of the Karman stability criterion (see reference 3.20 for review), an examination of predictions of the Strouhal frequency by a universal wake Strouhal frequency concept will be limited to several applications of the Bearman method just described. Furthermore, in an attempt to reduce errors due to wind tunnel interference, etc., predictions were limited to those sets of data where both drag and base pressure were measured in the same facility.

The results are shown in figure 3.3, and while only three sets of reliable base pressure and drag data for $M<0.2$ and covering a Reynolds number range were found, the prediction method does appear to substantiate that high levels of wake vortex shedding frequency can be expected in the Reynolds number range where the wake is relatively narrow. The Bearman points, calculated from the three tabulated values of base pressure and pressure drag presented in Table I of reference 3.20, appear to substantiate the trend in the critical Reynolds number range, while the corresponding calculations from the Bursnall and Loftin data (reference 2.7) extend the trend to the early portion of the supercritical range. In the upper supercritical range, the general level of the calculations based on Roshko's pressure and drag data is in qualitative agreement with the previously observed trend of reduced Strouhal frequency in this range where the wake is again widening. The detailed shape of the variation however is not reproduced.

It will be noted that the base pressure and pressure drag data from the study by Jones et. al. (reference 3.38) have not been used here to estimate

the Strouhal shedding frequency. The reason for this omission is that the pressure measurements were made with the gap between the fixed and instrumented sections of the cylinder in a configuration which was found to seriously disturb the flow and produce unreasonably high pressure drags, particularly in the critical and supercritical regions.

From the results of the estimates of the Strouhal vortex shedding frequency just described (figure 3.3), it appears that the narrowing of the wake in the critical and supercritical regions has a greater effect than the reduced wake velocity, and that increases in the vortex shedding frequency might be expected in this Reynolds number range. In addition, the estimated values are at least in qualitative agreement with the wake measurements presented in figure 3.2 and might reasonably be considered as additional evidence of the existence of high vortex shedding frequencies in the critical and supercritical Reynolds number ranges. However, an in-depth study of the applicability of the Bearman formulation to the wake characteristics in these high Reynolds number ranges may be required before coincidental agreement can be completely ruled out.

Somewhat related to the above discussion is the study of Shaw, presented in a rarely cited paper (reference 3.14) in which he develops an acoustic theory to explain vortex shedding characteristics. Briefly, it is based on the assumption that the flow about the cylinder is in acoustic vibration at a frequency determined by the perimeter of the cylinder. He shows reasonably good agreement with the Delany and Sorensen measurements for various cross-sectional shapes including the high Strouhal shedding frequencies in the supercritical Reynolds number range. However, in view of the fact that Shaw had to assume a harmonic mode for each case, and the fact that no independent critique of the basic concept appears to have been published, his results should not, at present, be considered as strong evidence in support of the high frequencies.

3.1.3 Effect of compressibility

Although data defining the effect of compressibility on the vortex shedding frequency over the Reynolds number range of interest in this paper is rather meager, it appears that some trends can be established as shown in figure 3.4. For comparison, the variation with Reynolds number for the incompresible case ($M<0.2$) is also shown. In the subcritical to

supercritical Reynolds number range, the incompressible wake measurements of Bearman (reference 3.37) are shown, and in the upper supercritical range, those of Delany and Sorensen. In the hypercritical range, the incompressible lift oscillation data of Jones et. al. were selected to provide consistency with their compressible flow data.

In the subcritical Reynolds number range, the compressible flow data of Naumann et. al. (reference 3.36) and of Murthy and Rose (reference 3.42) indicate the possibility of a slight reduction in Strouhal frequency with increasing Mach number. Once the critical Mach number is exceeded, the wake width tends to be fixed by shock-induced separation, and the Strouhal frequency remains at essentially the same value well into the Reynolds number range corresponding to that defined in incompressible flow as supercritical. This is shown by the shaded conjectural fairing in figure 3.4 based on the above mentioned data for a Mach number of approximately 0.45. This shock-induced separation precludes the wake narrowing that occurs with turbulent separation at subcritical Mach numbers, and therefore, the shedding frequency associated with shock-induced separation is essentially the same as with incompressible laminar separation. This, of course, results in a large effect of compressibility in the Reynolds number range, corresponding to the incompressible critical and lower supercritical ranges. In their study, Nauman et. al. observed that the shock waves alternated from one side of the cylinder to the other at the frequency of the vortex shedding.

In the upper supercritical range, a possible trend towards reduced vortex shedding frequency with increasing Mach number is observed by comparing the Delany and Sorensen data for $M<0.2$ with the conjectural band for $M=0.29$ developed from their data and the data of James et. al. In this shock-free subcritical Mach number range, the apparent reduction in frequency with increasing Mach number is probably associated with the increase in the adverse pressure gradient, due to compressibility, and the resulting increase in the vortex wake width, as discussed in section 1.1.3. It appears that in the wide-band random wake region increasing Mach number reduces the upper frequency level.

In the hypercritical Reynolds number range, the data point for $M=0.40$, obtained from Table IV of Jones et. al., indicates that the reduction in Strouhal frequency with increasing Mach number in the subsonic range extends into this Reynolds number range. However, as in the subcritical Reynolds number range, the effect of Mach number is considerably less than in the

critical and supercritical range. It should be noted that the data point presented for M=0.4 is that obtained by Jones et. al. in air with their data obtained in freon not being presented due to possible "real gas" effects for the high local Mach number conditions involved as discussed in section 1.1.3.

Data into the supercritical Mach number range is primarily limited to low Reynolds numbers with the data of Murthy and Rose (see reference 3.42) and Knowler and Pruden (see reference 3.28) indicating that between M=0.40 and M=0.80, the Strouhal frequency remains at about a constant value. In this regard, it is of interest to note that the extraction of the Strouhal frequency number from the vortex shedding patterns of three dimensional bodies of revolution at high angles of attack performed by Thomson and Morrison (see figure 15 of reference 3.39) using the impulse flow analogy also indicated little variation with crossflow Mach number below M=0.8 in the subcritical Reynolds number range.

In summary, it appears that for Mach numbers below about 0.80, the only major effects of compressibility occur in the critical and supercritical Reynolds number range where the narrow wake is progressively increased in width by the effect of compressibility on the adverse pressure gradient and separation point and finally by the shock-induced separation which occurs near the laminar separation point. For Reynolds numbers below and above this region, compressibility effects are minimized due to the similar location of the incompressible separation points and the shock-induced separation points.

For Mach numbers above 0.80 very little definitive information appears in the literature with regard to the vortex wake characteristics for cylinders in normal flow. It does appear, however, that above 0.90 no distinct vortex shedding frequencies have been observed in the wake (see reference 3.42 for example). Thomann (reference 3.34) suggests that supersonic flow stabilizes the separated shear layers. It might also be said that the fact that the wake boundaries converge rather rapidly behind cylinders at supersonic speeds may indicate that the lack of a distinct frequency might be analagous to the incompressible supercritical Reynolds number case with its narrow wake and no dominant vortex frequency.

With regard to the analysis of flow about three-dimensional bodies, the analysis of Thomson and Morrison (see figure 15 of reference 3.39), described earlier in the subsonic discussion is of considerable interest for transonic

and supersonic speeds. By using the impulse flow analogy to extract the Strouhal frequencies, they found a rapid increase of frequency with increasing Mach number for transonic and supersonic crossflows. Although no explanation was offered, it would appear that an increase in the Strouhal frequency number might be expected due to the reduced velocity behind the detached bow shock. Nevertheless, this is an area requiring further research which will be discussed in section 5 in connection with out-of-plane forces on three-dimensional bodies at high angles of attack.

3.2 Non-Circular Cylinders in Normal Flow

Vortex shedding frequency data for non-circular cylinders in flow normal to the cylinder axis is essentially limited to that of Delany and Sorensen (reference 3.30) and of Modi and Dikshit (reference 3.22). The former study covered a variety of cross-sectional shapes and in most cases included data through the critical range and into the low supercritical range. The latter study was limited to elliptical cross sections at subcritical conditions, and no further reference will be made to that study due to the emphasis in this paper on high Reynolds number.

A summary of the effect of cross-sectional shape on the vortex shedding frequency parameter for a series of shapes selected from the Delany and Sorensen study is presented in figure 3.5. In this figure, both the Strouhal number and the Reynolds number, R_w, are based on the maximum width, w, normal to the free stream velocity vector. Since Delany and Sorensen did not present results for the circular cylinder in the subcritical and critical range, the results of Bearman (reference 3.37) are utilized. The results indicate, as would be expected, that the effect of cross-sectional shape on the critical Reynolds number is consistent with that observed from the drag measurements (see section 1.2.1 and reference 3.30). Similarly, the effect of cross-sectional shape on the magnitude of the Strouhal number in the supercritical range follows the drag trends, with an increase in S accompanying a decrease in drag coefficient as might be expected from application of the "universal wake Strouhal frequency" concept described in the previous section. Unfortunately, no data appears to exist in the hypercritical range for non-circular cross sections. Likewise, no data appears to exist on the effects of compressibility for non-circular cross sections.

3.3 Cylinders in Oblique Flow

Available data on the vortex shedding frequencies of cylinders in oblique flow appears to be limited to the laminar separation case, well below the critical Reynolds number (see references 3.44 through 3.51). Of the above studies, Chiu and Lienhard (reference 3.47) have provided the most complete coverage of the flow incidence angle range and have shown that for the laminar separation case, the Strouhal vortex shedding frequency follows the independence principle rule which, in terms of angle of attack, α, (of interest for application to three-dimensional bodies of revolution), states that

$$S_\alpha = S_{\alpha=90^\circ} \sin \alpha ,$$

where S is based on free stream velocity and body diameter and sin accounts for the effect of angle of attack on the free-stream velocity component acting in the plane normal to the body axis.

Although no data appears to be available for the turbulent separation case of interest in this paper, it would be expected that the mutual influence of angle of attack and Reynolds number on the separation and wake characteristics, as in the case of the normal force, would play an important role in the effect of angle of attack on vortex shedding frequency. Research throughout the high Reynolds number range and for compressible flow is needed to identify such effects. This need appears to be particularly important with regard to vortex shedding and out-of-plane forces on three-dimensional bodies that will be discussed in section 5.

3.4 References

Selected Papers Related to Wake Structure

3.1 Strouhal, V.: Ueber eine besondere Art der Tonerregung, Widemann's Annalen der Physik und Chemie, Neue Folge, Band V, pp. 216-251, 1878.

3.2 Rayleigh, Lord: Acoustical Observations. II. Philosophical Magazine 5.5, Vol. 7, No. 42, March 1879.

3.3 Strutt, John Wiliam (Lord Rayleigh): Theory of Sound, Vol. II second edition, p. 413, 1896; reprinted by Dover Publications, NY.

3.4 Von Kármán, Th., Uber den Mechanismus des Widerstandes, den ein bewegter Körper in einer Flüssigkeit erfährt. Göttingen Nachrichten, math.-phys. Kl. 547 (1911).

3.5 Von Kármán, Th., Rubach, H.: Uber den Mechanismus des Flüssigkeitsund Luftwiderstandes. Phys. Z. 13, No. 2 (1912).

3.6 Föppl, Ludwig: Wirbelbewegung Hinter Einem Kreiszylinder. Sitzungsberichte der Mathematische-Physikalische Klasse der K.B. Akademie der Wissenschaften, Munich, Germany, Vol. 1, January-March, 1913, pp. 1-18.

3.7 Fage, A. and Johansen, F.C.: The Structure of Vortex Sheets. R. & M. No. 1143, British A.R.C., 1927; also Phil. Mag., ser. 7, vol. 5, no. 28, February 1928. pp. 417-441.

3.8 Fage, A.: The Air Flow Around a Circular Cylinder in the Region Where the Broundary Layer Separates from the Surface. R. & M. No. 1179, British A.R.C., 1928.

3.9 Fluid Motion Panel of the Aeronautical Research Committee and Others (S. Goldstein, ed.): Modern Developments in Fluid Dynamics. Vol. II. The Clarendon Press (Oxford), 1938.

3.10 Birkhoff, Garrett: Formation of Vortex Streets. Journal of Applied Physics, Vol. 24, No. 1, January 1953.

3.11 Roshko, A.: On the Development of Turbulent Wakes from Vortex Streets, NACA TN 2913, July 1953.

3.12 Roshko, A.: On the Drag and Shedding Frequency of Two-Dimensional Bluff Bodies, NACA TN 3169, July 1954.

3.13 Roshko, Anatol: On the Wake and Drag of Bluff Bodies. JAS, February 1955.

3.14 Shaw, R.A.: An Explanation of Vortex Shedding on the Basis of Pulses Travelling at the Speed of Sound. A.R.C. 18,455-F.M. 2406. 1st May 1956.

3.15 Roshko, A.: Experiments on the Flow Past a Circular Cylinder at Very High Reynolds Number. Journal of Fluid Mechanics. Vol. 10, pt. 3, 1961.

3.16 Bloor, M. Susan: The Transition to Turbulence in the Wake of a Circular Cylinder. Journal of Fluid Mechanics, Vol. 19, 1964.

3.17 Kronauer, R.F.: Predicting eddy frequency in separated wakes. Unpublished paper presented at the I.U.T.A.M. symposium on concentrated vortex motions in fluids. University of Michigan, Ann Arbor, MI, 6-11th July 1964.

3.18 Bloor, M.S. and Gerrard, J.H.: Measurements on Turbulent Vortices in a Cylinder Wake. Proceedings of the Royal Society of London, Ser. A., Vol.294, 1966, pp. 319-342.

3.19 Gerrard, J.H.: The mechanics of the formation region of vortices behind bluff bodies. J. Fluid Mech., Vol. 25, part 2, pp. 401-413, 1966.

3.20 Bearman, P.W.: On Vortex Street Wakes. J. Fluid Mech., Vol. 28, Pt. 4, pp. 625-641, 1967.

3.21 Berger, Eberhard and Wille, Rudolf: Periodic Flow Phenomena. Annual Review of Fluid Mechnics. Vol. 4, 1972.

3.22 Modi, V.J. and Dikshit, A.K.: Near-Wakes of Elliptic Cylinders in Subcritical Flow. AIAA Journal, Vol. 13, No. 4, April 1975.

3.23 Ericsson, L.E. and Reding, J.P.: Vortex-Induced Asymmetric Loads on Slender Vehicles. Rept. LMSC-D630807, Contract N60921-77C-0234, Lockheed Missiles & Space Co., Inc., Sunnyvale, CA, January 1979.

Reynolds Number and Mach Number Effects

3.24 Relf, E.F.: The Singing of Circular and Streamlined Wires. Aeronautical Research Com. R and M 825, 1921.

3.25 Relf, E.F. and Simmons, L.F.G.: The Frequency of Eddies Generated by the Motion of Circular Cylinders Through a Fluid, Aeronautical Research Com. R and M 917, 1924.

3.26 Tyler, E.: Vortex formation behind obstacles of various sections. Philosophical Magazine and Journal of Science, Ser. 7, 11 (1931), S. 849.

3.27 Blenk, H.; Fuchs, D.; Liebers, F.: Uber Messungen von Wirlbelfrequenzen, Luftahrtforschung 12 (1935), S. 38-41.

3.28 Knowler, A.E. and Pruden, F.W.: On the Drag of Circular Cylinders at High Speeds, R. & M. No. 1933, British A.R.C., 1944.

3.29 Koyasznay, L.S.G.: Hot-Wire Investigation of the Wake Behind Cylinders at Low Reynolds Numbers, Proc. Roy. Soc. (London) A, Vol. 198, p. 174, 1949.

3.30 Delany, N.K. and Sorensen, N.E.: Low-Speed Drag of Cylinders of Various Shapes, NACA TN 3038, 1953.

3.31 Drescher, H.: Messung der auf querangestromte Zylinder ausgeubten zeitlich veranderten Drucke, Z.F. Flugwiss 4, Heft 1/2, pp. 17-21, 1956.

3.32 Neely, K.K.; Etkin, B.; and Ribner, H.S.: 1958 Noise Research in Canada: Physical and Bio-acoustic Proc. 1st Int. Congr. Ar. Sci. Madrid (publ. by Pergamon Press, London, 1959).

3.33 Nakagawa, K.; Fujino, T.; Arita, Y.; Ogata, Y.; and Masaki, K.: An experimental investigation of aerodynamic instability of circular cylinders at supercritical Reynolds numbers. Proceedings of the 9th Japan National Congress for Appl. Mech., 1959.

3.34 Thomann, H.: Measurement of the Recovery Temperature in the Wake of a Cylinder and of a Wedge at Mach Numbers Between 0.5 and 3: Aeronautical Research Institute of Sweden Rep. 84, June 1959.

3.35 Fung, Y.C.: Fluctuating Lift and Drag Acting on a Cylinder in a Flow at Supercritical Reynolds Numbers. Journal of Aeronautical Sciences, November 1960.

3.36 Naumann, A.; Morsbach, M.; and Kramer, C.: The conditions of separation and vortex formation past cylinders. AGARD CP No. 4, 1966.

3.37 Bearman, B.W.: On vortex shedding from a circular cylinder in the critical Reynolds number regime. Journal of Fluid Mechanics, Vol. 37, pt. 3, pp. 577-585, 1969.

3.38 Jones, George W., Jr.; Cincotta, Joseph J.; and Walker, Robert W.: Aerodynamic Forces on a Stationary and Oscillating Circular Cylinder at High Reynolds Numbers. NASA TR R-300, 1969.

3.39 Thomson, K.D. and Morrison, D.F.: The Spacing, Position and Strength of Vortices in the Wake of Slender Cylindrical Bodies at Large Incidence, J. Fluid Mech., Vol. 50, Pt. 4, 1971, pp. 751-783.

3.40 Loiseau H. et Szechenyi, E.: Analyse expérimentale des portances sur un cylindre immobile soumis à un écoulement per pendiculaire à son axe à des nombres de Reynolds élevés. - Rech. Aerosp. n^0 1972-4, p. 279-291.

3.41 Loiseau, H. and Szechenyi, E.: Dynamic Lift on a Cylinder in High Reynolds Number Flow. IUTAM-IAHR, 1972.

3.42 Murthy, V.S. and Rose, W.C.: Form Drag, Skin Friction, and Vortex Shedding Frequencies for Subsonic and Transonic Crossflows on Circular Cylinder. AIAA Paper 77-687, Albuquerque, NM, June 27-29, 1977.

3.43 James W.D.; Paris, S.W.; and Malcolm, G.N.: Study of Viscous Crossflow Effects on Circular Cylinders at High Reynolds Numbers. AIAA Journal, December 1980, pp. 1066-1072.

Cylinders in Oblique Flow

3.44 Hanson, A.R.: Vortex Shedding from Yawed Cylinders, AIAA Journal, Vol. 4, No. 4, April 1966, p. 738.

3.45 Chiu, S.W.: The Boundary Layer Formation and Vortex Shedding on Yawed Cylinders, Washington State University, College of Engineering Bulletin 299, 1966.

3.46 Surry, J. and Surry D.: The Effect of Inclination on the Strouhal Number and Other Wake Properties of Circular Cylinders at Subcritical Reynolds Number, University of Toronto Institute for Aerospace Studies Tech. Note No. 116, August 1967.

3.47 Chiu, W.S. and Lienhard, J.H.: On Real Fluid Flow Over Yawed Circular Cylinders, Journal of Basic Engineering, Trans. ASME, Series D, Vol. 89, No. 4, December 1967, pp. 851-857.

3.48 Roshko, A.: Discussion to "On Real Fluid Flow Over Yawed Circular Cylinders," Journal of Basic Engineering, Trans. ASME, Series D, Vol. 91, No. 1, March 1969, p. 132.

3.49 Van Atta, C.W.: Experiments in Vortex Shedding from Yawed Circular Cylinders. AIAA Journal, Vol. 6, No. 5, May 1968, pp. 931-933.

3.50 Smith, R.A.; Moon, W.T.; and Kao, T.W.: Experiments on Flow About a Yawed Circular Cylinder. Journal of Basic Engineering, December 1971.

3.51 King, R.: Vortex Excited Oscillations of Yawed Circular Cylinders. Journal of Fluid Engineering, September 1977.

Some Additional Papers

3.52 Bouard, Roger and Coutanceau, Madeleine: The Early Stage of Development of the Wake Behind an Impulsively Started Cylinder for $40<R_e<10^4$. Journal of Fluid Mechanics, 1980, Vol. 101, Part 3, pp. 583-607.

3.53 Loc, T.P.; Daube, O.; Monnet, P.; and Coutanceau, M.: A Comparison of Numerical Simulation and Experimental Visualization of the Early Stage of the Flow Generated by an Impulsively Started Elliptic Cylinder. Numerical Methods in Laminar and Turublent Flow. Proceedings of the Third International Conference held in Seattle, WA, August 8-11, 1983.

3.54 Schewe, Gunter: On the force fluctuations acting on a circular cylinder in crossflow from subcritical up to transcritical Reynolds numbers, Journal of Fluid Mechanics, Vol. 133, 1983.

4. FORCES ON THREE-DIMENSIONAL BODIES

4.1 Bodies of Revolution

4.1.1 Flow regimes

With modern tactical aircraft and missiles encountering high angles of attack throughout much of their flight envelopes, the aerodynamic characteristics of the fuselage often play a dominant role in the flight behavior of the vehicle. Throughout a large portion of the angle of attack range, the flow about fuselage-type bodies is dominated by separation-induced vortex flows as illustrated by figure 4.1 (adapted from reference 4.42). Figure 4.1 illustrates the general trend of the boundaries separating the various flow regimes as a function of angle of attack and length along the body for ogive-cylinder types of bodies. In the low angle of attack range, and as long as the flow remains attached, a vortex-free flow exists over the length of the body, and the normal force (which is confined to the ogive) increases linearly with angle of attack. At an angle of attack of about 6° to 8°, the crossflow about the body begins to separate over the aft portion creating a pair of symmetrical, counter-rotating vortices fed by vortex sheets originating along the boundary layer separation lines on the cylinder. As the angle of attack increases further, the separation lines move toward the windward side of the body until the vortices completely dominate the lee-side flow. In this symmetric vortex flow regime, the influence of the vortices causes the normal force to increase rapidly in a non-linear manner similar to the vortex lift generated by highly swept wings.

Above about 25°, the vortices over the aft portion become asymmetric and when the angle of attack typically reaches about 40°, the entire vortex flow is asymmetric and characterized by alternating pairs of asymmetrical vortices. In this steady, or at least quasi-steady, asymmetric vortex-flow regime, large "out-of-plane" side forces are generated, and the normal force no longer increases as rapidly. At even higher angles of attack, there is a transition into the unsteady wake-type flow characteristic of cylinders normal to the flow. The "out-of-plane" side forces will be discussed in section 5.

Since the flows described above are generated by boundary layer separation, they are influenced considerably by Reynolds number, compressibility, and cross-sectional shape. While a rather large mass of data exists for subcritical Reynolds numbers, little is available in the supercritical regime and essentially none in the hypercritical range. The purpose of this section, therefore, is to present a reference list of those papers which deal with the higher Reynolds numbers and to use selected examples to illustrate some of the influences of supercritical Reynolds numbers as a possible aid in guiding research programs to be carried out in the new high Reyonlds number wind tunnels. First, however, some of the early investigations of the vortex flow on bodies of revolution will be reviewed briefly.

Much of the early research on bodies of revolution at angle of attack was related to the aerodynamic characteristics of airship hulls, and the "airship theory" developed by Munk (reference 4.1), published in 1924, is generally recognized as the key development in understanding the flow about bodies of revolution and the fundamental basis for the various slender body and slender wing theories subsequently developed for both attached and separated flows. Using a potential flow impulse analogy, he demonstrated that at angle of attack, the closed bodies of interest for airship hulls developed positive lift ahead of the maximum diameter and negative lift aft so that although there was no overall lift, there was an unstable pitching moment. However, even for the low angles of attack of interest at the time, some lift was developed which varied non-linearly with angle of attack, and Munk pointed out that this effect was associated with the fact that free vortices are created near the rear of the body in real viscous flow so that instead of a negative lift, a positive lift is produced over the aft portion.

The first detailed study of the flow field associated with these vortices appears to be that carried out by Harrington and reported in 1935 (reference 4.2). However, little progress was made in developing methods that predicted the nonlinear lift, particularly for high angles until the late 1940's. With the growing interest in maneuverable missiles and the lengthening of fuselage forebodies as a result, in part, of engines being located in the rear of jet fighter aircraft, the high angle of attack characteristics of bodies were rapidly becoming more important.

The first successful approach to the above problem was developed by Allen and published in 1949 (reference 4.3). In his approach, the development of the viscous crossflow along the length of the body was related to the time-dependent viscous flow past a two-dimensional cylinder started impulsively into motion with a velocity equal to Vsin . In this "impulse flow analogy" distance from the nose of the body is related to the time from the start of the cylinder motion.

Referring again to figure 4.1, the four flow regimes for the three-dimensional bodies, starting at zero angle of attack, correspond in general terms to the following stages of the impulsively-started cylinder flow: (1) the completely attached flow, (2) the formation of two counter rotating symmetrical vortices, (3) the asymmetric displacement of the two vortices, and (4) the formation of an alternating "street" of shed vortices.

To simplify the application, the variation of the cylinder drag during the early stages of the motion was ignored and steady state crossflow drag coefficients were applied along the body. The approach, known as the Allen "crossflow theory," was extensively evaluated by Allen and Perkins (reference 4.4), who also studies the vortex flow fields. Some pressure distribution and flow field studies have been selected and are listed as references 4.5 through 4.12.

The work of Allen and Perkins formed the basis for many of the semi-empirical methods developed since that time. While it is not the purpose of this paper to evaluate the various prediction methods, a list of some selected papers is included as references 4.13 through 4.27 for those interested in details of the various refinements to the basic method.

Progress is, of course, being made with methods that take advantage of the rapid development of high speed computers to model the actual three-dimensional viscous flow. However, the current inadequacy of transitional and turbulent boundary-layer flow modeling and high computer costs has generally limited the application of these approaches to Reynolds numbers below those in the critical range, and no references to these studies will be made.

4.1.2 Effects of angle of attack

While a great mass of experimental data on the aerodynamic characteristics of bodies of revolution for a wide range of Mach numbers

appears in the literature, there appears to be few studies covering both a large angle of attack range and the subcritical, critical, and supercritical Reynolds number ranges. One of the most complete studies covering these conditions appears to be that of Hartman (reference 4.40), and some of his results are presented in figure 4.2 for a high-fineness ratio, ogive-cylinder body at a Mach number of 0.5. The ogive has a fineness ratio of 3 and the cylinder a fineness ratio of 16. The results are presented in the form of total body normal force coefficient C_N (based on free-stream conditions and base area) as a function of Reynolds number based on free-stream velocity and the diameter of the cylindrical part of the body. Due to the possibly large sting support interference mentioned by Hartmann, his data presented here is limited to an angle of attack of 60^o.

The data presented in figure 4.2 illustrates the large reduction in critical Reynolds number (when based on diameter) with decreasing angle of attack. This is associated with the increasing streamline length as discussed previously in connection with two-dimensional oblique cylinders in incompressible flow (see section 2). However, for the case shown, the free-stream Mach number is constant (M=0.5), and since the crossflow Mach number varies from approximately 0.17 to 0.43 over the angle of attack range presented, some compressibility effects would be expected in the upper range, as discussed in section 1.1.3. Unfortunately, as indicated in section 1.1.3, two-dimensional compressibility effects in the critical Reynolds number range are not well enough defined to accurately apply them to the angle of attack case. Nevertheless, in an attempt to show at least qualitatively how changes in streamline length caused by changes in angle of attack can effect the boundary-layer separation, boundaries based on the "effective" Reynolds number concept discussed in section 2 are presented in figure 4.2. The boundary defining the beginning of the critical range has been approximated by $R = 4x10^5/K_\alpha$ and that defining the beginning of the supercritical range by $6.5x10^5/K_\alpha$. Since, as mentioned above, no attempt has been made to account for the moderate changes in the compressibility effects due to angle of attack, the constants in the above approximations for the boundaries have been selected to provide a reasonable match with the data for the intermediate angle of attack of 40^o. The variation of K_α (the ratio of the effective Reynolds number to the diameter Reynolds number) with angle of attack is presented in the table in section 2.2. In general, these boundaries appear to be reasonably consistent with the data, although the

data is not sufficient to define the supercritical regime at the high angles of attack. In addition to the basic angle of attack effect, the expected effect of compressibility in delaying the beginning of the critical Reynolds number range appears to be in evidence at 60^{o} angle of attack where the crossflow Mach number has reached 0.43.

Another point of interest illustrated by figure 4.2 is that for a constant Reynolds number, R_D, of about 3.5×10^5 all three flow regimes are encountered - the supercritical, critical, and subcritical - as the angle of attack is increased from 20^{o} to 60^{o}. The corresponding changes in the separation lines associated with the changes in effective Reynolds number increase the nonlinear behavior of the normal force above that associated with the increase due to the increase in crossflow dynamic pressure.

To provide some indication of the variation in the upper supercritical Reynolds number range, data for an angle of attack of 30^{o}, (from Foley's study, reference 4.34) is presented by the "flagged" symbols in figure 4.2.[1] Since Foley's data was obtained with a fineness ratio 7 cylindrical afterbody, the data has been adjusted to approximate a fineness ratio of 16 afterbody by increasing that part of the normal force acting on the afterbody (using slender-body theory to subtract the nose force) by the ratio of the fineness ratios. Despite the simplicity of the above adjustment, the resulting data appears to provide a reasonable extrapolation of Hartmann's data. For reference, the approximate boundary between the supercritical and hypercritical Reynolds number regimes, based on $6 \times 10^6 / K_\alpha$, is shown.

The overall results shown in figure 4.2 appear to reflect the general effects of Reynolds number anticipated from the two-dimensional oblique cylinder results described in section 2.2, although the level of the normal force in the upper supercritical region is somewhat higher than would be expected. This may be due to the fact that the method used to adjust Foley's data to approximate a fineness ratio of 16 may not properly adjust the contribution associated with the vortex flow. From the literature search, it appears that an experimental study covering the complete supercritical range and extending well into the hypercritical would be highly desirable.

---

[1] Foley's uncorrected data is used since for this high angle condition, where stable vortex flow exists, it would appear that a correction based on asymmetries observed near zero angle of attack would not be applicable.

With regard to compressibility effects, it must be kept in mind that a more accurate estimate of the boundaries, using the Esch factor, requires well-defined compressible flow data for the two-dimensional cylinder case that would allow the effect of the normal component of Mach number to be included.

Further illustrations of the significance of the flow regime encountered by slender bodies of revolution over the angle of attack and Reynolds number ranges are described with the aid of figures 4.3 and 4.4. In figure 4.3, the normal force data of figure 4.2 has been converted to the normal force coefficient on the cylindrical section based on planform area and crossflow dynamic pressure, $C_{N'_{cyl}}/\sin^2\alpha$, and presented as a function of the effective Reynolds number, R_{eff}, which is equal to $R_D K_\alpha$. This provides a convenient way to relate the normal force to the drag of a two-dimensional cylinder in flow normal to its axis which is representative of the 90° angle of attack case. The normal force on the cylindrical section was extracted by assuming that the force on the expanding nose section was essentially equal to the inviscid value, $\sin 2\alpha \cos \frac{\alpha}{2}$ (based on maximum cross-sectional area) and subtracting it from the total. The results presented for angles of attack of 20° and 30° are seen to agree reasonably well in the critical Reynolds number range, indicating that the effective Reynolds number factor, K_α, provides a reasonable means of assuring similar boundary layer conditions. The data from Tinling and Allen (reference 4.29), denoted by the flagged symbols, and extend the $\alpha=20^\circ$ data into the upper supercritical region.

In the supercritical region, the data for the two angles of attack do not collapse as well, due possibly to compressibility effects. In this regard, the data obtained by Hartmann at the higher angles of attack are not presented because the normal component of Mach number for those cases were in the region where compressibility effects are known to be important.

The drag coefficient variation for a circular cylinder normal to the flow, taken from figure 1.2, is also shown in figure 4.3. This provides an indication of the normal force parameter values that would be expected for the cylindrical portion of the three-dimensional body at $\alpha=90^\circ$ where an unsteady wake-type flow exists. Comparison of this curve with those for the lower angles of attack provides an indication of the effects of the stable vortex flow which characterizes the moderate angle of attack range. For subcritical Reynolds numbers, the comparison appears to indicate that, consistent with the results of section 2.2 for oblique two-dimensional

cylinders, the effect of angle of attack is relatively small. This is also consistent with the impulse flow analogy as can be shown by application of Sarpkaya's measured, time-dependent, impulsive flow drag for a two-dimensional cylinder in normal flow at subcritical Reynolds numbers (reference 4.17).

Unfortunately, no impulsive flow drag data is available for the other Reynolds number regimes. However, the large increase in $C_N'/\sin^2\alpha$ for $\alpha=20^o$ $\alpha=30^o$, relative to $\alpha=90^o$, seen in figure 4.3 in the supercritical range is consistent with the oblique cylinder results described in section 2.2. Some insight into the phenomena can be obtained from figure 4.4 where pressure distribution data, in the form of $C_p/\sin^2\alpha$, is compared for a two-dimensional case and a three-dimensional case for supercritical Reynolds numbers. Both sets of data are for an effective Reynolds number of about 0.88×10^6 with the three-dimensional body data being taken from Tinling and Allen's study (reference 4.29) and the two-dimensional cylinder data taken from Bursnall and Loftin (reference 2.7). Excellent agreement is seen on the windward half of the body. However, on the leeward half of the body, it appears that the vortex flow restricts the aft movement of the separation line, as well as inducing suction forces on the leeward portion of the body.

4.1.3 Compressibility effects

An extensive study of the effects of compressibility over a broad range of Reynolds numbers has been reported by Foley in reference 4.34. The effects of Mach number and Reynolds number on normal force coefficient for the body at an angle of attack of 30^o, taken from the above study, are presented in figure 4.5. The free stream Mach numbers range from 0.40 to 2.0, while the normal component of Mach number, $M \sin\alpha$, varies from 0.20 to 1.0. As in figure 4.2, the normal force coefficient is based, in the conventional manner for bodies alone, on the base area. Thus, because of the lower fineness ratio and moderate angle of attack (relative to figure 4.2), the coefficient level is greatly reduced and a different scale is selected to better illustrate the compressibility effects.

The general trends of the compressibility effects on this three-dimensional body at 30^o angle of attack are the same as those observed in the drag data for two-dimensional cylinders normal to the flow (see section 1.1.3). However, the magnitude of the forces illustrate the effect of the stable vortex flow that occurs on the three-dimensional bodies. Sizable

compressibility effects are observed, even in the subcritical crossflow Mach number range. Also, the large increase in normal force that occurs above a crossflow Mach number of 0.4, accompanied by a decrease in Reynolds number effect, is consistent with the shock induced separation conditions observed in the two-dimensional flow.

Again it appears that the research needs to be extended into the hypercritical Reynolds number range. A useful contribution would be to develop accurate Euler solutions for the inviscid shock induced separation case that would provide an asymptote for the very high Reynolds number conditions. Such solutions would provide useful information regarding the need for additional experiments to extend the shock boundary layer interaction results to higher Reynolds numbers.

Additional papers containing the effects of Reynolds number and Mach number on the aerodynamic characteristics of bodies of revolution can be found in the reference lists of both this section and section 5.

4.2 Bodies of Non-Circular Cross Section

4.2.1 Normal force characteristics

The cross sections of fuselages often depart from circles, and an example of the important effects of these shapes on the normal force is shown in figure 4.6, which is based on data obtained on fuselages similar to the space shuttle orbiter and reported by Brownson et. al. in reference 4.31. The data is for an angle of attack of 60^{o} and covers a range of windward corner radii for cross sections of modified rectangular shapes. The Mach number has been limited to values less than 0.2 to minimize compressibility effects. The normal force coefficient C_{N}' is based on the projected plan area of the fuselages, and the Reynolds number is based on the maximum width, W, which is more closely related to the boundary layer development ahead of the corner than is the body depth. The radius parameter, $r/_{W}$, covers the range from 0 to .086. In the subcritical range, it will be noted that only small increases in radius produce large normal force reductions relative to the sharp corner case. The corresponding decrease in critical Reynolds number, analagous to that encountered in two-dimensional flow (see section 1.2.1), emphasizes the importance of high Reynolds-number testing when investigating the implications of windward corner shape. The effects of

corner shape are of particular importance with regard to the local normal force and its impact on pitching moment.

Some effects of angle of attack and Mach number for the same shuttle type fuselage are presented in figures 4.7 and 4.8, which show data taken from the summary paper by Jorgensen and Brownson (reference 4.35). For these comparisons, the fuselage having $r/_W$=.063 has been selected. Figure 4.7 presents the data for a Mach number of 0.3 in the form of $C_N'/\sin^2\alpha$ as a function of an effective Reynolds number. In selecting the effective Reynolds number factor, it appeared probable that due to the reduced lateral perturbations, the streamline lengths would increase more rapidly with decreasing angle of attack for this flat bottom fuselage than for the circular fuselages. Therefore, instead of using K_α (section 2.2), the factor $1/\sin\alpha$ was used and as shown in figure 4.7, was found to collapse the data for angles of attack from 35^o to 50^o as well as could be expected using this simplified approach to the three-dimensional boundary layer development. For this angle of attack range, the normal component of Mach number, M $\sin\alpha$ is less than 0.23, so that the data is assumed to be reasonably free of compressibility effects. For the angle of attack of 70^o where the value of M $\sin\alpha$ has reached 0.28, there appears to be a consistent effect that may be attributed to compressibility promoting a more forward separation line in the vicinity of the small-radius corner with its steep adverse pressure gradient.

Regarding the effective Reynolds number factor selection, it should be noted that Esch (reference 4.38) selected $1/\sin^2\alpha$ and found a reasonably good correlation over the complete angle of attack range. However, the present author believes that the larger factor required in Esch's analysis is due to the probable mixture of subcritical and supercritical Mach numbers encountered in the high angle of attack range for the data he used.

To further illustrate the effects of compressibility, figure 4.8 presents the normal force parameter, $C_N'/\sin^2\alpha$ as a function of $R_W/\sin\alpha$ for free-stream Mach numbers of 0.2, 0.6, and 0.9, for angles of attack of 40^o and 70^o. For convenience in relating compressibility effects for the two angles of attack, the normal component of Mach number, M $\sin\alpha$, is also shown. The most prominent effect shown is the much greater influence of compressibility at the angle of attack of 40^o, where vortex flow would be expected, than at 70^o, where turbulent wake flow is expected. This difference in compressibility effect is particularly noteworthy in view of

the considerably lower levels of the normal component of Mach number for the 40^{o} angle of attack case. The fact that the vortex-induced force begins to increase at a relatively low value of $M \sin\alpha$ is presumed to be associated with the high velocity at the separation line for the small corner radius. For both angles of attack, the reduction in Reynolds number effects is observed for Mach numbers where shock induced separation would be expected.

In general, the primary importance of the fuselage normal force variation with Reynolds number is, of course, the contribution it makes to the aircraft pitching moment. An example of the effect of Reynolds number on the pitching moment of a forward-swept wing aircraft configuration at low speeds and an angle of attack of 80^{o}, taken from unpublished data obtained at NASA's Ames Research Center is presented in figure 4.9. In view of the long fuselage forebody, and the fact that the remainder of the fuselage is "blanketed" by the canard and wing, it is to be expected that the major effect of Reynolds number would be associated with the fuselage forebody. It is seen that as the Reynolds number increases, there is a large negative shift of the pitching moment consistent with the expected reduction in forebody normal force as the crossflow attaches further around the forebody. Such effects are important with regard to stall-spin characteristics, and some related data on this configuration can be found in reference 4.61.

The results presented in figure 4.9 are for cross sections with rather generous radii on the bottom corners; for smaller radii the critical Reynolds number would, of course, be higher, as indicated in figure 4.6.

The above results tend to emphasize the importance of simulating both the Mach number and the Reynolds number of the flight conditions in question, even for relatively low Mach number conditions, for these types of body cross sections. The new cryogenic wind tunnels offer important increased capability to accomplish this well into the hypercritical Reynolds number range where no data exists at present.

4.2.2 Side force characteristics

One of the most pronounced effects of non-circular bodies is the side forces they develop, particularly when the sideslip is combined with the high angles of attack encountered in maneuvers. For tactical aircraft, the major effects are usually confined to the fuselage forebody ahead of the wing and

the resulting side forces often produce yawing moments of magnitudes such that the complete aircraft can become statically unstable.

Section 1.2.2 demonstrated the importance of Reynolds number on the side forces developed on various two-dimensional non-circular cylinders with axes normal to the flow and at roll angles representing various combinations of angle of attack and sideslip. The implications of these side forces with regard to three-dimensional bodies were briefly discussed. Also discussed were some of the early aircraft configuration studies of non-circular fuselages which demonstrated the need for two- and three-dimensional research, and the reader is referred to section 1.2.2 for this background and associated references.

This section briefly describes some Reynolds number studies carried out on three-dimensional bodies in the high angle of attack range. Extensive studies on three-dimensional bodies having non-circular cross sections have been performed by Clarkson et. al. (reference 4.43) over an angle of attack range from 55° to 90°, and a portion of their results are presented in figure 4.10. The side force coefficient, $C_{Y'}$, acting on the forward portion of the fuselage is presented as a function of R_W for a constant flow incidence angle in the body crossflow plane of $\phi=+10^{\circ}$ (obtained by static roll angle) for various angles of attack. The angle ϕ represents the resultant flow angle in the crossflow plane for various combinations of angle of attack and sideslip.

The fuselage cross section was a square with rounded corners having non-dimensional radii of $\frac{r}{w}=0.245$ which is identical to one of the two-dimensional cylinders discussed in section 1.2.2. For angles of attack of 75 and 90° the resulting side force coefficients, based on side area, are quite similar to the two-dimensional results presented in figure 1.11, and illustrate the change in direction of the side force between subcritical and supercritical Reynolds number conditions as the flow attaches around the left front corner (see section A-A of figure 4.10). Inasmuch as a positive value of corresponds to a positive sideslip angle, it is seen that the nose portion would contribute a restoring moment at subcritical Reynolds numbers and diverging moment at supercritical Reynolds numbers. For configurations where the wing obstructs the crossflow aft of the nose, such effects as shown in figure 4.10 can have a profound effect on directional stability, and even more important, at these high angles of attack, on damping of the flat spin mode (to be shown later).

For the angles of attack of 45^{o} and 60^{o}, large Reynolds number effects still occur but are seen to have somewhat opposite trends. It would appear that this change is associated with the change from a disorganized wake type flow to the organized vortex type flow discussed in connection with circular bodies. For example, at the lower angles of attack, a strong vortex would be expected to form and be fed by the separation at the left front corner, in the cross-sectional view of figure 4.10, which produces suction forces accompanied by circulation changes such that the resulting force is opposite that at the higher angles of attack. At higher Reynolds numbers where the flow remains attached further around the corner, the vortex strength is reduced and a reduction in side force occurs.

An example of the Reynolds number sensitivity of space shuttle orbiter type bodies at high angles of attack combined with sideslip is presented in figure 4.11, from the study by Brownson et. al. (reference 4.31). Again, the side force coefficient, $C_{Y'}$, is presented as a function of the Reynolds number based on the maximum width of the body. The angle of attack is 60^{o}, the flow incidence angle, ϕ, is 10^{o}, and the non-dimensional corner radii r/w, is 0.086. Also shown is the corresponding data from the two-dimensional cylinder study, reviewed in section 1.2.2, for the square cylinder having non-dimensional corner radii r/w of 0.080. The two-dimensional side force has been adjusted to the condition of $\alpha=60^{o}$ by reducing its magnitude by $\sin^{2}\alpha$ to account for the reduced crossflow dynamic pressure. Since the effective Reynolds number for the $\alpha=60^{o}$ case is higher than for the $\alpha=90^{o}$ case, the Reynolds numbers for the two-dimensional data have been reduced for purposes of comparison. It should be noted, however, that instead of the K_{α} term presented in section 2.2 for circular bodies, the factor $\sin\alpha$ has been used as discussed in section 4.2.1. Although such corrections are very approximate, and changes in the lee-side flow can occur that are not accounted for, the two sets of data demonstrate the same trend of side force with Reynolds number.

The major consequence of the above side force characteristics is usually, of course, its effect on the vehicle's directional stability. An example of such an effect of Reynolds number on the directional stability, $C_{n_{\beta}}$, is presented in figure 4.12 for the complete configuration of the space shuttle orbiter. This data is for an angle of attack of approximately 20^{o} and was taken from the paper by Bornemann et. al. (reference 4.41). The data

points represent static directional stability measurements made in various wind tunnels with several models which resulted in a variety of stability levels. However, when the data was plotted as a function of the Reynolds numbers associated with the various size models and tunnel pressures, the trend illustrated in figure 4.12 emerged. The results indicate that while the configuration is stable at low Reynolds numbers, it becomes unstable at high Reynolds numbers. This again illustrates the importance, particularly for non-circular forebodies, of testing at sufficiently high Reynolds numbers to assure separation characteristics similar to the full scale vehicle, or of developing accurate transition-control techniques. It will be noted that the change in directional stability is consistent with the side force results presented in the previous figure, for a body alone having a cross section similar to the shuttle oribter nose. Although the body alone data was for a much higher angle of attack, it appears possible that with the upwash from the wing increasing the local angle of attack at the nose section, side force variations similar to those of the previous figure could be developed on the nose, and that they would provide the observed trend in directional stability. The long moment arm from the center of gravity amplifies, of course, the effect of the side force developed on the nose. It should be pointed out that these results include any forces induced on the aft portion of the vehicle by the vortex flows generated by the forebody separations.

The new high Reynolds number facilities offer an opportunity to carry out a systematic study of this and other viscous dominated flows on the space shuttle orbiter and other configurations at, or near, full scale conditions.

4.2.3 Autorotation characteristics

Another consequence of the long fuselage forebodies ahead of the wing, which are characteristic of modern jet fighter-type aircraft, is the major role they can play in regards to the aircraft's spin characteristics. Prior to the evolution of these long forebodies, the fuelage's influence in spinning was usually small. However, in the mid-1950's, several aerodynamic research programs began to demonstrate not only the strong influence of the longer forebodies but the critical effects of their cross-sectional shape and of Reynolds number. The early portions of this research were influenced considerably by the discovery in the Langley spin tunnel that the model of the F8U aircraft experienced a flat fast spin. These programs included, in

addition to the spin tunnel studies, one-degree-of-freedom autorotation tests of the F8U in the flat spin mode over a range of Reynolds numbers and a fundamental study of the crossflow characteristics of a wide range of two-dimensional non-circular cylinders over a wide Reynolds number range. These latter two programs demonstrated the strong influence of cross-section shape and Reynolds number and the results relative to the F8U are briefly summarized with the aid of figure 4.13. From their two-dimensional cylinder research, Polhamus et. al. (reference 4.49) established a probable autorotation boundary for rectangular and square cross sections with rounded corners as a function of the Reynolds number (based on the corner radius and the ratio ot the corner radius to the width of the cross section) as shown in figure 4.13. In the same time period, Clarkson (reference 4.48) was carrying out the F8U autorotation tests in which he established a Reynolds number that separated autorotation from damping charcteristics for the fuselage forebody and his results, converted to the parameters described above, are also shown in figure 4.13. The lower Reynolds number of the boundary for the F8U cross section relative to the modified rectangular cross sections is probably due to a less adverse pressure gradient expected for the somewhat elliptical shape as well as three-dimensional relief. Both studies predicted the importance of Reynolds number which was substantiated by comparisons of the F8U spin tunnel results by Kliner et. al. (reference 4.44) and the full scale aircraft flight results by Alley (reference 4.45). These results also shown in figure 4.13, indicated that, in fact, the airplane was not susceptible to the flat spin observed in the spin tunnel.

As a result of the above studies, the current practice in the spin tunnel tests is to develop a forebody flow control device for each configuration to simulate high Reynolds number damping characteristics. This is accomplished through the aid of static tests carried out over a Reynolds number range in a conventional pressure tunnel as has been described by Chambers et. al. (reference 4.51). Some of the results of these static tests can be found in references 4.52 through 4.55. Although this approach has been fairly successful, uncertainties associated with the lack of rotary motion in the Reynolds number tests and possible incompatabilities between the flow control devices required for the yaw and pitch modes are causes for some concern.

Recently, Clarkson et. al. have established a general research program utilizing a one-degree-of-freedom rig similar to the earlier F8U rig, but with angle of attack variation capability. This program includes force and

moment data, detailed pressure distribution measurements, and surface flow visualization for a series of body shapes over a Reynolds number range. This technique should offer, in addition to the basic research results, an improved method of flow control development for use in improving simulation in low Reynolds number spin tunnels. An example of the side force (indicative of the damping or propelling moment) measured on this rig, over a range of Reynolds numbers is shown in figure 4.14 for a fuselage having a square cross section with non-dimensional corner radii, r/w, of 0.245 (see reference 4.56). Also shown is the side force measured on a two-dimensional cylinder of the same cross section for a flow incidence angle, ϕ, of 10^{o} (from figure 1.11). The corresponding helix angle for the rotational tests was 7.6^{o} and the strong similarity of the results is apparent. Both types of tests indicate a shift from a prospin condition at low Reynolds numbers to an antispin condition at higher Reynolds numbers as the flow attaches around the left front corner in the cross-section sketch. A detailed description of the flow is presented in section 1.2.2. Additional results from the spin rig can be found in references 4.56 through 4.58

As pointed out in section 1.2.2, cross-sectional shapes such as the modified squares might be expected to encounter additional Reynolds number effects in the higher ranges as the flow eventually closes more completely around the aft corners. Therefore, it would be advantageous to carry out tests similar to those described above in the new high Reynolds number tunnels and obtain actual full scale conditions.

4.3 References

Some Early Studies

4.1 Munk, Max M.: The Aerodynamic Forces on Airship Hulls. NACA rep. 184, 1924.

4.2 Harrington, R.P.: An Attack on the Origin of Lift of an Elongated Body. Daniel Guggenheim Airship Inst., Publication 2, 1935.

4.3 Allen, H. Julian: Estimation of the Forces and Moments Acting on Inclined Bodies of Revolution of High Fineness Ratio. NACA RM A9126, 1949.

4.4 Allen, H. Julian and Perkins, Edward W.: A Study of Effects of Viscosity on Flow Over Slender Inclined Bodies of Revolution. NACA Rep. 1048, 1951.

Some Selected Pressure and Flow Field Studies

4.5 Werle, H.: Separation on axisymmetrical bodies at low speed. Rech. Aero. 90:3-14, 1962.

4.6 Fiechter, M.: Wirbelsysteme Schlanker Rotationskorper, ISL 10/66 (1966).

4.7 Lamont, P.J. and Hunt, B.L.: Pressure and Force Distributions on a Sharp-Nosed Circular Cylinder at Large Angles of Inclination to a Uniform Subsonic Stream. Journal of Fluid Mechanics, 76, 3, 1976, pp. 519-559.

4.8 Yanta, W.J. and Wardlaw, A.B.: Laser Doppler Velocimeter Measurements of Leeward Flowfield on Slender Bodies at Large Angle-of-Angle. AIAA Paper 77-660, 1977.

4.9 Werle, H.: Tourbillons de corps fuseles aux incidences eleves. L'Aero. L'Astro., no. 79, 1979-6.

4.10 Owen, F.K. and Johnson, D.A.: Wake Vortex Measurements of an Ogive Cylinder at α=36 Degrees. Journal of Aircraft, September 1979, pp. 577-583.

4.11 Schwind, R.G. and Mullen, J.: Laser Velocimeter Measurements of Slender Body Wake Vortices. AIAA Paper 79-0302, 1979.

4.12 Wardlaw, A.B. and Yanta, W.J.: The Flow Field About and Forces on Slender Bodies at High Incidence. AIAA Paper 80-0184, 1980.

Some Prediction Methods

4.13 Hopkins, E.J.: A Semi-empirical Method for Calculating the Pitching Moment of Bodies of Revolution of Low Mach Numbers, NACA RM A51C14, 1951.

4.14 Hill, J.A.F.: A Non-Linear Theory of the Lift on Slender Bodies of Revolution, NavOrd Report 5338, Proceedings U.S. Navy Symposium on Aeroballistics, 1954.

4.15 Kelly, H.R.: The Estimation of Normal-Force, Drag, and Pitching-Moment Coefficients for Blunt-Based Bodies of Revolution at Large Angles of Attack, J. Aeron, Sci. Vol. 21,8 (1954), pp. 549-555.

4.16 Bryson, A.E.: Symmetric Separation on Circular Cylinders and Cones. Journal of Applied Mechanics, December 1959.

4.17 Sarpkaya, T.: Separated flow about lifting bodies and impulsive flow about cylinders. AIAA Journal, Vol. 4, No. 3, March 1966, p. 414.

4.18 Saffell, Bernard F., Jr.; Howard, Millard L.; and Brooks, Eugene N., Jr.: Method for Predicting the Static Aerodynamic Characteristics of Typical Missile Configurations for Angles of Attack to 180 Degrees. Rep. 3645, Naval Ship Research and Development Center, March 1971.

4.19 Thomson, K.D. and Morrison, D.F.: The spacing, position and strength of vortices in the wake of slender cylindrical bodies at large incidence. Journal of Fluid Mechanics, Vol. 50, Part 4, 1971, p. 751.

4.20 Angelucci, S.B.: A Multivortex Method for Axisymmetric Bodies at Angle of Attack. Journal Aircraft, Vol. 8, No. 12, December 1971, pp. 959-966.

4.21 Thomson, K.D.: The Estimation of Viscous Normal Force, Pitching Moment, Side Force, and Yawing Moment on Bodies of Revolution at Incidences up to 90^{o}. Australian Weapons Research Est., WRE-Rep. 782, 1972.

4.22 Jorgensen, Leland H.: Prediction of Static Aerodynamic Chracteristics for Space-Shuttle-Like and Other Bodies at Angles of Attack from 0^{o} to 180^{o}. NASA TN D-6996, 1973.

4.23 Wardlaw, A.G.: Prediction of normal force, pitching moment, and yawing on bodies of revolution on angles of attack up to 50 degrees using a concentrated vortex flow-field model, 1973, NOLTR 73-209.

4.24 Jorgensen, Leland H.: Estimation of Aerodynamics for Slender Bodies Alone and with Lifting Surfaces at α's from 0^{o} to 90^{o}. AIAA J., Vol. 11, no. 3, March 1973, pp. 409-412.

4.25 Jorgensen, Leland H.: A Method for Estimating Static Aerodynamic Characteristics for Slender Bodies of Circular and Non-circular Cross Section Alone and with Lifting Surfaces at Angles of Attack from 0^{o} to 90^{o}. NASA TN D-7228, 1973.

4.26 Jorgensen, Leland H.: Prediction of Static Aerodynamic Characteristics for Slender Bodies Alone and with Lifting Surfaces to Very High Angles of Attack. NASA TR R-474, 1977.

4.27 Baker, William B., Jr.: An Aerodynamic Coefficient Prediction Technique for Slender Bodies with Low Aspect Ratio Fins at Mach Numbers from 0.6 to 3.0 and Angles of Attack from 0 to 180 Degrees. AEDC-TR-77-97, Air Force Flight Dynamics Laboratory, Wright-Patterson Air Force Base, Ohio, March 1978.

Effects of Reynolds Number and Mach Number

4.28 Jorgensen, Leland H. and Treon, Stuart L.: Measured and Estimated Aerodynamic Characteristics for a Model of a Rocket Booster at Mach Numbers from 0.6 to 4 and at Angles of Attack from 0^{o} to 180^{o}. NASA TN X-580, 1961.

4.29 Tinling, Bruce E. and Allen, Clyde Q.: An Investigation of the Normal Force and Vortex-Wake Characteristics of an Ogive-Cylinder Body at Subsonic Speeds. NASA TN D-1297, April 1962.

4.30 Atraghji, E.G.: The Influence of Mach Number, Reynolds Number, Semi-Nose Angle and Roll Rate on the Development of the Forces and Moments over a Series of Long Slender Bodies of Revolution at Incidence. National Research Council of Canada, NAE 5 x 5/0020, March 1967.

4.31 Brownson, Jack J.; Graham, Ralph E.; and Banducci, David: Static Stability Characteristics of Manned Spacecraft Center Straight-Wing Space Shuttle Oribiter: Effect of Reynolds Number and Body Corner Radius at M<0.5. NASA TM X-62,054, 1971.

4.32 Brownson, Jack, J. and Whitnah, A.M: Static Stability Chracteristics of a Manned Spacecraft Center Straight-Wing Space Shuttle Orbiter: Effect of Reynolds Number and Body Corner Radius (M=0.6-1.35). NASA TM X-62,056, 1971.

4.33 Peterson, Victor L.; Katzen, Elliott D.; Axelson, John A.; Brownson, Jack J.; Cliffone, Donald L.; Cleary, Joseph W.; Intrieri, Peter F.; Malcolm, Gerald N.; and Mellenthin, Jack A.: Static and Dynamic Aerodynamics of Space Shuttle Vehicles. Presented at NASA Space Shuttle Technology Conference, March 2-4, 1971, pp. 311-373. NASA TM X-2272, 1971.

4.34 Foley, J.E.: Results of a Study of Mach Number and Reynolds Number on the Crossflow Drag Characteristics of Ogive-Cylinder and Ogive-Cylinder-Frustrum-Cylinders at Angles of Attack to 30 Degrees. NASA CR-61356, October 1971.

4.35 Jorgensen, Leland H. and Brownson, Jack J.: Effects of Reynolds Number and Body Corner Radius on Aerodynamic Characteristics of a Space Shuttle-Type Vehicle at Subsonic Mach Numbers. NASA TN D-6615, 1972.

4.36 Jorgensen, Leland H. and Nelson, Edgar R.: Experimental Aerodynamic Characteristics for a Cylindrical Body of Revolution with Various Noses at Angles of Attack from 0^{o} to 58^{o} and Mach Numbers from 0.6 to 2.0. NASA TM X-3128, 1974.

4.37 Jorgensen, Leland H. and Nelson, Edgar R.: Experimental Aerodynamic Characteristics for Bodies of Elliptic Cross Section at Angles of Attack from 0^{o} to 58^{o} and Mach Numbers from 0.6 to 2.0. NASA TM X-3129, 1975.

4.38 Esch, Helmut: The Influence of Reynolds Number on the Normal-Force Characteristic of Slender Cylindrical Bodies. ESA TT-170, 1975.

4.39 Johnson, J.D. and Winkler, G.W.: Force Tests of a 0.88 percent Scale 142-Inch Diameter Solid Rocket Booster (MSFC Model Number 461) in the NASA/MSFC High Reynolds Number Wind TUnnel (SA13F) NASA CR-144,617. May 1976.

4.40 Hartmann, Klaus: Ueber den Einfluss der Reynoldzahl auf die Normalkraefte schlanker Flugkoerperruempfe. Zeitschrift fur Flugwissenschaften und Weltraumforschung, Vol. 2, No. 1, 1978, pp. 22-35.

4.41 Bornemann, W.E. and Surber, T.E.: Aerodynamic Design of the Space Shuttle Orbiter. Paper 11, AGARD CP 247, 1979.

4.42 Chapman, G.T. and Keener, E.R.: The Aerodynamics of Bodies of Revolution at Angles of Attack to 90^{o}. AIAA Paper 79-0023.

4.43 Clarkson, M.H.; Malcolm, G.N.; and Brittain, V.A.: Aerodynamic Characteristics of Bodies with Non-circular Cross Sections at High Angles of Attack. AIAA Paper No. 82-0056, 1982.

Some Papers Related to Aircraft Spinning

4.44 Klinar, Walter J.; Lee, Henry A.; and Wilkes, Faye L.: Free-Spinning Tunnel Investigation of a 1/25-Scale Model of the Chance Vought XF8U-1 Airplane. NACA RM SL56L315, December 1956.

4.45 Alley, J.R.: Model XF8U-1/F8U-1 Airplane Part II Spin Demonstration Plus Additional Investigation and Demonstration of Spins with the Aileron Control Held Full Against the Spin - XF8U-1 Bureau No. 138900, Chance Vought Aircraft Rep. No. 10638, January 1957.

4.46 Neihouse, A.I.; Klinar, J.J.; and Scher, S.H.: Status of Spin Research for Recent Airplane Designs, NASA RM L57F12, August 1957.

4.47 Polhamus, E.C.: Effect of Flow Incidence and Reynolds Number on Low-Speed Aerodynamic Characteristics of Several Noncircular Cylinders with Applications to Directional Stability and Spinning, NACA TN 4176, January 1958.

4.48 Clarkson, M.H.: Autorotation of Fuselages. Aeronautical Engineering Review, Vol. 17 February 1958.

4.49 Polhamus, Edward C.; Geller, Edward W.; and Grunwald, Kalman J.: Pressure and Force Characteristics of Noncircular Cylinders as Affected by Reynolds Number with a Method Included for Determining the Potential Flow about Arbitrary Shapes. NASA TR R-46, 1959.

4.50 Clarkson, Mark H.; Malcolm, Gerald N.; and Chapman, Gary T.: Experimental Determination of Post-Stall Rotary Derivatives for Airplane-Like Configurations at Several Reynolds Numbers. AIAA Paper 75-171, AIAA 13th Aerospace Science Meeting, Pasadena, CA, January 20-22, 1975.

4.51 Chambers, Joseph R.; Bowman, James S., Jr.; and Malcolm, Gerald N.: Stall/Spin Test Techniques used by NASA. AGARD CP-199, 1975.

4.52 Kaufmann, Ronald C.; Scher, Stanley H.; and Cohen, Lee E.: Static Aerodynamic Characteristics of a 1/7-Scale Model of the F-5A Airplane at Angles of Attack from 0 to 90 Degrees and Angles of Sideslip from -10 to 30 Degrees for a Mach Number of 0.20. NASA TM X-62,339, April 1974.

4.53 Hedstrom, C. Ernest; Scher, Stanley H.; and Clasen, Daniel J.: Low-Speed Static Aerodynamic Characteristics of an 0.05-Scale Tail-Less Model of the A-10 Airplane at High Angles of Attack. NASA TM X-62,340, April 1974.

4.54 Petroff, Daniel N.; Scher, Stanley H.; and Sutton, Carl E.: Low Speed Aerodynamic Characteristics of a 0.08-Scale YF-17 Airplane Model at High Angles of Attack and Sideslip. NASA TM 78438, April 1978.

4.55 Keener, Earl R. and Howell, Michael H.: Static Aerodynamic Characteristics of a 1/9-Scale Model of the F-16 Airplane at Angles of Attack of $\pm 90^{\circ}$ and Angles of Sideslip of $\pm 30^{\circ}$ at a Mach number of 0.20. NASA TM 78435, September 1978.

4.56 Clarkson, M.H.; Malcolm, G.N.; and Chapman, G.T.: Experimental Post-stall Rotary Aerodynamic Coefficients for Airplane-Like Configurations. AIAA Journal, Vol. 13, No. 8, August 1976, pp. 565-570.

4.57 Malcolm, G.N. and Clarkson, M.H.: Wind Tunnel Testing with a Rotary-Balance Apparatus to Simulate Aircraft Spin Motions. Proceedings of AIAA 9th Aerodynamic Testing Conference, June 1976, pp. 143-146.

4.58 Malcolm, G.N.: New Rotation-Balance Apparatus for Measuring Airplane Spin Aerodynamics in the Wind Tunnel. J. of Aircraft, Vol. 16, No. 4, April 1979, pp. 264-268.

4.59 Lugt, Hans J.: Autorotation of an elliptic cylinder about an axis perpendicular to the flow. J. Fluid Mechanics (1980), Vol. 99, Part 4, pp. 817-840.

4.60 Yoshinaga, T.; Tate, A.; and Inove, K.: Approximate Calculation of Aerodynamic Coefficients for Rotating Slender Bodies at 90 Degrees Incidence. Journal of Spacecraft and Rockets, Vol. 19, No. 1, 1982.

4.61 Moore, M. and Frei, D.: X-29 Forward Swept Wing Aerodynamic Overview. AIAA Paper No. 83-1834, July 1983.

5. OUT-OF-PLANE FORCE

5.1 Background

5.1.1 Early studies

As the angle of attack of a body of revolution increases, the crossflow separation induced vortex pairs eventually become asymmetric even for the symmetric body at zero sideslip. This can result in a large out-of-plane side force producing a sudden and sometimes uncontrollable yawing moment. Some of the early studies are listed as references 5.1 through 5.12.

The first photographs of these asymmetric vortices to be published were those of Allen and Perkins in 1951 (reference 5.1). They pointed out that on long missiles at high angles of attack, "the discharge of a vortex street should promote asymmetry of forces on the tail surfaces and manifest itself as a tendency to unexpected and erratic rolling ..." The anticipated effect on long missiles with stabilizing fins was soon confirmed by wind tunnel tests as reported by Mead in early 1952 (reference 5.2) and in 1953 by Gowen (reference 5.3), who reported on vertical tail buffeting caused by asymmetric vortex flow.

With regard to forces and moments developed on the body itself, Allen and Perkins also suggested that "the aperiodic changes in the discharged street of vortices might induce, for a pitched body, undesirable forces and moments in yaw." In the latter part of 1952, Cooper et. al. published the results of a study at M=1.59 which demonstated the out-of-plane forces and moments anticipated by Allen and Perkins and, in addition, indicated the cyclic variation in local side force along the body length (reference 5.4). In 1953, Letko (reference 5.5) published the first low speed measurements of out-of-plane forces and moments on slender bodies at high angles of attack and demonstrated the effectiveness of a ring or other roughness at the nose in greatly reducing the undesirable yawing moments. Also in 1953, Perkins and Dennis (reference 5.6) established the angle of attack at which the asymmetric and unsteady vortex flow began to decrease with increasing nose fineness ratio, and then established a boundary relating these two parameters. A study of the yawing moment at zero sideslip was also made in connection with spin stabilized rockets by Dunn in 1954 (reference 5.9).

Some early work in England was reported by Fink in 1953 (reference 5.11) and by Maltby and Peckham in 1956 (reference 5.12). During this same period, studies established that, although the asymmetric vortex patterns were still present, the large out-of-plane forces and moments encountered at low speeds were essentially eliminated at supersonic speeds. Representative of this research are the papers published by Allen and Perkins (reference 5.1), Gowen and Perkins (reference 5.8), and Gapcynski (reference 5.10).

Thus, the general features of the asymmetric vortex flow, the resulting out-of-plane forces, the cyclic variation of local side force, and the importance of nose shape and Mach number had been uncovered by the mid 1950's. However detailed research, the development of prediction methods, and the search for practical methods of reducing the magnitude of the forces lagged during the next fifteen years because the aircraft and missiles of that time were not, in general, operating in the high angle of attack range. However, in the late 1960's and early 1970's, interest was renewed as new fighter aircraft designs began to penetrate the high angle of attack range during maneuvers. At the high angles of attack involved the large yawing moment which can result from the side force at zero sideslip can be a major contributor to the so-called "nose slice" or "yaw off" - a divergence in yaw resulting in an incipient departure. Providing adequate control power for these high angle of attack asymmetric flow conditions is a major problem for modern tactical aircraft that can encounter angles of attack approaching 60^{o} in combat maneuvers. This and other stability and control problems encountered in the design of modern fighter aircraft have recently been reviewed by Skow and Erickson (reference 5.20). Examples of review papers dealing with the fluid dynamic aspects of the asymmetric vortex flows and resulting out-of-plane forces are listed as references 5.13 through 5.22 with the recent paper by Hunt (reference 5.21) providing a summary of the overall subject.

With regard to basic data papers, the reference list has been restricted primarily to those that include studies of Reynolds number and/or Mach number effects in the subsonic and transonic range (consistent with the subject of the present paper). The large mass of low speed, subcritical Reynolds number data, as well as supersonic data, can be located within the reference lists of the cited papers.

Because of the many recent papers dealing with various aspects of this flow, and because of the overall summary by Hunt, the discussion in the

present paper will be limited primarily to certain effects of Reynolds number and a discussion of those areas where higher Reynolds number data might be needed.

Although the resulting yawing moments are generally more important to vehicle controllability, the side forces and their distributions have been selected as a more convenient means of discussing the general phenomena associated with asymmetric vortex flow.

5.1.2 Some general characteristics

A typical variation of the out-of-plane force with angle of attack for an ogive-cylinder configuration is shown in figure 5.1. At a moderate angle of attack, vortex flow develops but is initially symmetrical. At some higher angle of attack, the vortices become asymmetrical with the asymmetry either being initiated at the rear of a relatively long afterbody in accordance with the impulse flow analogy or at the apex of a slender, pointed nose. The side force resulting from the vortex asymmetry increases with angle of attack due primarily to the increase in the normal component of dynamic pressure. However, the corresponding increase in normal velocity increases the vortex shedding rate, resulting in a second pair of asymmetric vortices of opposite asymmetry, and the overall side force is reduced. Eventually, as the angle of attack increases further, the steady vortex flow transitions into the unsteady wake-type flow associated with cylinders normal to the flow, and the time-averaged side force returns to zero.

For aircraft-type bodies, it appears that since the wing generally blankets the flow over much of the fuselage, the onset of vortex asymmetry is associated with the apex of the nose, as mentioned above for short bodies. Keener and Chapman (reference 5.34) have proposed that since asymmetric vortex flows and the resulting rolling moments have been observed in tests of slender sharp-edge wings where the separation lines are fixed, asymmetry in separation lines on slender pointed bodies of revolution are not necessarily the cause of vortex asymmetry; instead it can result from a "hydrodynamic instability" of the vortices themselves. Woolard (reference 5.38) arrived at a similar conclusion by showing that the onset angles for slender wings and cones can be analytically related by a slender body mapping procedure. More recently, Dyer et. al. (reference 5.39) have shown, with an inviscid model of the flow about a slender cone, that asymmetrical vortices can form with the

separation lines disposed symmetrically. These and other papers related to hydrodynamic instability are listed as in references 5.29 through 5.40.

Figure 5.2 illustrates some of the evidence of "hydrodynamic instability" as a cause for vortex asymmetry. On the left are results of tests of slender delta wings that show the boundary between symmetric and asymmetric vortex flow in terms of α/δ, the ratio of angle of attack to semi-apex angle, versus the semi-apex angle. On the right are the results of the inviscid theory for cones in terms of α/δ versus the location of the assumed symmetrical separation lines. Experimental data for cones indicate the boundary occurs at a value of $\frac{\alpha}{\delta}$ of about 2.0, which is in reasonable agreement with the calculations of Dyer et. al. and about one-half of the value for the delta wings.

From these results and available experimental data, it appears that the onset angle of attack may not be critically dependent upon Reynolds number. However, as will be shown, the characteristics beyond onset are highly Reynolds number dependent.

5.2 Ogive-Cylinder at Constant α

The recent study by Lamont (reference 5.57) produced a rather complete set of data with regard to the detailed effects of Reynolds number on the out-of-plane force for an ogive-cylinder covering the subcritical, critical, and supercritical regimes. While only a portion of his study has been published to date, that which has been published provides considerable insight into the Reynolds number efects of interest in this paper. The variation of the maximum out-of-plane force, $C_{Y_{o\ max}}$, with Reynolds number, R_D, for an angle of attack of 40^o from Lamont's study is presented in figure 5.3. The model was a body of revolution having an ogive nose of 3.5 diameters in length and a cylindrical afterbody of 4.0 diameters in length of which 6 diameters from the apex were pressure instrumented. The model was rolled during the tests to assure that the maximum side force was obtained.

It will be noted that in preparing figure 5.3, this author utilized the actual sign of the side force rather than using the absolute value, $|C_{Y_{o\ max}}|$ presented by Lamont. The parameter, $|C_{Y_{o\ max}}|$, is often useful when comparing results from different models or different runs since the direction of the vortex asymmetry and the resulting side force sign are generally established by random disturbances in the wind tunnel or slight asymmetries

in nose shape. This method of presentation, however, obscures the changes in sign of the overall side force that are caused by changes in Reynolds number. These changes are sometimes encountered in the critical range and are believed to be associated with the change in vortex shedding frequency. The actual signs used in figure 5.3 were deduced from the longitudinal distributions of local side force.

In figure 5.3, it will be noted that $C_{Y_{o\ max}}$ decreases with increasing Reynolds number, reaching a value of zero at about $R_D=7x10^5$ and then changes sign. With further increases in Reynolds number, the sign again reverses, and at the highest supercritical Reynolds number tested, $R_D=4x10^6$, the out-of-plane force returns to a value similar to the subcritical value. While much of the reduction in the critical range can be attributed to the well-known reduction in vortex strength as the separation line moves aft, the change of sign appears to be associated with the change in period of the cyclic variation of local side force along the length of the body. This is illustrated in figure 5.3 by the small inset plots showing the measured longitudinal distributions of the local side force for three Reynolds numbers. It will be noted that near the peak negative value of out-of-plane force, the period of the cyclic variation has been reduced to about one-half of its subcritical value and the negative loop establishes the overall sign of the side force. In the upper supercritical Reynolds number range, the period returns to a value similar to the subcritical case, and a return to a positive value of side force coefficient results. The cyclic variation of side force along with body is, of course, associated with the alternating asymmetric vortex pairs resulting from periodic vortex shedding, and it can be shown by the impulsive flow analogy that the vortex spacing varies inversely as $S \tan\alpha$, where S is the Strouhal frequency for a two-dimensional cylinder normal to the flow (see reference 5.61) having the same separation line location. Although the analogy has been successfully demonstrated in the subcritical range (see reference 5.50, for example), no such analysis covering a wide range of Reynolds numbers in which the various flow regimes are encountered has been found in the literature. However, the detailed data set of Lamont's offers an opportunity to explore this aspect and the result of a preliminary attempt is illustrated in figure 5.4.

In figure 5.4, Lamont's local side force distributions along the body are presented for several Reynolds numbers on the left portion of the figure. The Reynolds numbers were selected such that they could be

reasonably characterized by the laminar, transitional, or fully turbulent separation boundaries identified by Lamount (see figure 2, reference 5.57). The corresponding two-dimensional Strouhal vortex shedding parameter, S, was then estimated from figure 3.2 of this paper. While the choice of a value for the shedding parameter was straightforward for the laminar and high Reynolds number turbulent cases, the values to use for the transitional and low Reynolds number turbulent cases were not so apparent because of the variation of the boundary-layer state along the length of the body. Consequently, for the purpose of this paper, the shedding frequency parameters for the latter two cases were chosen as those values appropriate for the longitudinal station at which the first peak in the side force distribution occurs. Consequently, using Bearman's data, a subcritical value of S equal to 0.20 was used for the laminar separation case, a value in the center of the critical range equal to 0.32 for the transitional case, and a value in the supercritical range of 0.46 for the low Reynolds number fully turbulent case. A value of 0.26 based on Roshko's data was used for the high Reynolds number fully turbulent case. It should be noted that Lamont's boundary layer states were used rather than R_D since it is difficult to relate the effective Reynolds number on the ogive to the two-dimensional case.

Using the values of S shown in the table, the ratio of c_y/c_n is plotted versus $\frac{X}{D}(S)\tan\alpha$ on the right portion of figure 5.4. The use of c_y/c_n is an attempt to reduce the effect of vortex strength variations with Reynolds number. While the amplitudes do not collapse, it is interesting to note that the periods, in terms of $\frac{X}{D}(S)\tan\alpha$ are essentially the same. From this it appears that the three-dimensional body data may support the suggestion made in section 3.1, that while the two-dimensional vortex shedding frequency content in the critical and most of the supercritical range is of the "wide-band random" type, the upper frequency level characterizes shedding from three-dimensional bodies at angles of attack where steady asymmetric vortex flow exists. This conclusion, however, must be considered as tentative since the above use of the impulse flow analogy is strictly applicable only for constant diameter bodies and the method of using the two-dimensional data of figure 3.2 could be questioned.

To further investigate the above observations, it would appear desirable to make pressure measurements on a high fineness ratio ogive cylinder in order to define the cyclic variations of the out-of-plane side force over the

constant diameter section in the supercritical and hypercritical Reynolds number ranges. The new high Reynolds number cryogenic tunnel offers the opportunity to accomplish this over a range of subsonic and transonic Mach numbers.

5.3 Isolated Ogive Forebodies

5.3.1 General characteristics

The above discussion dealt with the effect of Reynolds number on C_{Y_o} at a constant angle of attack. However, additional insight with regard to the effects of Reynolds number can be derived by examining how the first and second peaks in the cyclic variation of C_{Y_o} change with angle of attack. Inasmuch as the sense of the vortex asymmetry is random and dependent on disturbances associated with model imperfections, tunnel flow, etc., a sign convention has been adopted as an aid in clarifying trends. In this convention, all signs are reversed, when necessary, to provide a positive sign for the first peak in the subcritical Reynolds number range. An example of the effect of Reynolds number on these peak values is presented in figure 5.5 for a fineness ratio 5.0 tangent ogive forebody alone at M=0.25. The data illustrate the basic variation with angle of attack for a subcritical and supercritical Reynolds number as obtained from the data of Keener et. al. (figure 6 of reference 5.52) and defines the first and second peaks. For the subcritical Reynolds number case shown, as angle of attack increases it appears that two opposing effects occur that play dominant roles in the variation of the out-of-plane force with angle of attack. One effect is the increase in crossflow dynamic pressure, which is proportional to $\sin^2\alpha$, while the other is an increase in vortex shedding frequency which, according to the impulse flow analogy, is proportional to tan . The latter effect manifests itself. of course, as a reduced longitudinal spacing between the shed vortices (see reference 5.60, for example). In the angle of attack range where asymmetrical vortices first start to develop, the increasing crossflow dynamic pressure dominates and the out-of-plane force increases with angle of attack. However, the increase in vortex shedding frequency with increasing angle of attack compresses the cyclic variation of the out-of-plane force along the isolated forebody length and the resulting growth in the reversed force loop over the aft, larger diameter, portion of the forebody eventually

reverses the trend with angle of attack and for the case shown, the overall out-of-plane force is essentially zero when an angle of attack of about 65^{o} is reached, and at higher angles a two-dimensional wake type of flow develops.

In the critical and low supercritical Reynolds number range, the reduced vortex strength associated with the leeward movement of the separation lines tends to reduce the out-of-plane force. However, as illustrated by the supercritical case of figure 5.5, an additional effect combines with those described in the previous paragraph to further change the character of the variation with angle of attack. This effect is assumed to be an increase in vortex shedding frequency due to supercritical separation as discussed above in connection with figure 5.3. As a result of this additional increase in vortex shedding frequency and the associated further compression of the cyclic force variation, the counteracting reversed force loop becomes prominent at a lower angle of attack and above about 35^{o} completely dominates with the overall out-of-plane force changing sign and the maximum force now occurring at the peak of the resulting second force loop. It will be noted that this effect of Reynolds number is consistent with Lamont's results for a constant angle of attack of 40^{o} shown in figure 5.3.

To illustrate further the effect of Reynolds number on the peak out-of-plane forces, figure 5.6 presents the variation of the first and second peaks in the force variation as defined by figure 5.5. The variation of these two peaks with Reynolds number has been extracted from the angle of attack data of reference 5.52. Also shown, as a vertical band, is an indication of the critical Reynolds number as defined from the normal force data of reference 5.52. The results illustrate the decrease in the magnitude of the first peak with increasing Reynolds number and illustrate the reversed sign and magnitude increase for the second peak as Reynolds number is increased in the supercritical region. The large reduction of the first peak with increasing Reynolds number and the opposite sign and magnitude increase for the second peak with increasing Reynolds number appear consistent with the above discussion of the interacting effects of crossflow dynamic pressure and vortex shedding frequency. It is recognized, of course, that the details of these trends are modulated by the complicated interactions between the vortex flow, boundary layer state, and separation line variations over expanding bodies. For details of the boundary layer changes, the reader is referred to Lamont's recent paper (reference 5.57).

In view of the large variation in the magnitude of the second peak in the supercritical Reynolds number range and the fact that the two-dimensional studies described in section 3.1.1 suggest additional changes in the vortex shedding characteristics in the hypercritical range, research to higher Reynolds numbers appear desirable.

5.3.2 Effect of fineness ratio

The effect of fineness ratio on the C_{Y_o} variation with Reynolds number is illustrated in figure 5.7 which is based on the data of Keener et. al. (references 5.51 and 5.52). The data for the fineness ratio of 5.0 is the same as that presented in figure 5.6 except that, in the interest of clarity, the data for the first peak at supercritical Reynolds numbers is eliminated since the peak absolute values occurred at the second peak. In the subcritical range reducing the fineness ratio to 3.5 appears to have only minor effects implying that as a result of the low frequency of vortex shedding at subcritical Reynolds numbers, no appreciable reversed side force loop was developed on either body. Other effects such as differences in body side area, crossflow dynamic pressure, etc. can also contribute, however, and further study is required before a complete understanding can be attained. In the supercritical Reynolds number range, there is a well-established trend with the reduced fineness ratio body producing considerably less side force. Aside from the fact that the reversed side-force loop on the low fineness ratio body begins its growth at a higher angle of attack, possibly limiting the growth, it is again not clear how much of a role the aforementioned factors play in this effect.

5.3.3 Effect of cross section

Although in general, the forebodies of aircraft fuselages are not axisymmetric or even composed of sheared circular cross sections, research relative to the out-of-plane force has been devoted almost entirely to the axisymmetric case. While some research has been performed, for example that of Krouse (reference 5.41), Keener et. al. (reference 5.52), and Skow and Erickson (reference 5.20), it appears that it is limited primarily to force data and that only Keener et. al. have covered a significant Reynolds number range for non-axisymmetric bodies.

In their study, Keener et. al. investigated the effects of modifying their circular tangent ogive forebodies to elliptical cross-sectional shapes for a case with major axis vertical (narrow side-on) and one with major axis horizontal (broad side-on). Their results have been summarized by Hunt in Figure 72 of reference 5.21 in terms of the maximum side force coefficient as a function of Reynolds number. Expecting the side force, for the same maximum width, to be greatest for the ellipse with the "narrow side-on" Hunt described as an anomaly the implication that it developed, in general, the lowest side force. However, there are several factors, not discssed by Hunt, which tend to shed additional light on the experimental results.

First, as can be seen from the two-dimensional data of Delany and Sorensen (reference 1.45) and Polhamus et. al. (reference 1.52), the critical Reynolds number for the ellipse with the major axis vertical (particularly when based on maximum width as in Hunt's figure) is considerably lower than that with the major axis horizontal. This shift, due primarily to the differences in magnitude of the adverse pressure gradients, greatly amplifies the differences in side force at a given Reynolds number since subcritical and critical boundary layer conditions are being compared in Hunt's figure 72. Second, the strengths of the shed vortices are greater, for the same body width for the ellipse with the "broad side-on" due to the higher velocities at the separation lines. The greater vortex strength will, of course, tend to offset the effect of the reduced side area. Other factors include the difference in planform fineness ratio which can result in changes in the angle of attack for the onset of vortex asymmetry and the associated differences in "crossflow" dynamic pressure at the angle of attack for maximum side force.

In an attempt to clarify the effects of cross section, particularly with regard to the Reynolds number effects of interest in this paper, the data of Keener et. al. are analyzed in figures 5.8 and 5.9. Several factors were considered in making the comparisons. The tangent ogive forebody having an elliptical "cross section" reported by Keener et. al. was designed such that with the major axis horizontal, it has the same planform as the fineness ratio 3.5 tangent-ogive forebody of circular cross section, and with the major axis vertical, it has the same planform as the fineness ratio 5.0 circular cross-section body. Therefore, in attempting to illustrate the effect of cross-sectional shape, the comparisons are made herein for the same planform fineness ratios and with the side force coefficient based on the

area of a circle of diameter equal to the ellipse planform width at the base. Also, to provide some degree of consistency in relation to the length of streamline run between the stagnation line and the beginning of the adverse pressure gradient for the different shapes, the Reynolds numbers are based on the maximum body dimension (in plane of major axis) at the base in all cases. Finally, following the approach used in the previous section, it is indicated whether the maximum side force shown occurred at the first or second peak in the variation with the angle of attack.

In view of the difficulties involved in establishing that the maximum side force for each condition is indeed being encountered, the lack of pressure distribution measurements, questions associated with cyclic variations resulting from vortex shedding frequencies, etc., the data presentation and discussion which follows must be considered a tentative attempt to establish some trends with cross section.

Figure 5.8 presents the comparison between the circular and narrow side-on elliptical cross sections for the tangent ogive forebodies of fineness ratio 5.0. For the subcritical case where the separation lines would be expected to be near the maximum body width location for both forebodies, the narrow side-on elliptical shape generated the largest side force coefficient with the increase being approximately equal to the side area ratio. At supercritical Reynolds numbers, the maximum side force coefficients occur at the second peak because of the increased vortex shedding frequency, and the magnitude for the narrow side-on elliptical cross section is now considerably lower than for the circular cross section. This reduction is presumed to be associated with the rather large reduction in vortex strength due to the more complete flow closure for the more "streamlined" shape in the turbulent separation region, which more than offsets the larger side area. The benefit of a more "streamlined" cross section was suggested during the early studies of the problem in 1951 by Allen and Perkins (reference 5.1) as a possible solution to the out-of-plane force problem for configurations for which inclined flight occurs essentially in one plane. However, for modern, highly maneuverable aircraft, flight at high angles of attack is not confined to one plane, and the reduced directional stability associated with the elliptical nose with major axis vertical is, of course, highly undesirable.

Although the narrow side-on ellipse is of little interest for aircraft forebodies, the results of figure 5.8 illustrate the potential peril in attempting to accurately establish the effects of cross section and to select

forebody shape if the data is confined to subcritical Reynolds numbers. It is also possible that the trends obtained in the supercritical range are not representative of full-scale conditions because there could possibly be further changes in vortex shedding frequency in the hypercritical Reynolds number range. These possible effects need to be investigated in the new high Reynolds number wind tunnel up to full-scale conditions.

A comparison of the circular and "broad side-on" elliptical cross sections for the tangent ogive forebodies of fineness ratio 3.5 is presented in figure 5.9. To be noted is the higher critical Reynolds number for the elliptic cross section associated primarily with the more severe adverse pressure gradient, and the reduction in maximum side force at both subcritical and supercritical Reynolds numbers relative to the circular cross section. Also to be noted is the reduced magnitude of the maximum side force at supercritical Reynolds numbers. Again, the need for full-scale Reynolds number data is illustrated, and such tests should include the combined effects of Reynolds number and Mach number to assure adequate simulation of the vortex shedding frequency and the separation line locations.

Comparing figures 5.8 and 5.9 in the supercritical range, the much larger reduction in maximum side force for the "narrow side-on" elliptical cross section than for the "broad side-on" elliptical cross section when compared with their corresponding circular cross section forebodies is striking. This benefit of the more "streamlined" shape, which has been discussed earlier, has sometimes been interpreted as inconsistent with the benefits in reduced out-of-plane force obtained with the "shark nose" configuration of the recent Tiger Shark version of the F-5 aircraft (see reference 5.20). It would appear, however, that the primary source of the "shark nose" benefit is derived from the very large forebody apex angle, an early established trend with regard to delaying the onset of vortex asymmetry. The major benefit of the accompanying flat elliptical cross section, aside from "area rule" considerations, is presumed to be an improvement in directional stability.

5.4 Compressibility Effects

As mentioned earlier, studies in the early 1950's demonstrated that while asymmetric vortex flow also appears at supersonic speeds, the resulting out-of-plane forces and moments were essentially eliminated. More recently,

studies have been made in the high subsonic and transonic range, of particular interest in this paper, as well as the supersonic range. Briefly, these studies established that depending upon the body nose shape and fineness ratio, the side force tends to vanish at freestream Mach numbers as low as 0.8, and as expected, that the reduction was primarily related to the crossflow Mach number, M $\sin\alpha$. This is illustrated by figure 5.10 which has been prepared utilizing the subsonic and transonic data on an ogive-cylinder configuration reported by Pick (reference 5.42). Presented is the maximum out-of-plane force $C_{Y_{o\ max}}$, as a function of both freestream Mach number, M, and its normal component, M $\sin\alpha$, where the value of α is that corresponding to $C_{Y_{o\ max}}$ at each Mach number. The results indicate a rapid decrease in the out-of-plane force occurring when the normal component of Mach number reaches approximately 0.4 which is close to the critical Mach number for two-dimensional circular cylinders. The force rapidly decreases and is essentially eliminated for normal components of Mach number, M $\sin\alpha$, in the range from 0.5 to 0.6. Similar trends have been observed by other investigators and Hunt's survey paper (reference 5.21) presents results from several of these studies. Of the various phenomena which can contribute to this reduction in side force (see reference 5.42), it is likely that the reduced sensitivity of the separation lines to wake effects for the case of shock-induced separation is the primary cause.

Inasmuch as the angle of attack at which the onset of vortex asymmetry occurs is strongly related to the forebody nose angle, it follows that the onset of compressibility effects in terms of freestream Mach number should be dependent upon forebody nose angle for a given angle of attack. Such a relationship has been demonstrated by Keener et. al. (reference 5.48) from tests of various forebody shapes. For example, their results indicated that the reduction in maximum side force due to compressibility effects was delayed to a considerably higher freestream Mach number as the nose fineness ratio was increased from 3.5 to 5.0. The fineness ratio 5.0 nose, with its smaller nose angle and resultant lower angle of attack for onset of vortex asymmetry, reaches a higher freestream Mach number before the crossflow Mach number, M $\sin\alpha$, reaches the onset of important compressibility effects. From this, they suggest that since the onset of vortex asymmetry has been shown to occur at an angle of attack approximately equal to twice the nose semi-apex angle, the Mach number at which the side force has reduced to near zero can be approximated from the expression M $\sin(2\delta) \approx 0.5$.

For the free-stream Mach numbers where strong compressibility effects were encountered, it appears that the Reynolds numbers were subcritical in the above study. There also seems to be little, if any, data in the literature at combined supercritical Mach numbers and supercritical Reynolds numbers for cases in which the nose was rotated to assure the attainment of maximum side force. Since the angle of attack for onset of vortex asymmetry appears to be relatively insensitive to Reynolds number, it might follow that the free-stream Mach number corresponding to supercritical crossflow Mach number will also be relatively insensitive to Reynolds number. However, it should be kept in mind that this comment relative to Reynolds number effects is based on forebody alone results, and that with a sizable afterbody present, such phenomena as the cyclic variation in vortex asymmetry along the body length could produce interacting effects of Mach number and Reynolds number, particularly in the critical Reynolds number range. Again, the new high Reynolds number wind tunnel facilities should provide insight into these possible interactions.

5.5 References

Some Early Studies

5.1 Allen, H. Julian and Perkins, Edward W.: Characteristics of Flow Over Inclined Bodies of Revolution. NACA RM A50L07, 1951.

5.2 Mead, Merrill H.: Observations of Unsteady Flow Phenomena for an Inclined Body Fitted with Stabilizing Fins. NACA RM A51K05, 1952.

5.3 Gowan, Forrest E.: Buffeting of a Vertical Tail on an Inclined Body at Supersonic Mach Numbers. NACA RM A53A09, 1953.

5.4 Cooper, M.; Gapcynski, J.P.; and Hasel, L.E.: A Pressure-Distribution Investigation of a Fineness-Ratio-12.2 Parabolic Body of Revolution (NACA RM-10) at M-1.59 and Angles of Attack to 36°, NACA RM L52G14a, October 1952.

5.5 Letko, W.: A Low-Speed Experimental Study of the Directional Characteristics of a Sharp-Nosed Fuselage Through a Large Angle of Attack Range at Zero Angle of Sideslip, NACA TN 2911, 1953.

5.6 Perkins, Edward W. and Dennis, David H.: Inclined Bodies at High Supersonic Speeds. NACA conference on aerodynamics of High-Speed Aircraft. July 8-10, 1953.

5.7 Perkins, E.W. and Kuehn, D.M.: Comparison of the Experimental and Theoretical Distributions of Lift on a Slender Inclined Body of Revolution at M=2, NACA RM A53E01, 1953.

5.8 Gowen, F.E. and Perkins, E.W.: A Study of the Effects of Body Shape on the Vortex Wakes of Inclined Bodies at a Mach Number of 2, NACA RM A53I17, 1953.

5.9 Dunn, Eldon L.: A Low-Speed Experimental Study of Yaw Forces on Bodies of Revolution at Large Angles of Pitch and Zero Angle of Sideslip. U.S. Naval Ordinance Test Station TM-1588, 1954.

5.10 Gapcynski, J.P.: An Experimental Investigation of the Flow Phenomena over Bodies at High Angles of Attack at a Mach Number of 2.01. NACA RM L55H29, 1955.

5.11 Fink, P.T.: Some Low Speed Aerodynamic Properties of Cones - Experiments done in the Imperial College Aeronautical Laboratory. ARC 17,632, 1953.

5.12 Maltby, R.L. and Peckham, D.H.: Low Speed Studies of the Vortex Patterns Above Inclined Slender Bodies Using a New Smoke Technique. RAE TN AERO 2482, 1956.

Some Additional Papers

5.13 Chapman, G.T.; Keener, E.R.; and Malcolm, G.: Asymmetric Aerodynamic Forces on Aircraft Forebodies at High Angles of Attack - Some Design Guides, Paper No. 16, AGARD Meeting on Stall/Spin Problems of Military Aircraft, Ames Research Center, Moffett Field, CA, November 18-21, 1976.

5.14 Wardlaw, A.B., Jr.: High Angle of Attack Missile Aerodynamics, Paper 5, AGARD LS-98, March 1978.

5.15 Skow, A.M. and Titiriga, A., Jr.: Forebody-Wing Vortex Interations and their Influence on Departure and Spin Resistance, Paper 6, AGARD CP-247, September 1978.

5.16 Tobak, M. and Peake, D.J.: Topology of Two-Dimensional and Three-Dimensional Separated Flows, AIAA-79-1480, July 1979.

5.17 Ericsson, L.E. and Reding, J.P.: Vortex-Induced Asymmetric Loads in 2-D and 3-D Flows. AIAA-80-0181, January 1980.

5.18 Peake, D.J. and Tobak, M.: Three-Dimensional Interactions and Vortical Flows with Emphasis on High Speeds, AGARD-ograph, March 1980.

5.19 Ericsson, L.E. and Reding, J.P.: Steady and Unsteady Vortex-Induced Asymmetric Loads on Slender Vehicles, Journal of Spacecraft and Rockets, Vol. 18, March - April 1981.

5.20 Skow, A.M. and Erickson, G.E.: Modern Fighter Aircraft Design for High Angle of Attack, AGARD Lecture Series No. 121, High Angle of Attack Aerodynamics, March 1982.

5.21 Hunt, B.L.: Asymmetric Vortex Forces and Wakes on Slender Bodies. AIAA Paper 82-1336, September 1982.

5.22 Reding, J.P. and Ericsson, L.E.: Maxmium Vortex-Induced Side Force Revisited. AIAA Paper No. 83-0458, January 1983.

Pressure and Flow Fields

5.23 Flechter, M.: Über Wirbelsysteme an Schlanken Rotationskörpern and Ihren Einfluss auf die Aero-dynamischen Beiwerte, Deutsch-Franzosisches Forschungsinstitut, Saint-Louis, 1966, Bericht 10/66.

5.24 Yanta, W.J. and Wardlaw, A.B.: Laser Doppler Velocimeter Measurements of Leeward Flowfields on Slender Bodies at Large Angle of Attack, AIAA Paper 77-660, 1977.

5.25 Schwind, R.G. and Mullen, J.: Laser Velocimeter Measurements of Slender Body Wake Vortices, AIAA Paper 79-0302, 1979.

5.26 Yanta, W.J. and Wardlaw, S.B.: Multi-Stable Vortex Patterns on Slender, Circular Bodies at High Incidence, AIAA Paper 81-0006, 1981.

5.27 Dexter, P.C. and Fowler, J.W.: Pressures on a Slender Axisymmetric Body at High Angle of Attack in a Very Low Turbulence Level Air Stream. University of Bristol, Report No. PCD 8201, January 1982.

5.28 Yanta, W.J. and Wardlaw, S.B., Jr.: The Secondary Separation Region on a Body at High Angles of Attack. AIAA Paper 82-0343, 1983.

Some Papers Related to Hydrodynamic Instability

5.29 Föppl, Ludwig: Wirbelbewegung Hinter Einem Kreiszylinder, Zitsungsberichte der Mathematische-Physikalische Klasse der K.B. Academie der Wissenschaften, Munich, Germany, Vol. 1, January-March 1913, pp. 1-18.

5.30 Shanks, R.E.: Low-Subsonic Measurements of Static and Dynamic Stability Derivatives of Six Flat-Plate Wings Having Leading-Edge Sweep Angles of 70^{o} to 84^{o}. NASA TND-1822, 1963.

5.31 Bird, J.D.: Tuft-Grid Surveys at Low Speeds for Delta Wings, NASA TND-5045, February 1969.

5.32 Polhamus, E.C.: Predictions of Vortex-Lift Characteristics by a Leading-Edge Suction Analogy, Journal of Aircraft, Vol. 8, April 1971, pp. 193-199.

5.33 Fox, Charles H. and Lamar, John E.: Theoretical and Experimental Longitudinal Aerodynamic Characteristics of an Aspect Ratio 0.25 Sharp-Edge Delta Wing at Subsonic, Supersonic, and Hypersonic Speeds. NASA TN D-7651, August 1974.

5.34 Keener, E.R. and Chapman, G.T.: Similarity in Vortex Asymmetries over Slender Bodies and Wings. AIAA Journal, Vol. 15, September 1977, pp. 1370-1372.

5.35 Schwind, R.G. and Mullen, Jnr., J.: Laser-velocimeter measurements of slender-body wake vortices. AIAA Paper 79-0302, 1979.

5.36 Peake, D.J.; Owen, F.K.; and Johnson, D.A.: Control of Forebody Vortex Orientation to Alleviate Side Forces, AIAA Paper No. 80-0183, January 1980.

5.37 Ericsson, L.E. and Reding, J.P.: Steady and Unsteady Vortex-Induced Asymmetric Loads on Slender Vehicles. Journal of Spacecraft and Rockets, Vol. 18, March-April 1981, pp. 97-109.

5.38 Woolard, Henry W.: Similarity Relation for Vortex-asymmetry on Slender Pointed Forebodies. AIAA Journal, Vol. 20, No. 4, April 1982.

5.39 Dyer, D.E.; Fiddes, S.P.; and Smith, J.H.B.: Asymmetric Vortex Formation from Cones at Incidence - A Simple Inviscid Model. Aeronautical quarterly, November 1982.

5.40 Fiddes, S.P. and Smith, J.H.B.: Calculations of Asymmetric Separated Flow Past Circular Cones at Large Angles of Incidence. Paper presented at the AGARD Symposium on Missile Aerodynamics held in Trondheim, Norway, September 20-22, 1982.

Reynolds Number and Mach Number Effects

5.41 Krouse, John R.: Induced Side Forces on Slender Bodies at High Angles of Attack and Mach Numbers of 0.55 and 0.80, NRSDC Test Report, March 1971.

5.42 Pick, G.S.: Investigation of Side Forces on Ogive-Cylinder Bodies at High Angles of Attack in the M=0.5 to 1.1 Range. AIAA Paper No. 71-570, June 1971.

5.43 Jorgensen, L.H. and Nelson, E.R.: Experimental Aerodynamic Characteristics for a Cylindrical Body of Revolution with Various Noses at Angles of Attack from 0^{o} to 58^{o} and Mach Numbers from 0.6 to 2.0, NASA TM X-3128, 1974.

5.44 Keener, E.R and Chapman, G.T.: Onset of Aerodynamic Side Forces at Zero Sideslip on Symmetric Forebodies at High Angles of Attack, AIAA Paper 74-770, 1974.

5.45 Nelson, R.C. and Fleeman, E.L.: High Angle of Attack Aerodynamics on a Slender Body with a Jet Plume, J. Spacecraft and Rockets, Vol. 12, No. 1, pp. 12-16, January 1975.

5.46 Keener, E.R. and Taleghani, J.: Wind Tunnel Investigations of the Aerodynamic Characteristics of Five Forebody Models at High Angles of Attack at Mach Numbers from 0.25 to 2. NASA TM X-73,076, 1975.

5.47 Keener, Earl R. and Valdex, Jose: Side Forces on a Tangent Ogive Forebody with a Fineness Ratio of 2.5 at High Angles of Attack and Low Speed. NASA TM X-73,176, 1976.

5.48 Keener, E.R.; Chapman, G.T.; and Kruse, R.L.: Effects of Mach Number and Afterbody Length on Onset of Asymmetric Forces on Bodies at Zero Sideslip and High Angles of Attack, AIAA Paper No. 76-66, January 1976.

5.49 Deffenbaugh, F.D. and Koerner, W.G.: Asymmetric Wake Development and Associated Side Force Missiles at High Angles of Attack, AIAA Paper No. 76-364, July 1976.

5.50 Lamont, P.J. and Hunt, B.L.: Pressure and Force Distributions on a Sharp-Nose Circular Cylinder at Large Angles of Inclination to a Uniform, Subsonic Stream, Journal of Fluid Mechanics, Vol. 76, Pt. 3, 1976, pp. 519-559.

5.51 Keener, E.R.; Chapman, G.T.; Cohen, L.; and Talaghani, J.: Side Forces on a Tangent-Ogive Forebody with a Fineness Ratio of 3.5 at High Angles of Attack and Mach Numbers from 0.1 to 0.7, NASA TM X-3437, February 1977.

5.52 Keener, E.R.; Chapman, G.T.; Cohen, L.; and Talaghani, J.: Side Forces on Forebodies at High Angles of Attack and Mach Numbers from 0.1 to 0.7. Two Tangent Ogives, Paraboloid and Cone, NASA TM X-3438, February 1977.

5.53 Jorgensen, L.H.: Prediction of Static Aerodynamic Characteristics for Slender Bodies Alone and With Lifting Surfaces to Very High Angles of Attack, NASA TR R-474, 1977.

5.54 Przirembel, C.E.G. and Shereda, Donald E.: Aerodynamics of Slender Bodies at High Angles of Attack. Journal of Spacecraft, Vol. 16, January - February 1979.

5.55 Kruse, R.L.; Keener, E.R.; Chapman, G.T.; and Glaser, G.: Investigation of the Asymmetric Aerodynamic Characteristics of Cylindrical Bodies of Revolution with Variations in Nose Geometry and Rotational Orientation at Angles of Attack to 58° and Mach Numbers to 2, NASA TM 78533, September 1979.

5.56 Lamont, P.J.: Pressure Measurements on an Ogive-Cylinder at High Angles of Attack with Laminar, Transitional, or Turbulent Separation, AIAA 80-1556, January 1980.

5.57 Lamont, P.J.: The Complex Asymmetric Flow over a 3.5D Ogive Nose and Cylindrical Afterbody at High Angles of Attack, AIAA 82-0053, January 1982.

5.58 Hessman, F.W.: High Angle of Attack Aerodynamic Characteristics for a Finless TVS Missile Configuration. AIAA 82-1337, August 1982.

5.59 Lamont, P.J.: Pressures Around an Inclined Ogive Cylinder with Laminar, Transitional, or Turbulent Separation. AIAA Journal, Vol. 20, No. 11, November 1982.

Some Prediction Methods

5.60 Thomson, K.D. and Morrison, D.F.: On the Asymmetric Shedding of Vortices from Slender Cylindrical Bodies at Large Angles of Yaw, WRE Tech Note HSA 106, May 1965.

5.61 Thomson, K.D. and Morrison, D.F.: The Spacing, Position, and Strength of Vortices in the Wake of Slender Cylindrical Bodies at Large Incidence, Journal of Fluid Mechanics, Vol. 50, Pt. 4, 1971, pp. 751-783.

5.62 Thomson, K.D.: The Estimation of Viscous Normal Force, Pitching Moment and Yawing Moment on Bodies of Revolution at Incidences up to 90°, Australian W.R.E. Report 789 (W.R.&D.), 1972.

5.63 Lamont, P.J. and Hunt, B.L.: Out-of-Plane Force on a Circular Cylinder at Large Angles of Inclination to a Uniform Stream, Aeronautical Journal of the Royal Aeronautical Society, Vol. 77, January 1973, pp. 41-45.

5.64 Wardlaw, A.B., Jr.: Prediction of Normal Force, Pitching Moment, and Yaw Forces on Bodies of Revolution up to 50 Degrees Using a Concentrated Vortex Flow-Field Model. NOL TR 73-209, October 1973.

5.65 Marshall, F.J. and Deffenbaugh, F.D.: Separated Flow Over Bodies of Revolution Using an Unsteady Discrete-Vorticity Cross Wake. NASA CR-2414, June 1974.

5.66 Wardlaw, A.B.: Prediction of Yawing Force at High Angle of Attack, AIAA Journal, Vol. 12, August 1974, pp. 1142-1144.

5.67 Kao, H.C.: Side Forces on Unyawed Slender Inclined Aerodynamic Bodies, Journal of Aircraft, Vol. 12, March 1975, pp. 142-150.

5.68 Kuhn, Gary D.: Evaluation of a Theoretical Method for Calculating Side-Force Onset on Bodies of Revolution. Nielsen Engineering & Research, Inc., TR 96, September 1975.

5.69 Fidler, J.E. and Bateman, M.C.: Asymmetric Vortex Effects on Missile Configurations, Journal of Spacecraft, Vol. 12, November 1975, pp. 674-681.

5.70 Deffenbaugh, F.D. and Koerner, W.G.: Asymmetric Wake Development and Associated Side Force on Missiles at High Angles of Attack. AIAA Paper No. 76-364, July 1976.

5.71 Lamont, P.J. and Hunt, B.L.: Prediction of Aerodynamic Out-of-Plane Forces on Ogive-Nosed Circular Cylinders, Journal of Spacecraft, Vol. 14, No. 1, 1977, pp. 38-44.

5.72 Spangler, S.B.; Perkins, S.C., Jr.; and Mendenhall, M.R.: Prediction of Lateral Aerodynamic Loads on Aircraft at High Angles of Attack. AGARD CP-247, 1978, paper no. 29.

5.73 Mendenhall, M.R.; Spangler, S.B.; and Perkins, S.C., Jr.: Vortex Shedding for Circular and Non-circular Bodies at High Angles of Attack. AIAA Paper No. 79-0026, January 1979.

5.74 Dahlem, V.: Semi-Empirical Prediction Method for Induced Side Forces on Missiles at High Angles of Attack. AIAA Paper No. 79-0025, January 1979.

5.75 Graham, J.E. and Hankey, W.L.: Computation of the Asymmetric Vortex Pattern for Bodies of Revolution. AIAA Paper No. 82-0023, January 1982.

5.76 Botnan, Jan. I.: Asymmetric Forces on Slender Bodies at High Angles of Attack. Paper presented at the AGARD Symposium on Missile Aerodynamics held at Trondheim, Norway, September 20-22, 1982.

Some Additional Papers

5.77 Tobak, M. and Peak, D.J.: Topology of Three-Dimensional Separated Flows. NASA TM-81294, 1981.

5.78 Keener, Earl R.: Oil Flow Separation Patterns on an Ogive Forebody. AIAA Journal Vol. 21, No. 4, April 1983.

5.79 Dexter, P.C.: A Study of Asymmetric Flow Over Slender Bodies at High Angles of Attack in a Low Turbulence Environment. AIAA Paper No. 84-0505. January 1984.

6. SOME RECOMMENDED RESEARCH

Throughout the paper some of the areas where additional research would be useful have been pointed out, particularly with regard to extensions to higher Reynolds numbers. As a possible aid in defining research projects for the National Transonic Facility on bodies at high angles of attack, this section itemizes some of the more pertinent research areas mentioned in the paper. To assist in relating the recommended research items to particular NTF research models, they are grouped under "bodies of revolution" and "bodies of non-circular cross section". Also, under each body type, the subjects addressed follow the order of the main body of the paper. Priorities, therefore, are not implied by the order of the research recommendation. It is anticipated that, in general, possible adoption of any of the recommendations and assignment of priorities will be influenced by models currently planned for the NTF that could be adapted and future models will, of course, be influenced by aircraft technology needs at that time.

In addition to the three-dimensional research, there are several areas where fundamental research using two-dimensional models would be beneficial. However, in view of the initial emphasis on three-dimensional testing in the NTF, no definitive recommendations will be made here with regard to two-dimensional research except to point out that, in the absence of wall turntables and balances, some fundamental research could be performed with cylinders at fixed flow incidence angles and with surface pressure orifices. Some fruitful areas of two-dimensional research can be selected from the sections on cylinders in the main body of the paper.

Bodies of Revolution

Since the forces normal to the axis of revolution for any combination of angle of attack and sideslip can be resolved from the normal force and out-of-plane side force variation with angle of attack, only those two forces will be discussed.

Normal Force

Although the major effects of Reynolds number on normal force occur in the critical range, the review indicated evidence of rather large effects in

the supercritical range at subcritical Mach numbers that are not well defined at present. Essentially, no data is available in the hypercritical Reynolds number range. It is, therefore, recommended that an ogive-cylinder body-of-revolution model having a fineness ratio of approxmately 10 be tested over a wide Reynolds number range with emphasis on the supercritical and hypercritical regimes for angles of attack up to at least 45^{o}. The study should include compressibility effects for normal components of Mach number up to at least 0.60 at the high angles of attack.

An aid to this experimental research would be the development of accurate Euler solutions for the inviscid, shock-induced separation case to provide an indication of the asymptote for the very high Reynolds number conditions prior to eventual high Reynolds number Navier-Stokes solutions.

Out-Of-Plane Force

The analysis of two-dimensional and three-dimensional vortex shedding evidence, as related by the impulsive flow analogy, leads to a tentative conclusion that in the supercritical Reynolds number range, the vortex shedding rate for the three-dimensional ogive-cylinder is related to the upper level of the wide-band random frequency spectra for the two-dimensional circular cylinder normal to the flow. For this case, the Strouhal number is more than twice the subcritical value. It is, therefore, recommended that an ogive-cylinder pressure model of at least 10 diameters in length be tested over a wide Reynolds number range in an attempt to more completely define the changes in the period of the cyclic variation of the out-of-plane side force along the body Reynolds number well into the hypercritical range. Also, large effects of Mach number are expected in the supercritical Reynolds number range and normal components of freestream Mach number of at least 0.5 should be investigated in the 40^{o} to 45^{o} angle of attack range. The compressibility study should be extended into the hypercritical Reynolds number range if model loads will allow.

Bodies of Non-circular Cross Section

Bodies of non-circular cross section are highly sensitive to Reynolds number effects, and the data and analysis presented in the main body of this paper indicates many areas where research at higher Reynolds numbers would be

valuable. Although a few suggestions for extending the research are made in this section, final selections for models and test programs should, of course, be made by an examination of the many two-dimensional and three-dimensional flow examples given in the body of the paper in the light of cross-sectional shapes of practical interest at the time.

Normal Force

As in the case of the bodies of revolution, little data exists in the upper supercritical Reynolds number range and beyond. An even greater shortage of data exists with regard to compressibility effects which are particularly important due to the higher flow acceleration encountered around non-circular bodies. While large effects of Reynolds number on the normal force produced by non-circular bodies are illustrated in the body of the paper, it is believed that, in general, the shape selected for Reynolds number and compressibility studies in the NTF should probably be based on the more critical effects associated with asymmetric flows discussed in the following sections.

Side force Due to Sideslip

One of the most pronounced Reynolds number dependent flows encountered by bodies at high angles of attack is that associated with non-circular bodies in sideslip. The analysis of both two-dimensional and three-dimensional data illustrated that changes in the sign of the side force with Reynolds number can occur and data for the space shuttle orbiter demonstrated that such force changes on the forebody are of sufficient magnitude to cause a directional instability as the Reynolds number is increased. Of particular interest from a research standpoint is the square cross section having rounded corners for which the two-dimensional analysis indicated the possibility of additional changes in sign of the sideforce, at Reynolds number beyond those for which data is available, due to asymmetric closure of the flow around the leeward corners as influenced by vortex flow generated at the windward corners. It is, therefore, recommended that studies at high Reynolds numbers on bodies of non-circular cross section include, at least, a square shape with rounded corners and that consideration be given to forebody tests on a complete aircraft model as well as a relatively high fineness-

ratio body alone. Tests of the shuttle orbiter model in the NTF should, of course, include directional stability studies over a wide Reynolds number and Mach number range.

Out-Of-Plane Force

Except for certain elliptical cases, there appears to be little information on the Reynolds number dependence on the side force at zero sideslip generated by bodies of non-circular cross sections at high angles of attack. Those non-circular cross sections which develop large Reynolds number dependent side forces due to sideslip would be expected to be particularly sensitive to the asymmetric flow produced at angles of attack where the lee-side vortices become asymmetric. In addition, the review of the two-dimensional cylinder data indicated a large effect of cross-sectional shape on the Strouhal frequency in the critical Reynolds number range which might be expected to influence the vortex shedding and, therefore, the period of the cyclic variation of the side force along the body length. In view of these anticipated Reynolds number effects and their importance with regard to high angle of attack flying qualities, it would appear desirable to investigate at least one non-circular cross section body as part of the early research in the NTF in order to better define a more complete research program.

7. SYMBOLS

a	speed of sound
A_b	base area
A_p	planform area
$\bar{c}$	wing mean-aerodynamic chord
c_d	drag coefficient of two-dimensional cylinders, lift for unit length/qW
c_{d_p}	pressure drag coefficients
c	lift coefficient of two-dimensional circular cylinders, lift for unit length/qD
C_m	pitching-moment coefficient, pitching moment/$qS_w\bar{c}$
c_n	normal-force coefficient of two-dimensional circular cylinders, normal force per unit length/qD
C_n	yawing-moment coefficient, yawing moment/$qS_w\bar{c}$
C_N	normal-force coefficient of three-dimensional bodies, normal force/qA_b
C_N'	normal-force coefficient of three-dimensional bodies, normal force/qA_p
C_{N_β}	directional stability parameter (rate of change of yawing moment with sideslip)
C_p	pressure coefficient
C_{p_B}	base-pressure coefficient
c_y'	sideforce coefficient in body axis, side force per unit length/qh
C_{Y_o}	sideforce coefficient at zero sideslip (out-of-plane force coefficient), side force/qA_b
$C_{Y_{o\ max}}$	maximum out-of-plane force coefficient
D	cylinder diameter
h	body height or spoiler projection
L	body length

ℓ	distance to forebody geometric centroid
M	Mach number, V/a
n	frequency of vortex shedding from one side of body
q	dynamic pressure, $\frac{\rho V^2}{2}$
r	corner radius, or sand roughness height
R_D	Reynolds number based on maximum diameter, $\frac{\rho VD}{\mu}$
R_{eff}	Reynolds number based on an effective streamline length (see section 2.2.2)
R_h	Reynolds number based on body height, $\frac{\rho Vh}{\mu}$
R_r	Reynolds number based on corner radius, $\frac{\rho Vr}{\mu}$
R_w	Reynolds number based on body width, $\frac{\rho Vw}{\mu}$
S	Strouhal number, $\frac{nD}{V}$ or $\frac{nW}{V}$
S_w	wing area
V	freestream velocity
W	maximum width of body (D for circle)
X	distance from body nose, or distance behind cylinder
α	angle of attack
β	angle of sideslip
δ	azimuthal angle defining spoiler location, also semi-apex angle
ϕ	flow incidence in plane normal to axis of cylinder
θ	azimuthal angle (θ=0 is on windward side)
θ_s	azimuthal angle defining location of separation line
η	drag proportionality factor ($\frac{\text{finite span drag}}{\text{infinite span drag}}$)
ρ	free-stream air density
μ	free-stream air viscosity
ω	rolling angular velocity

8. ACKNOWLEDGEMENT

The author gratefully acknowledges the many helpful suggestions made by Dr. Robert M. Hall and Thomas B. Gainer, of the Langley Research Center during review of the text.

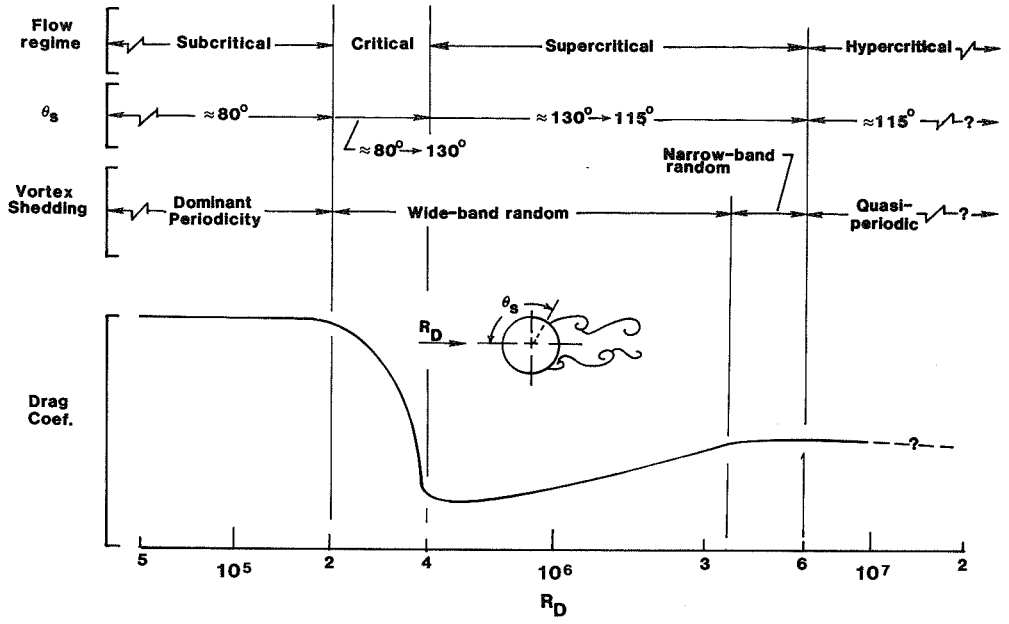

Figure 1.1 Identification of flow regimes to be discussed relative to circular cylinders.

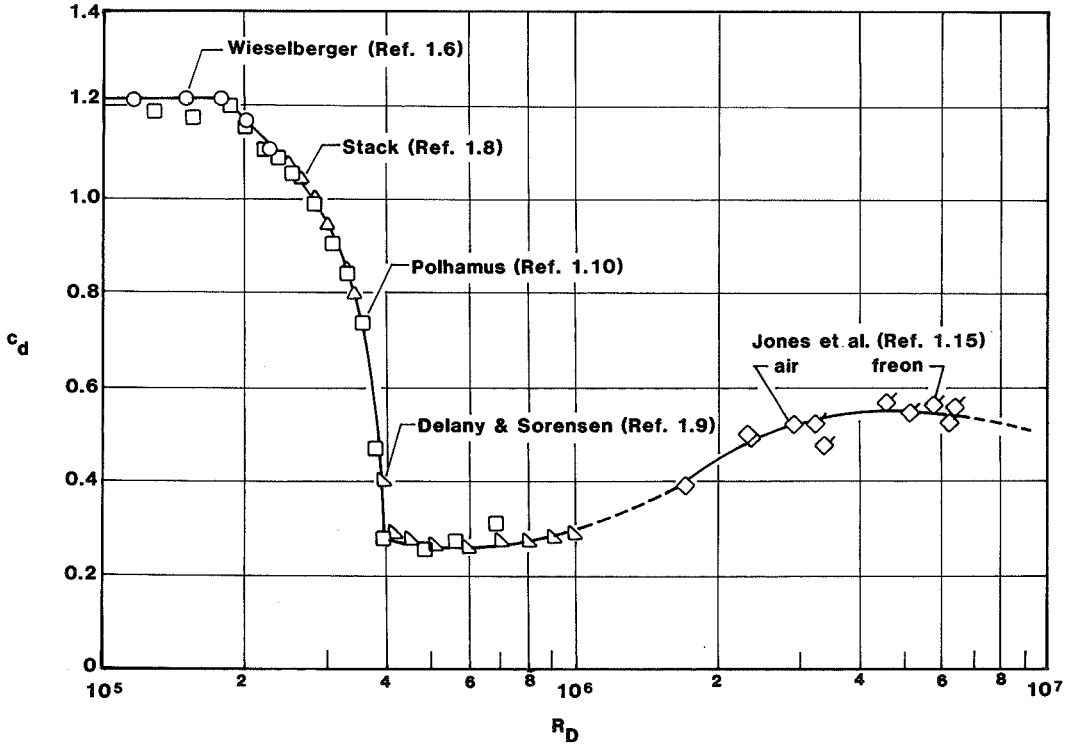

Figure 1.2 Drag coefficient for smooth circular cylinders. M = 0.15.

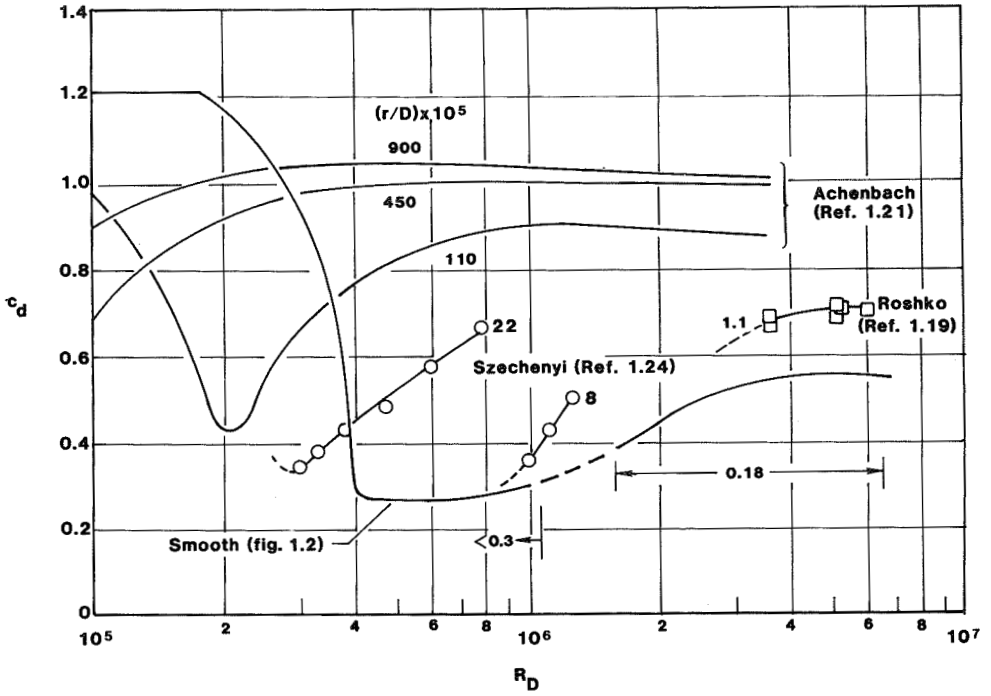

Figure 1.3 Effect of distributed roughness on the drag coefficient of circular cylinders. M = 0.15.

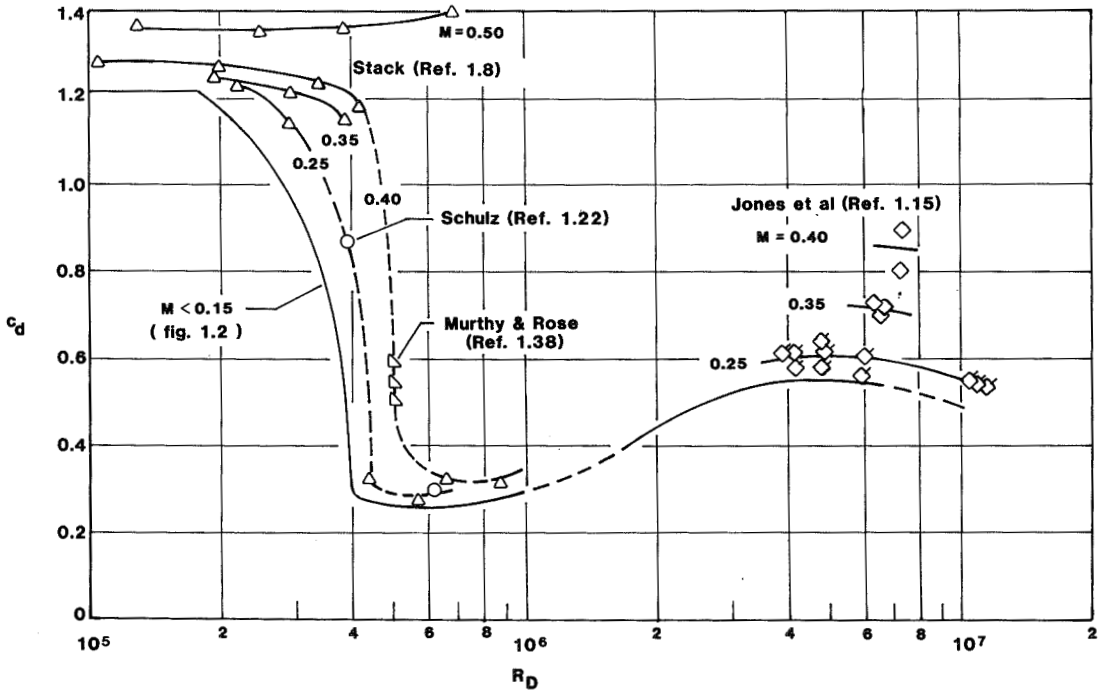

Figure 1.4 Effect of Mach number on drag coefficient of smooth circular cylinders.

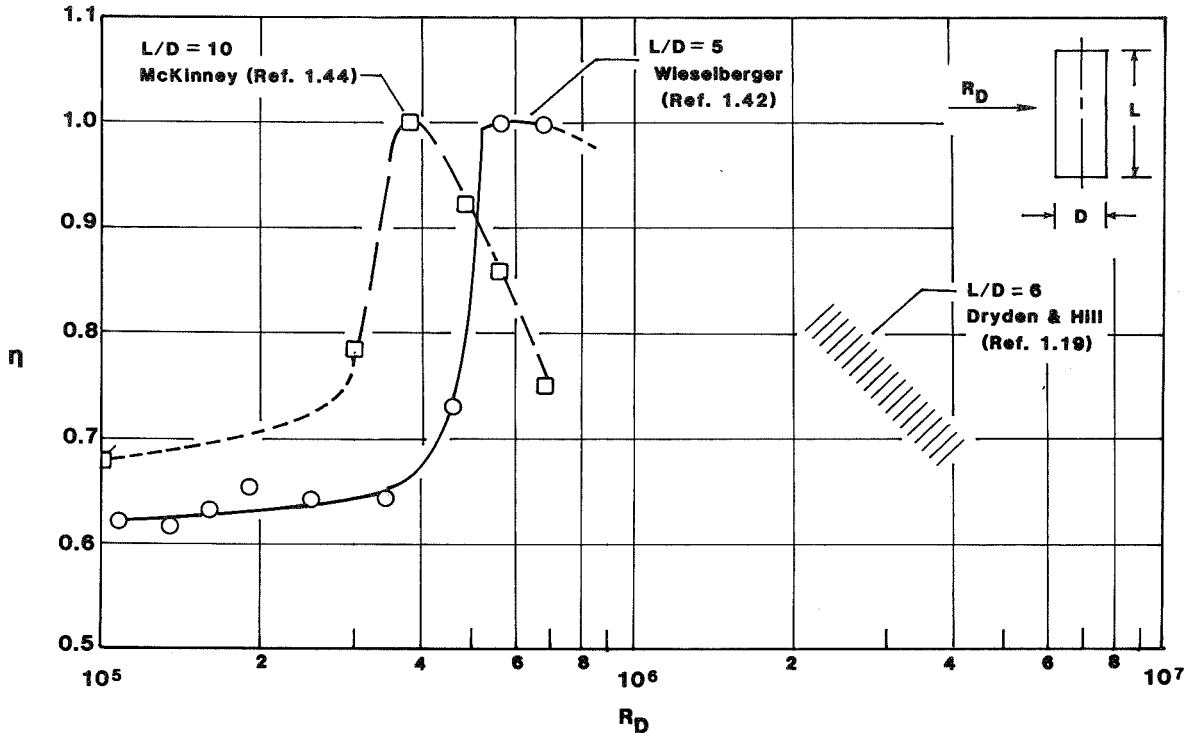

Figure 1.5. Finite-span drag proportionality factor.

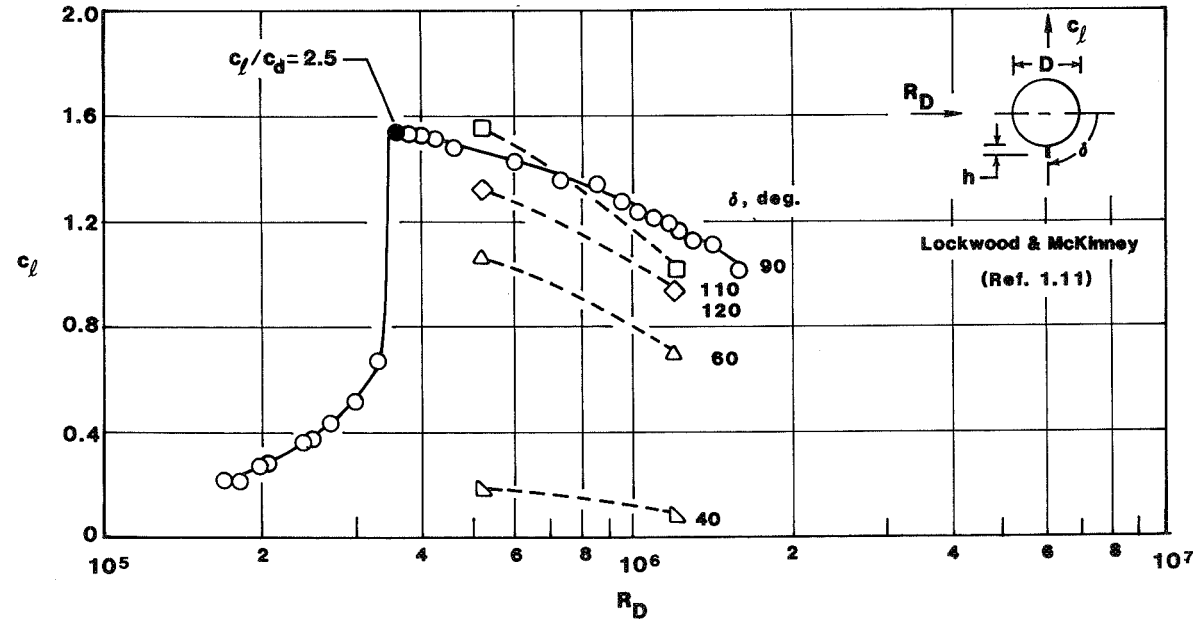

Figure 1.6 Effect of spoiler orientation angle on lift coefficient for circular cylinder. h/D = 0.06.

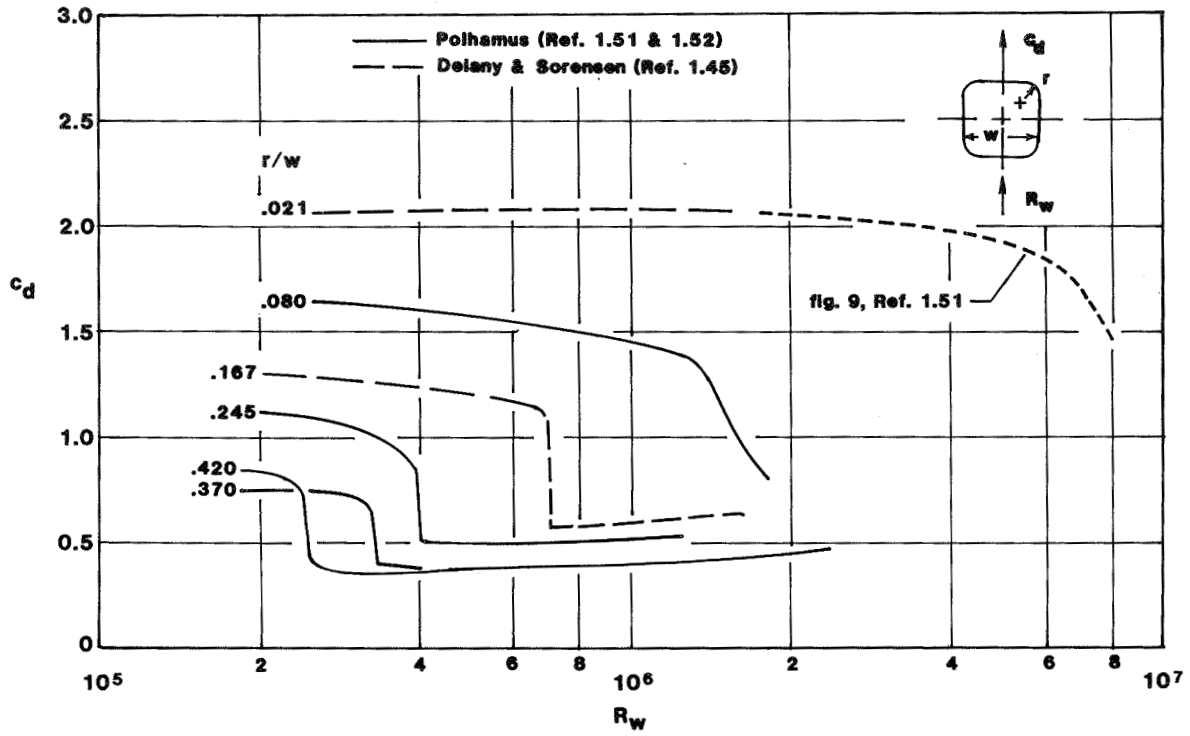

Figure 1.7 Influence of corner radius on drag coefficient of modified square cylinders.

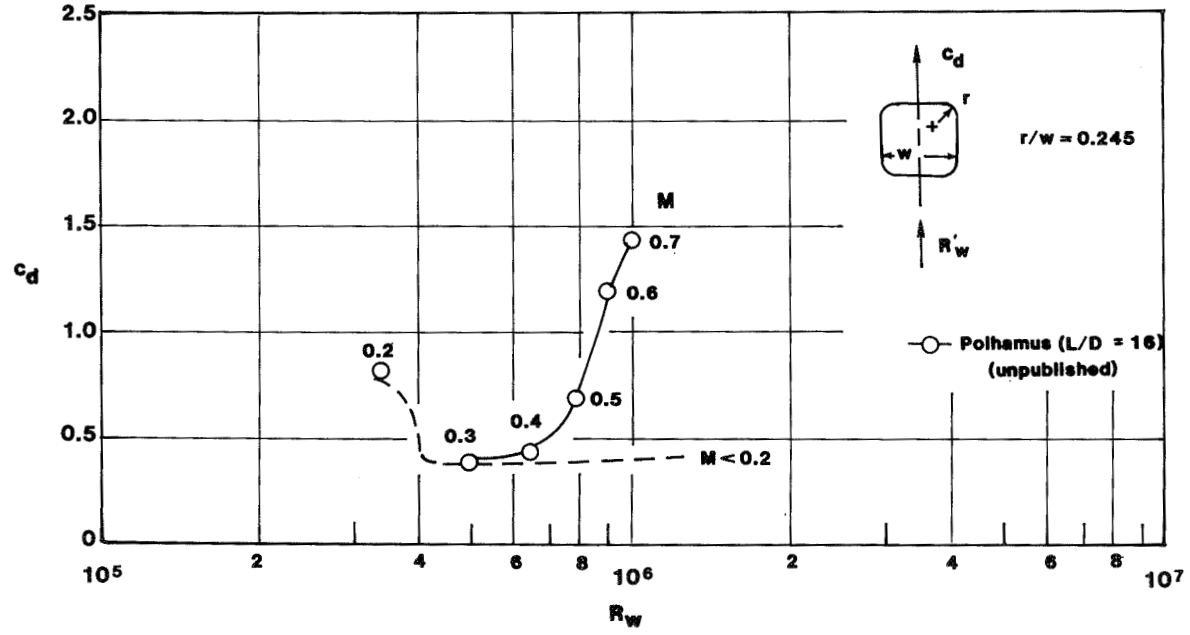

Figure 1.8 Effect of Mach number on the drag coefficient of a modified square cylinder.

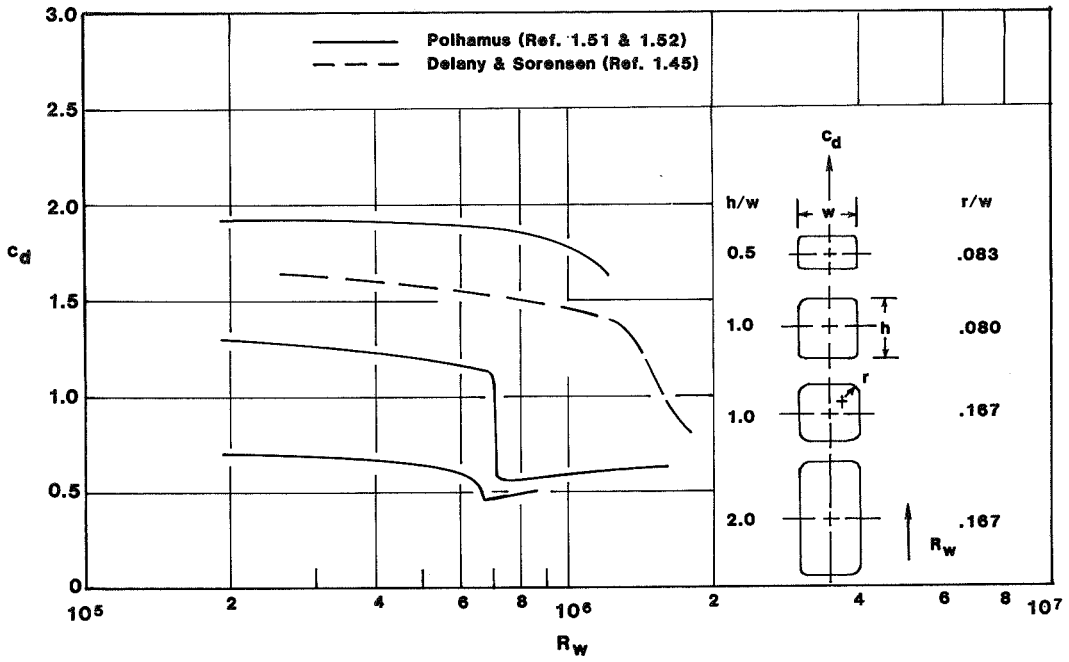

Figure 1.9 Effects of height-to-width ratio on drag coefficients of modified rectangular cylinders.

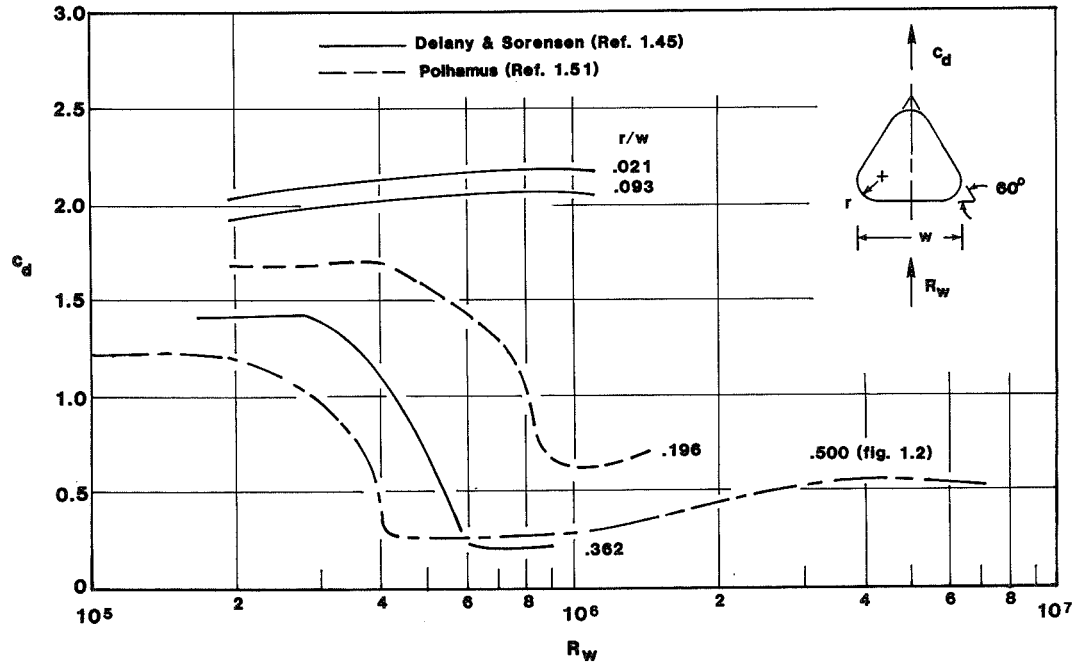

Figure 1.10 Effect of corner radius on the drag coefficient of modified triangular cylinders.

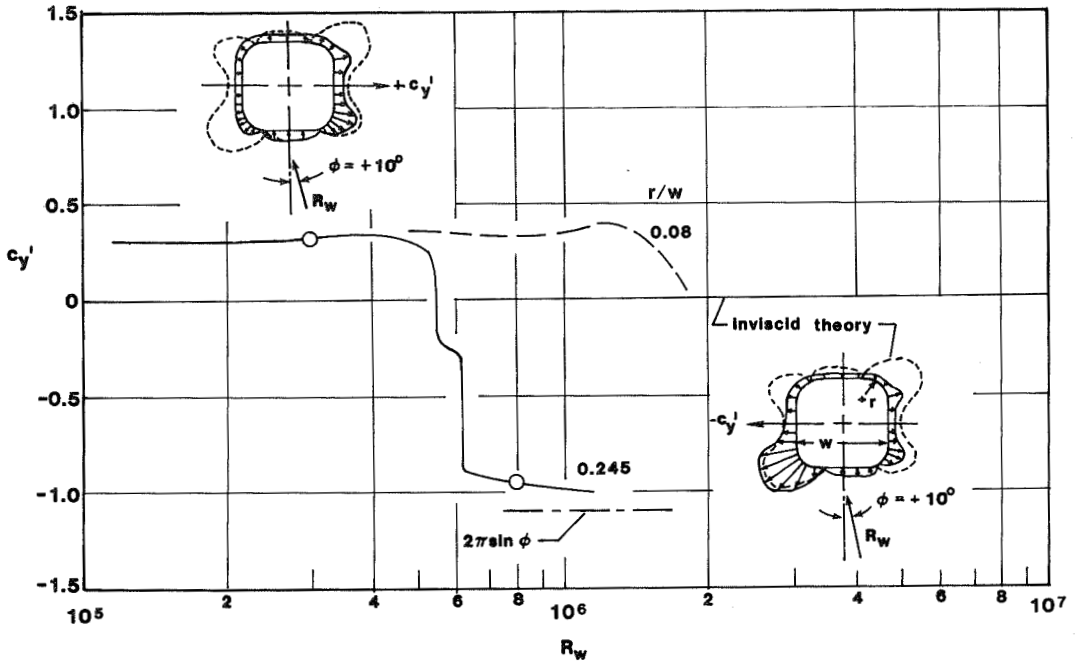

Figure 1.11 Influence of corner radius on the side force coefficient developed on modified square cylinders (reference 1.51 and 1.52).

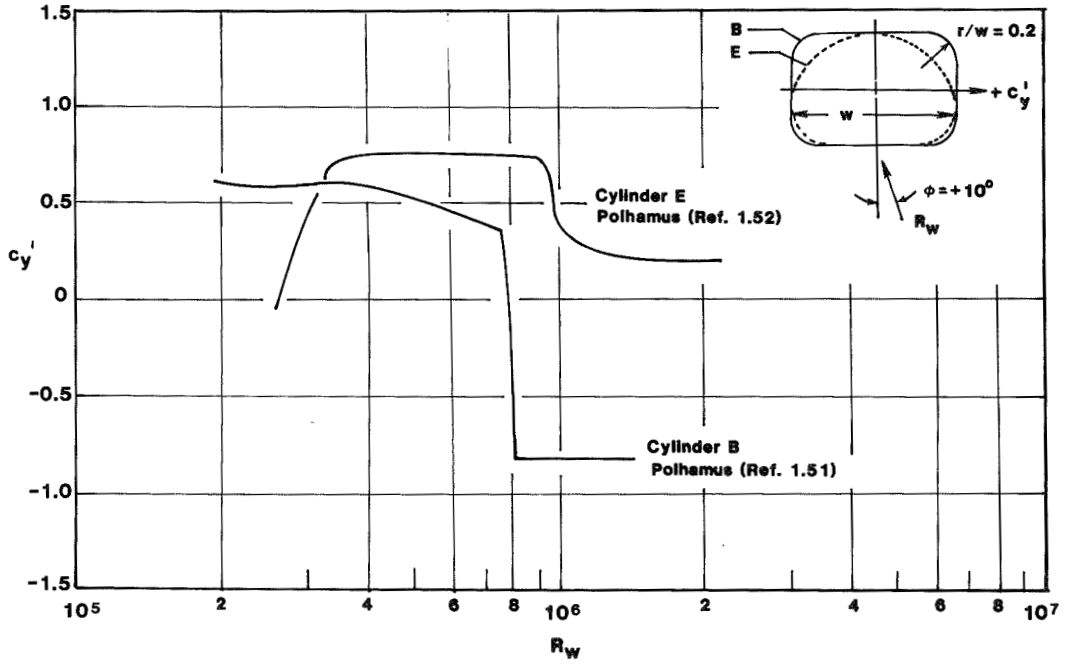

Figure 1.12 Effect of leeward shape on the side force coefficient of modified rectangular cylinders.

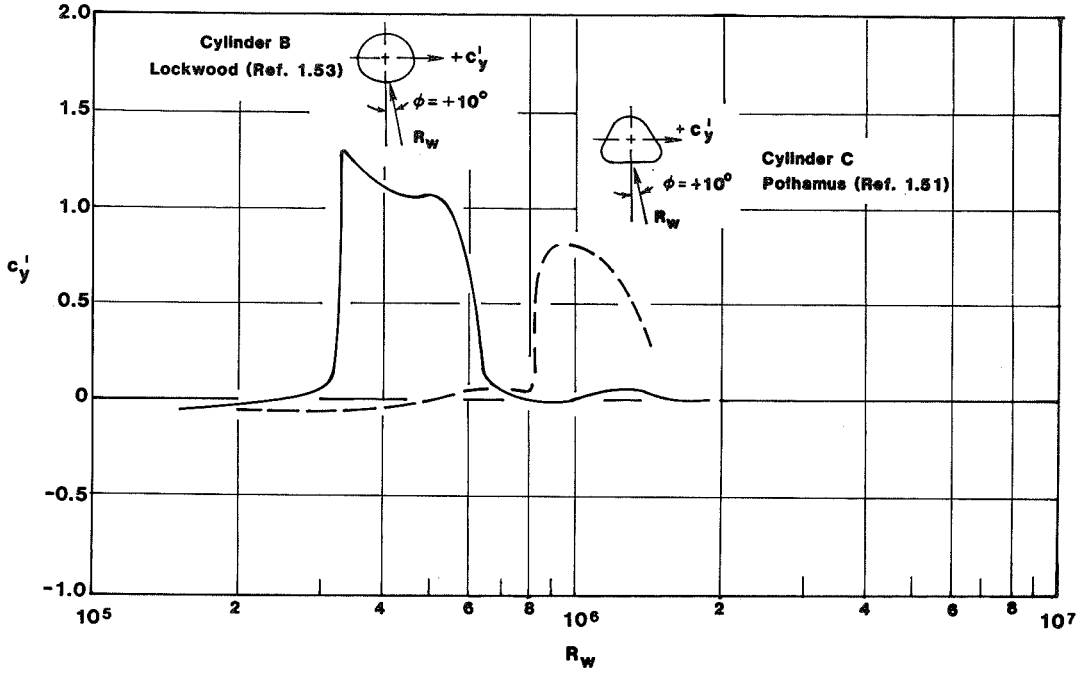

Figure 1.13 Effect of windward corner radius on side force spike developed by modified triangular cylinders.

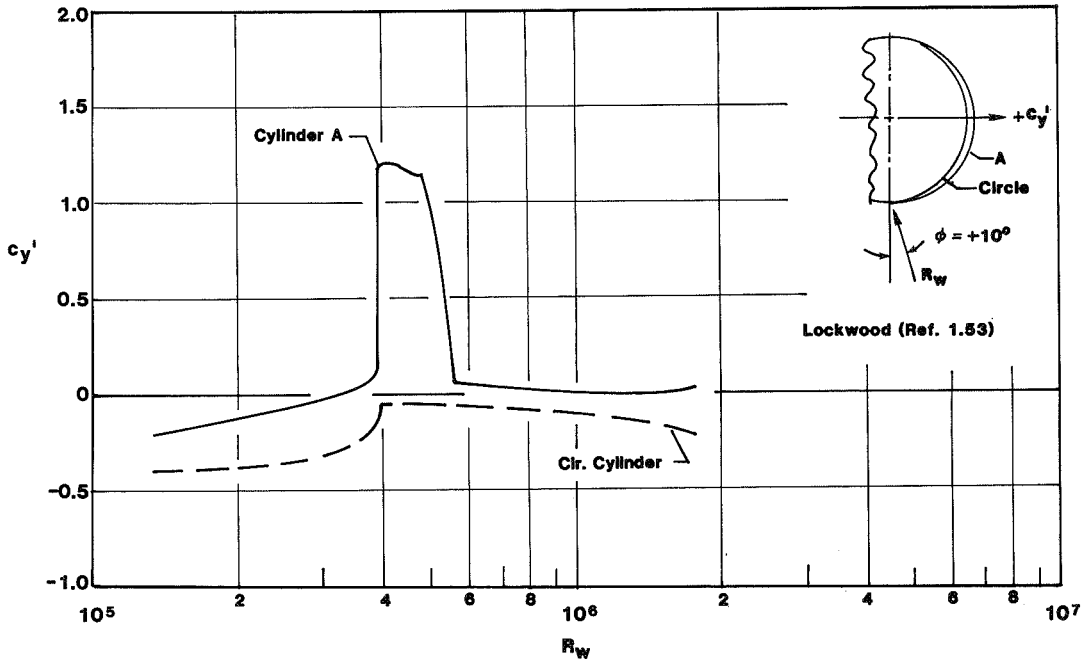

Figure 1.14 Influence of slight contour distortion on side force coefficient of circular cylinder.

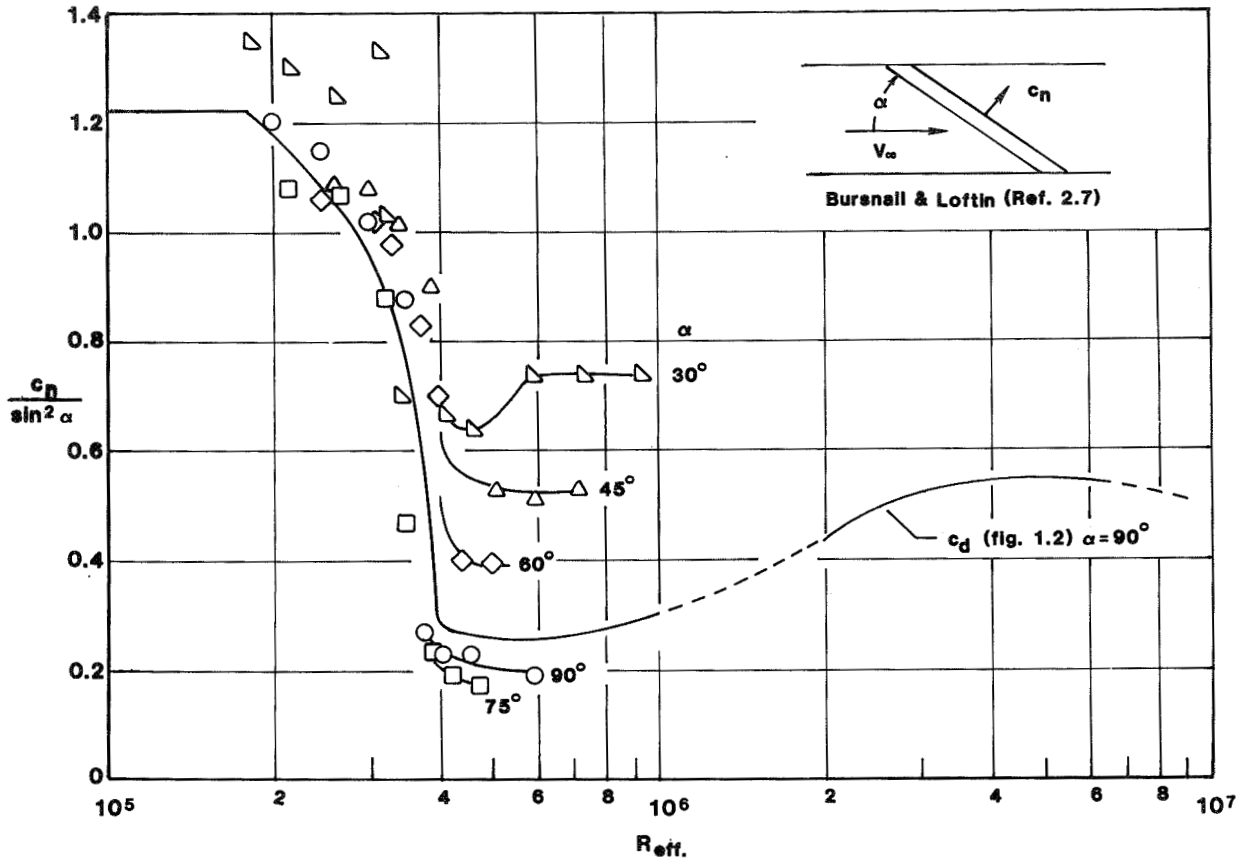

Figure 2.1 Effect of angle of attack on normal force coefficient parameter for circular cylinder.

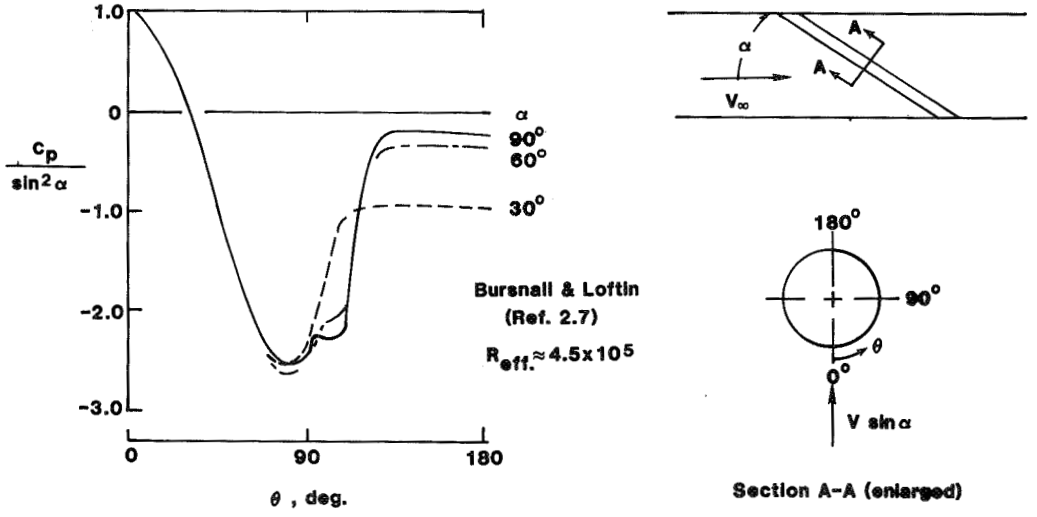

Figure 2.2 Comparison of normalized pressure coefficient parameter for circular cylinder at various angles of attack.

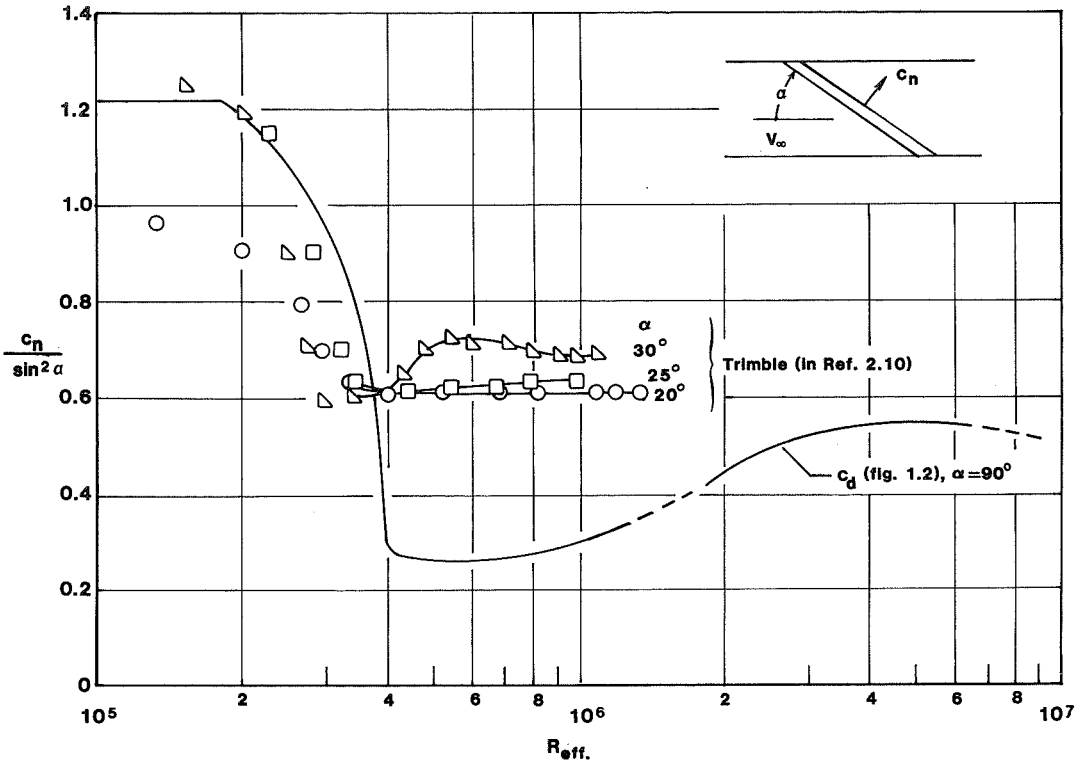

Figure 2.3 Effect of angle of attack on normal force coefficient parameter for circular cylinder.

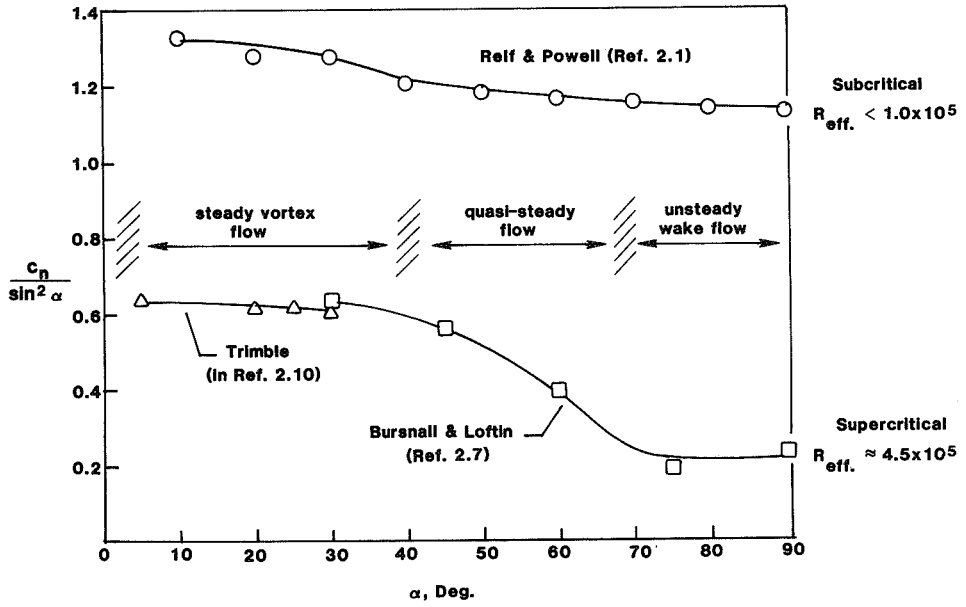

Figure 2.4 Variation of circular cylinder normal force coefficient parameter, with angle of attack for subcritical and supercritical conditions.

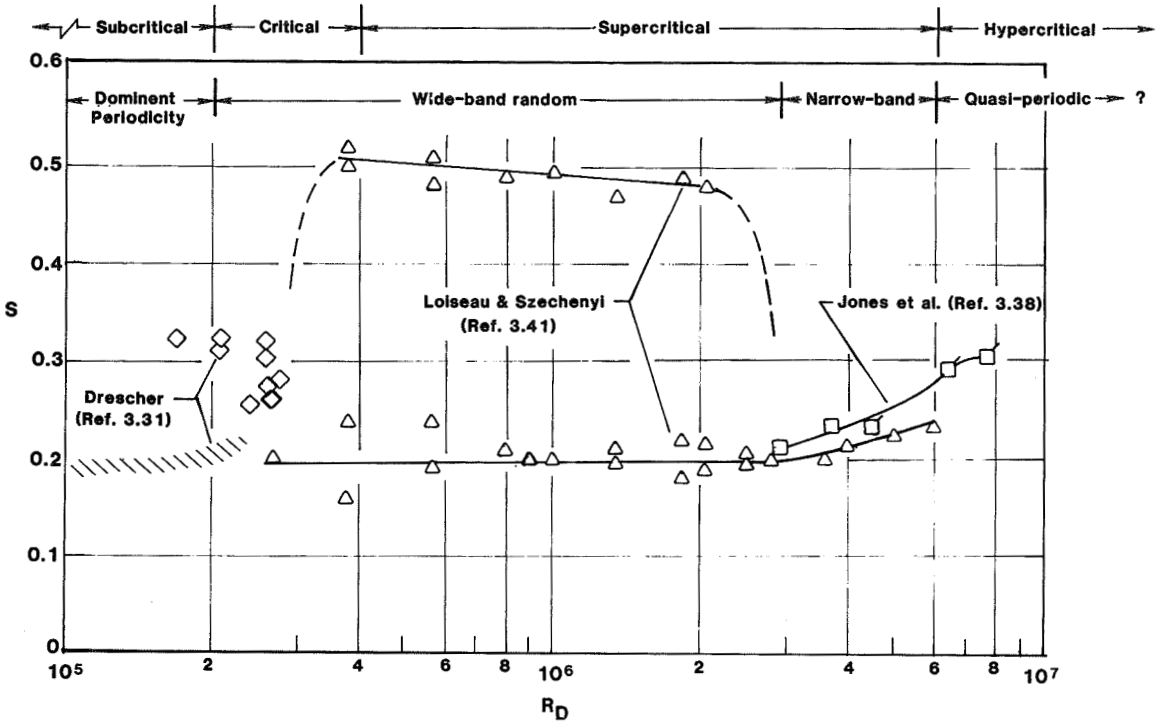

Figure 3.1 Circular cylinder Strouhal numbers from surface pressures and lift.

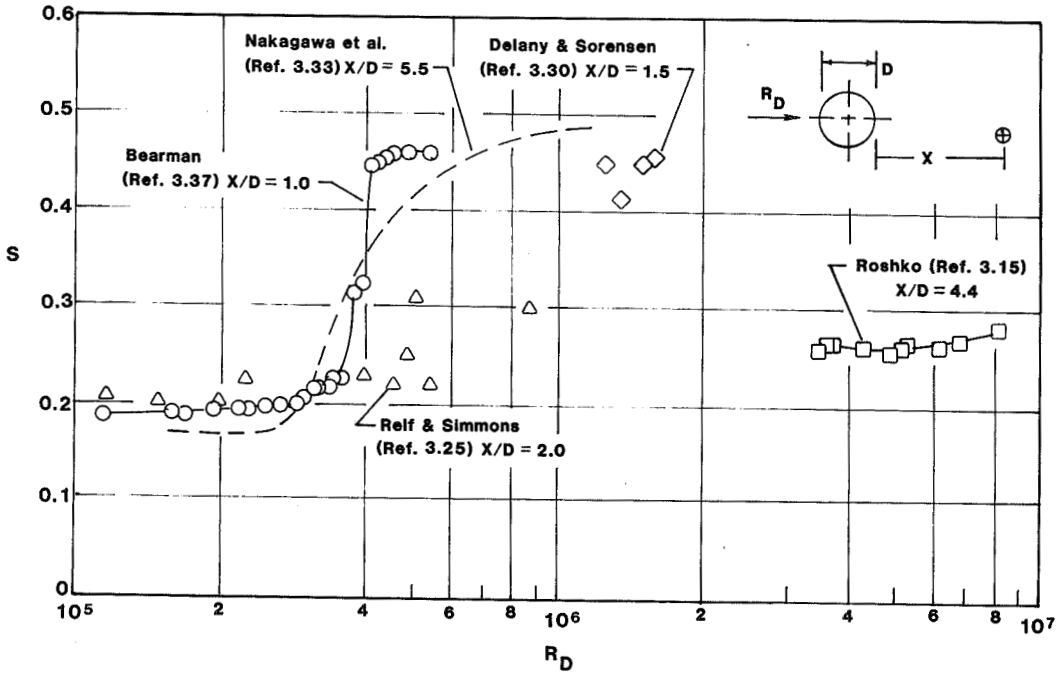

Figure 3.2 Circular cylinder Strouhal numbers from wake measurements.

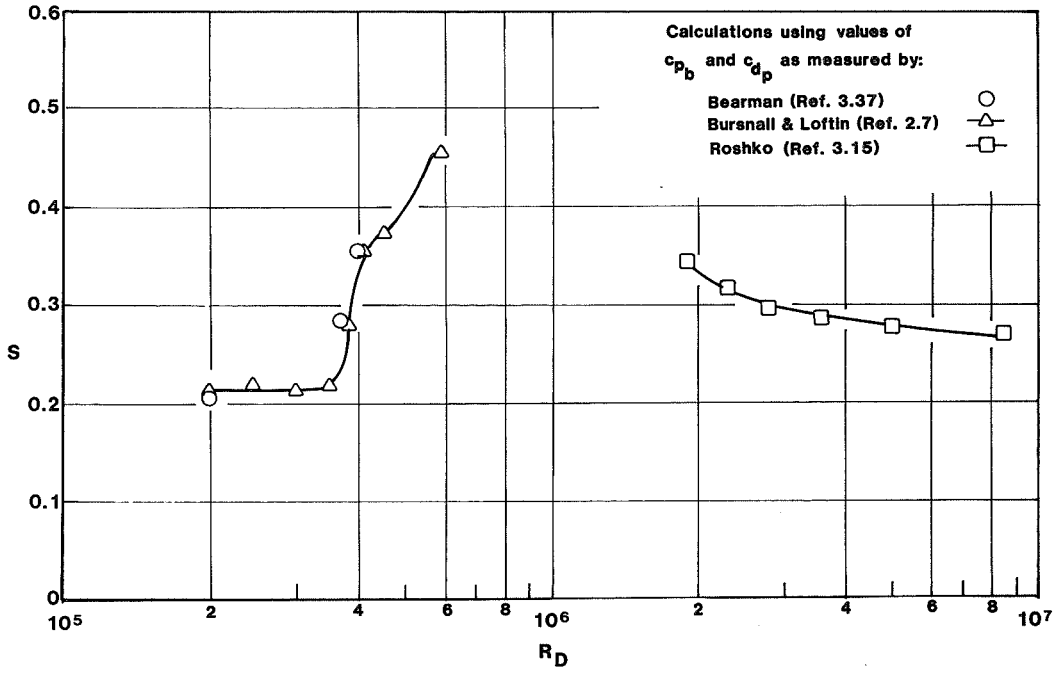

Figure 3.3 Calculations using Bearman's universal vortex wake frequency concept (reference 3.20).

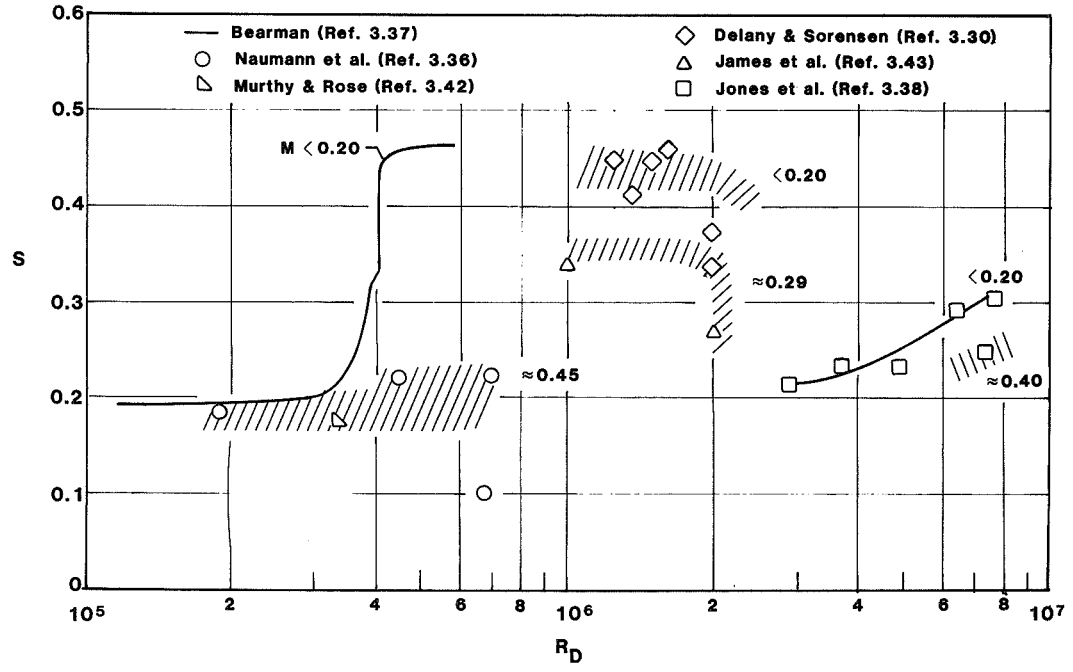

Figure 3.4 Effects of Mach number on Strouhal number for circular cylinders.

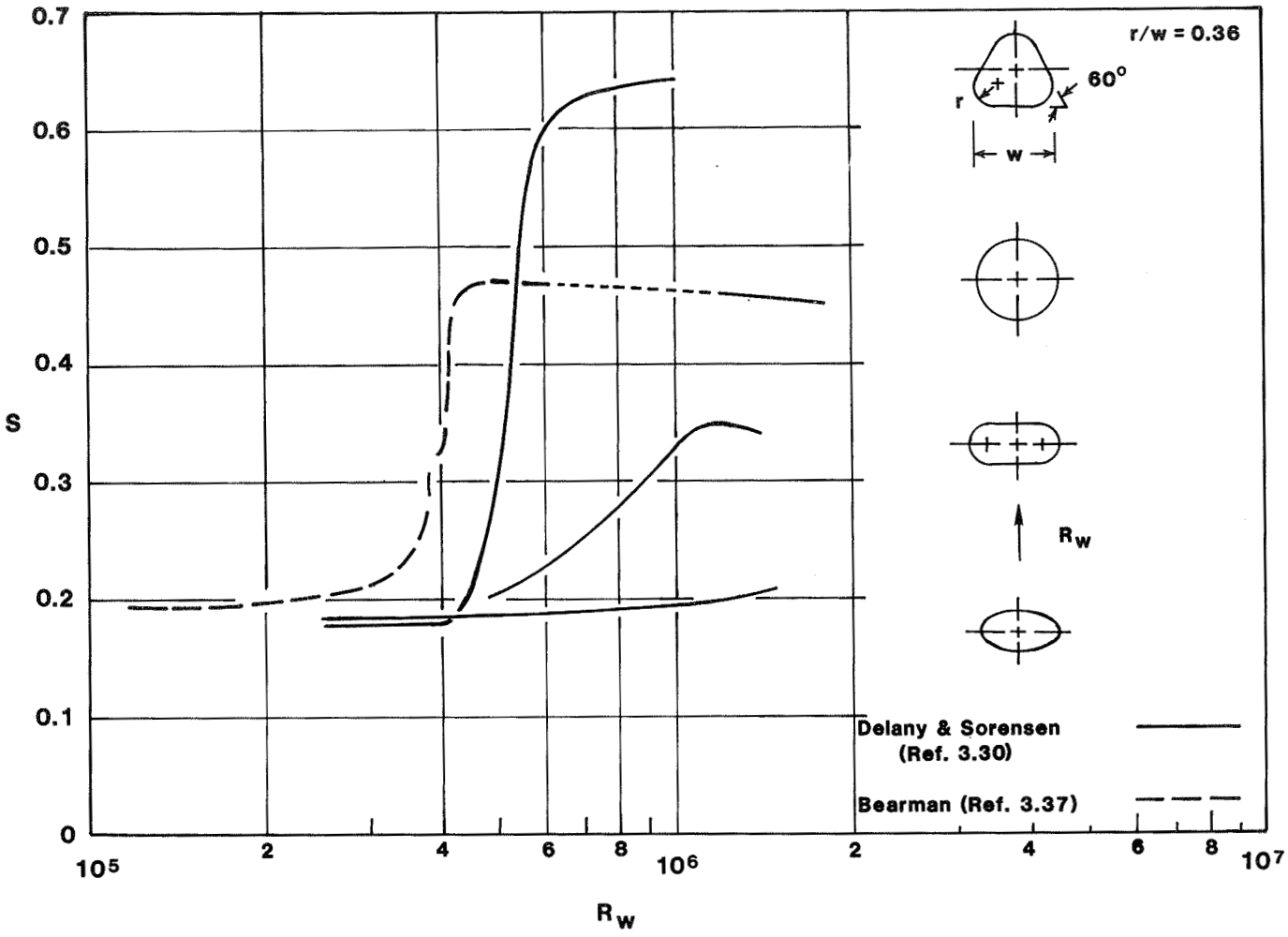

Figure 3.5 Influence of cross section on Strouhal number.

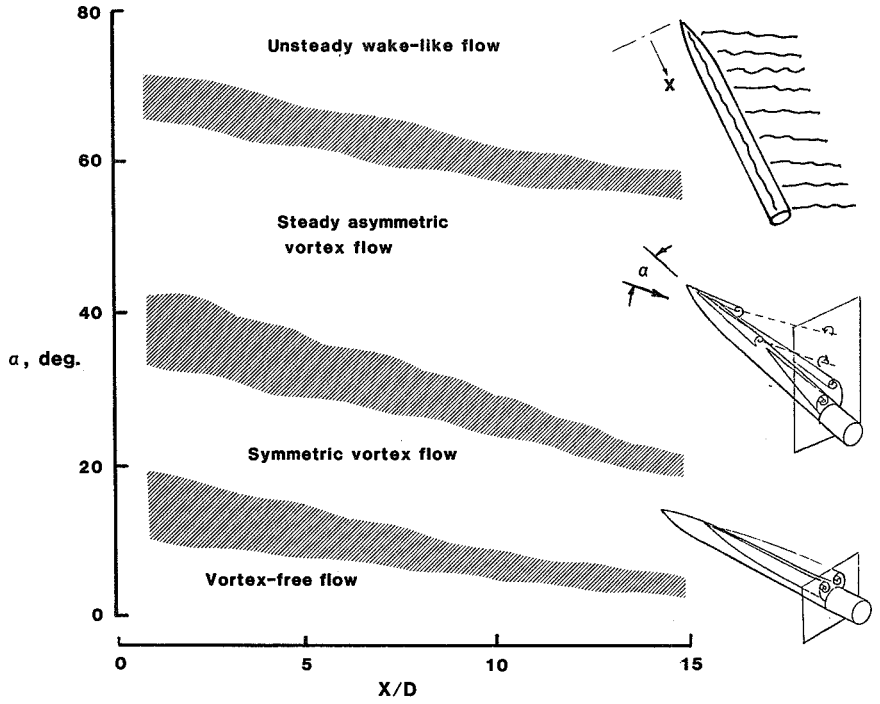

Figure 4.1 Approximate flow regimes for slender bodies of revolution. Adapted from reference 4.42.

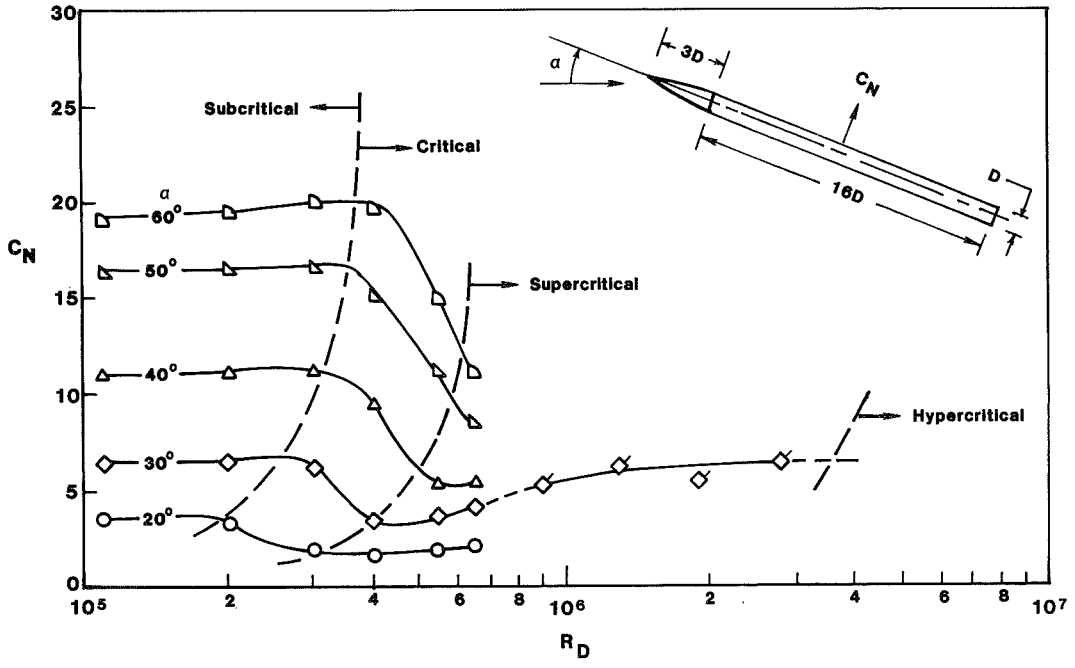

Figure 4.2 Effect of angle of attack on the normal force coefficient for a slender body of revolution. M = 0.5. Data from Hartmann (reference 4.40).

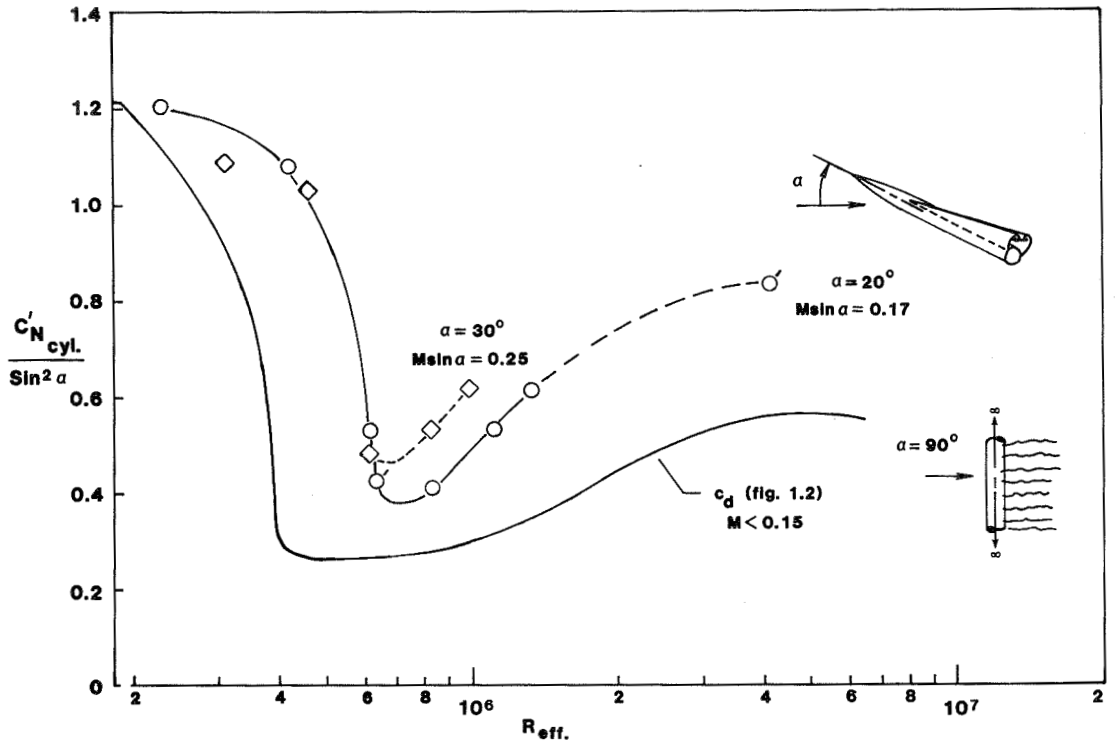

Figure 4.3 Indication of vortex contribution to normal force coefficient parameter.

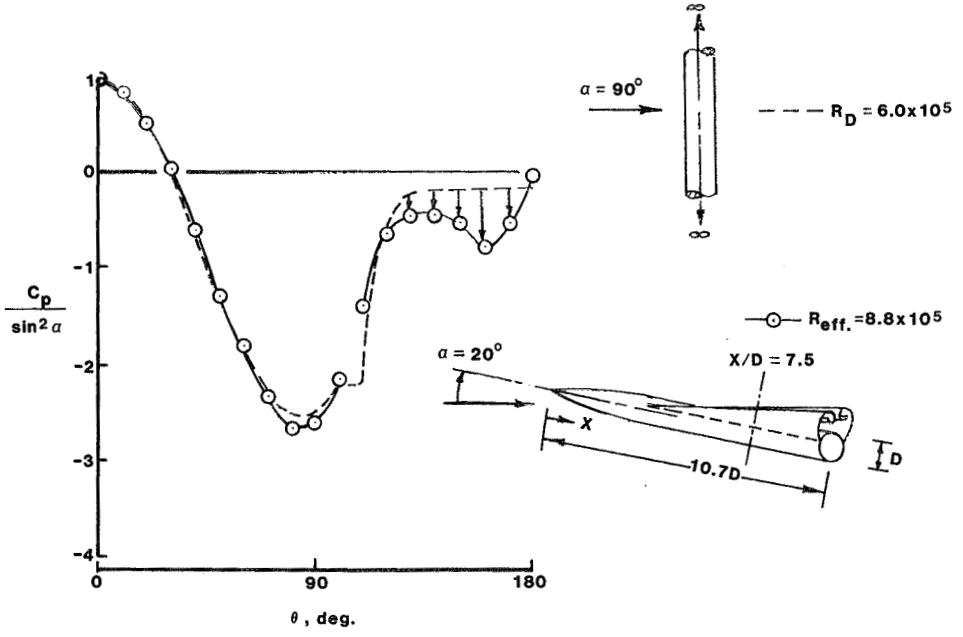

Figure 4.4 Effect of vortex flow on pressure distribution.

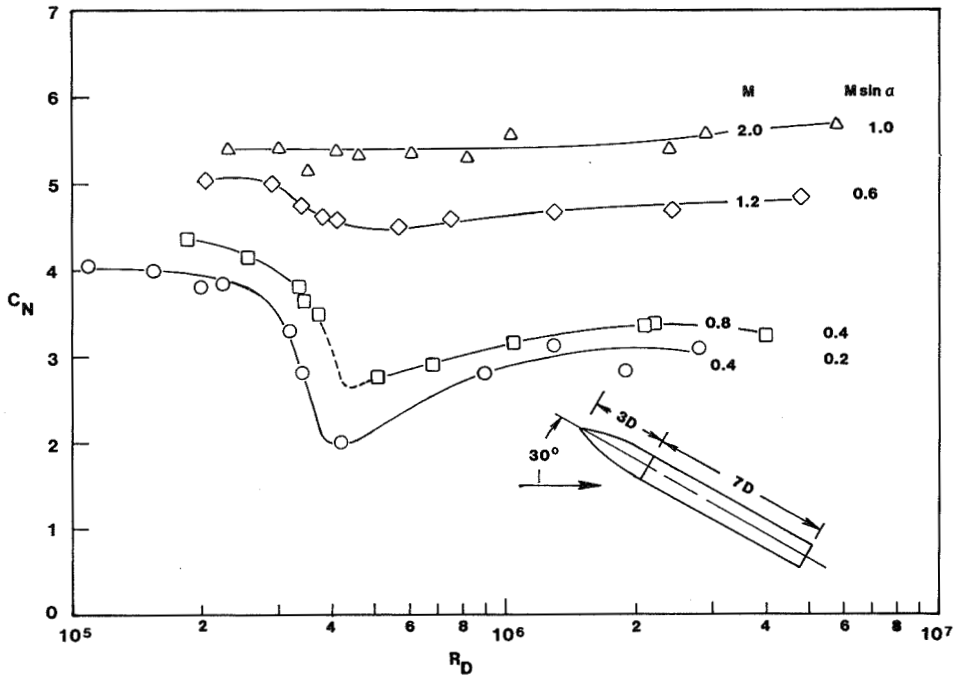

Figure 4.5 Effect of Mach number on normal force coefficient for slender body of revolution. Data from Foley (reference 4.34).

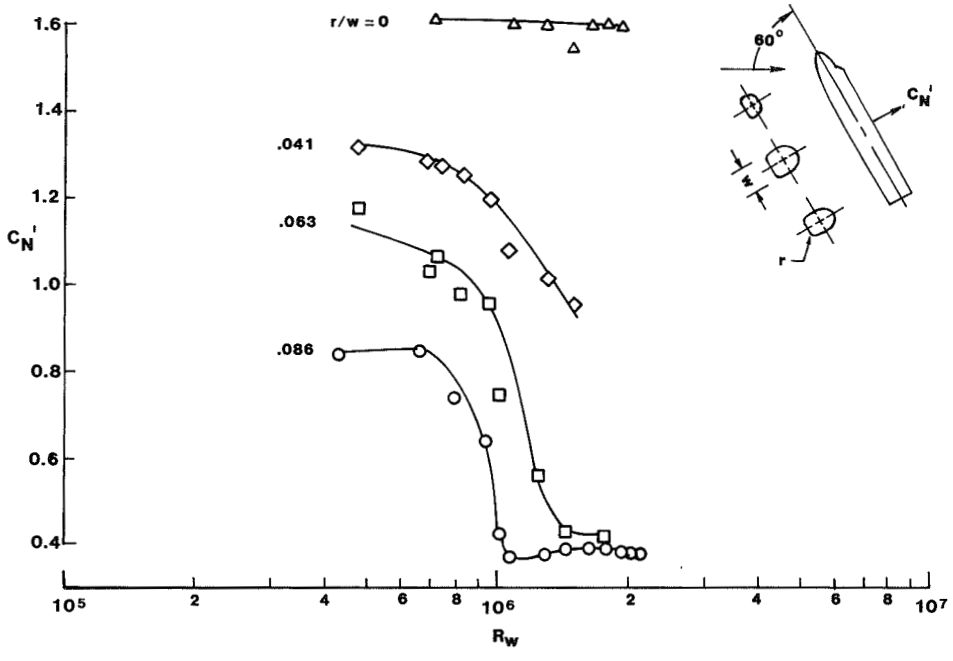

Figure 4.6 Effect of corner radius on normal force coefficient for shuttle orbiter-type fuselage. Data from Brownson, et. al. (reference 4.31).

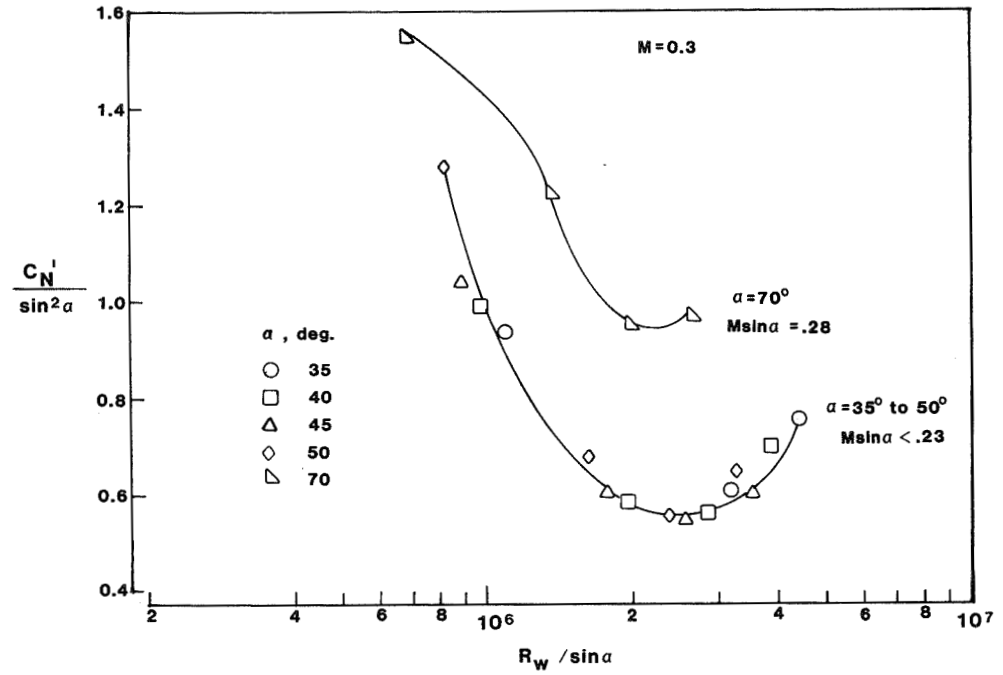

Figure 4.7 Variation of normal force parameter with an effective Reynolds number for shuttle orbiter-type fuselage. r/w = .063. Data from Jorgensen and Brownson (reference 4.35).

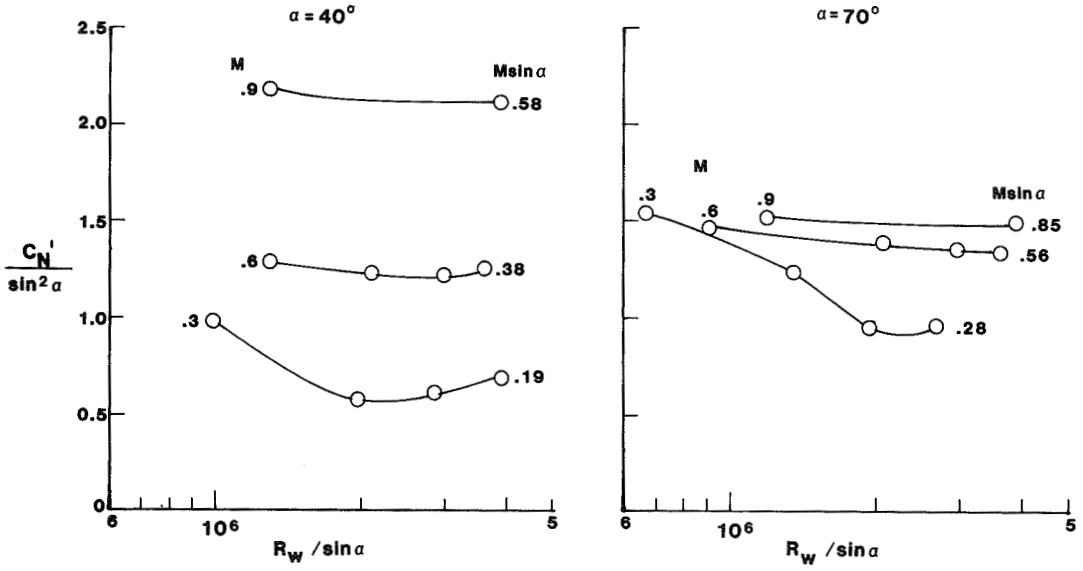

Figure 4.8 Variation of normal force coefficient parameter with Mach number for shuttle orbiter-type fuselage. r/w = .063. Data from Jorgensen and Brownson (reference 4.35).

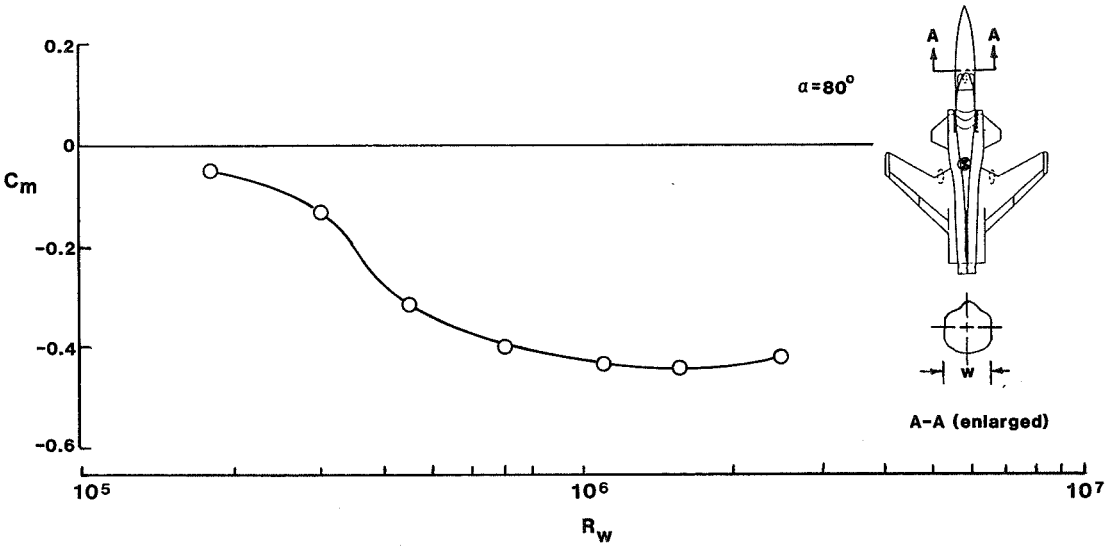

Figure 4.9 Pitching moment coefficient for forward swept wing configuration. Data from Whipple et. al. (reference 4.61).

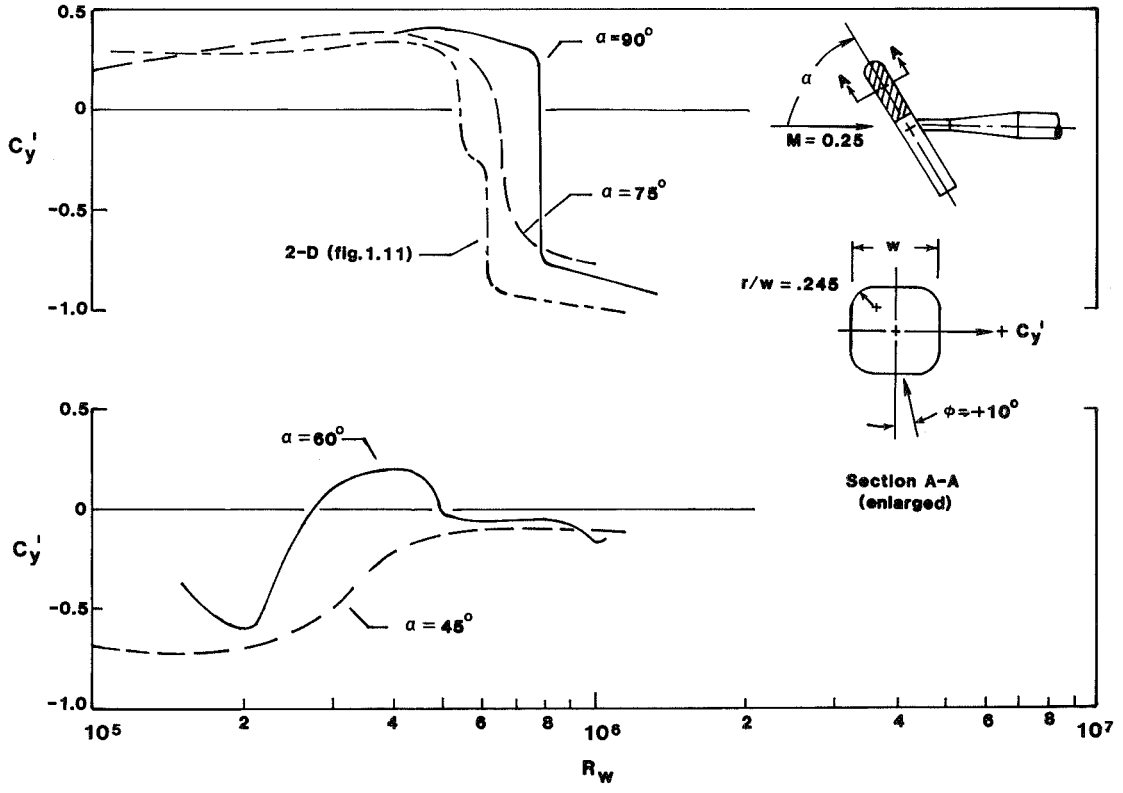

Figure 4.10 Effect of angle of attack on side force coefficient for body with modified square cross section. Data from Clarkson et. al. (reference 4.43).

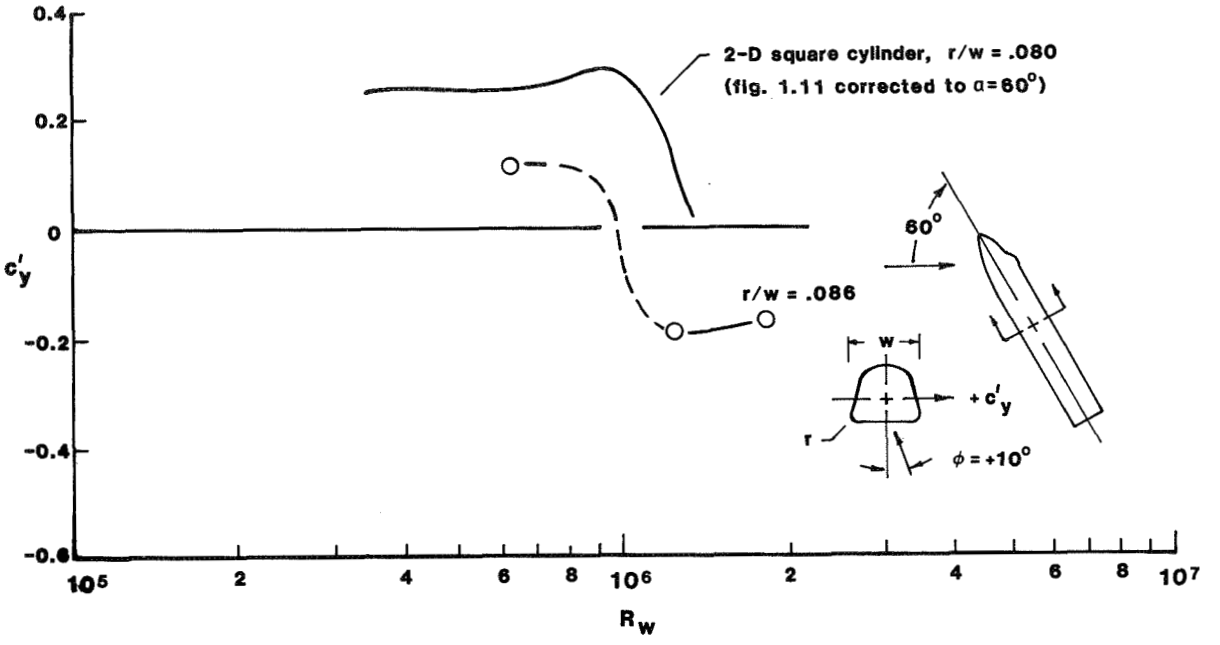

Figure 4.11 Side force coefficient for shuttle orbiter type fuselage. Data from Brownson et. al. (reference 4.31).

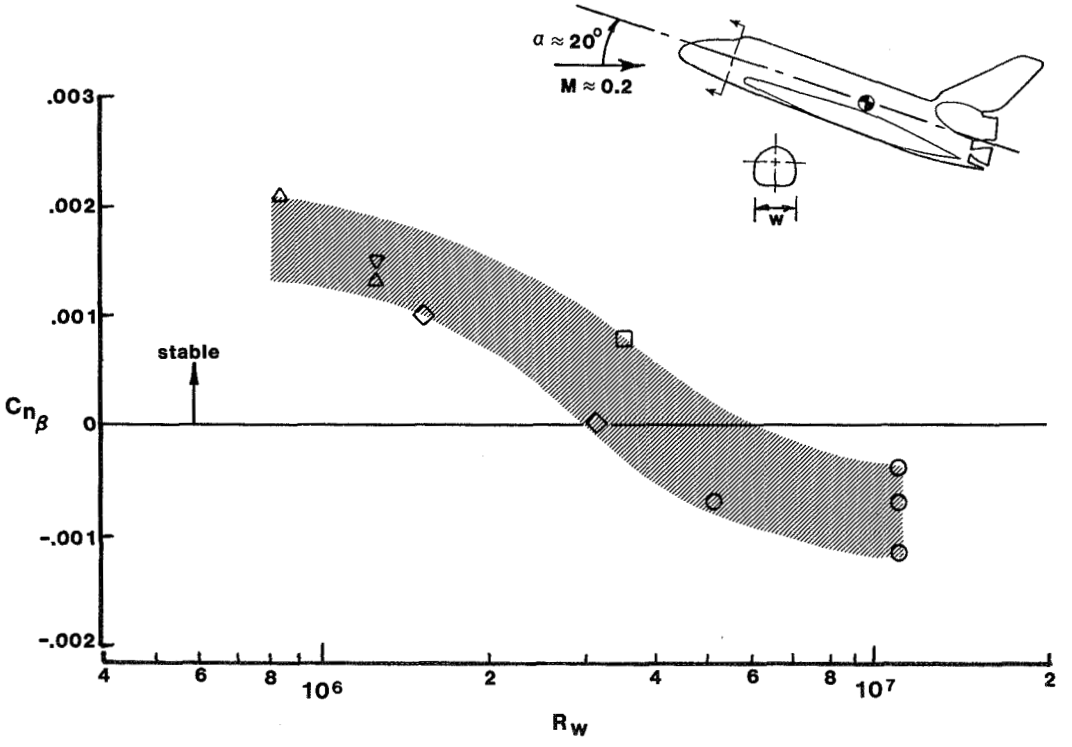

Figure 4.12 Directional stability variation for shuttle orbiter. Data from Bornemann and Surber (reference 4.41).

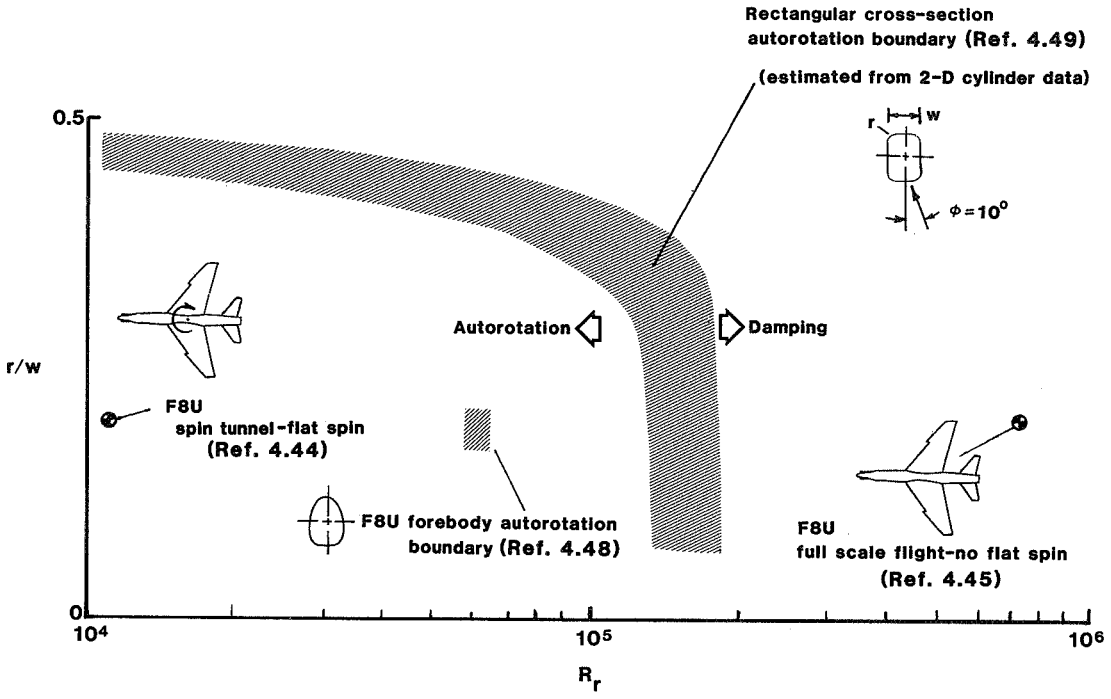

Figure 4.13 Autorotation boundaries for some non-circular cross-section bodies.

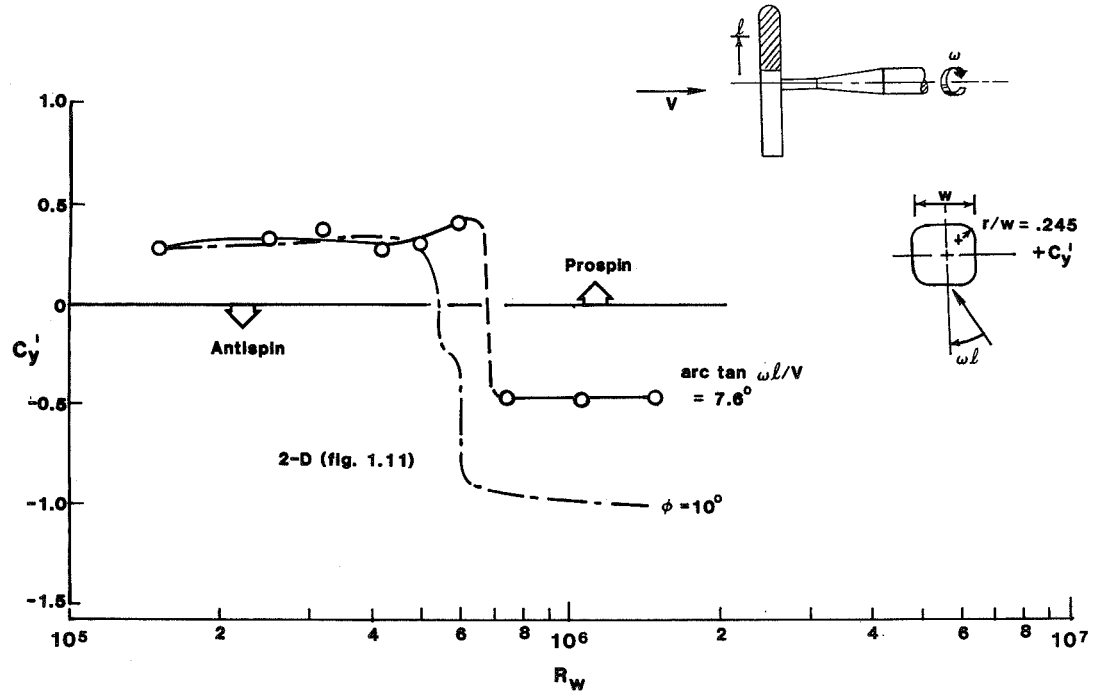

Figure 4.14 Forebody side force coefficient produced by spin motion. Data from Clarkson et.al. (reference 4.56).

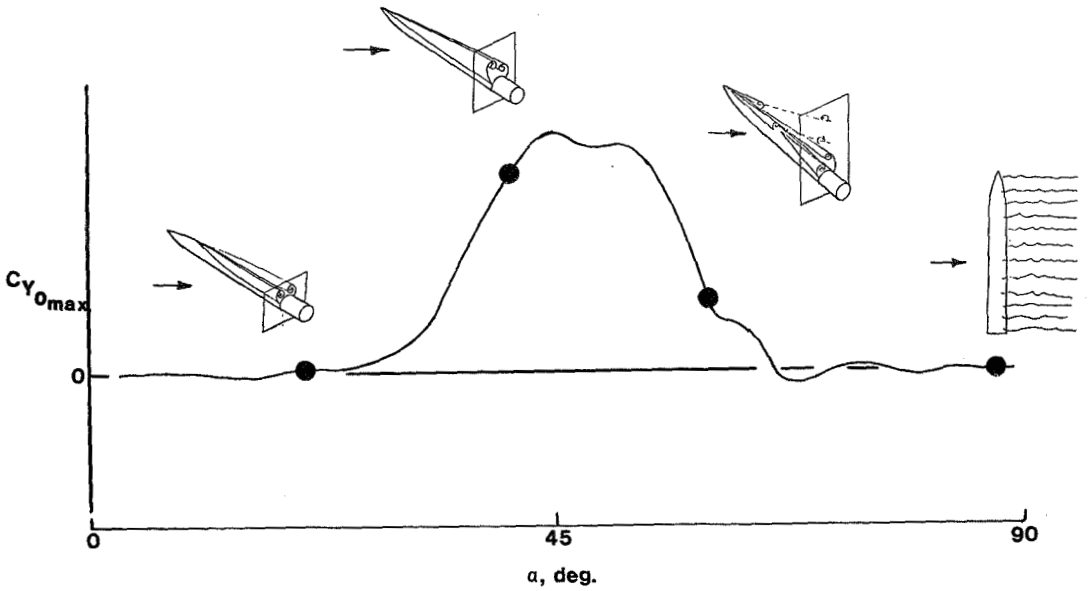

Figure 5.1 Typical variation of out-of-plane force and vortex patterns with angle of attack.

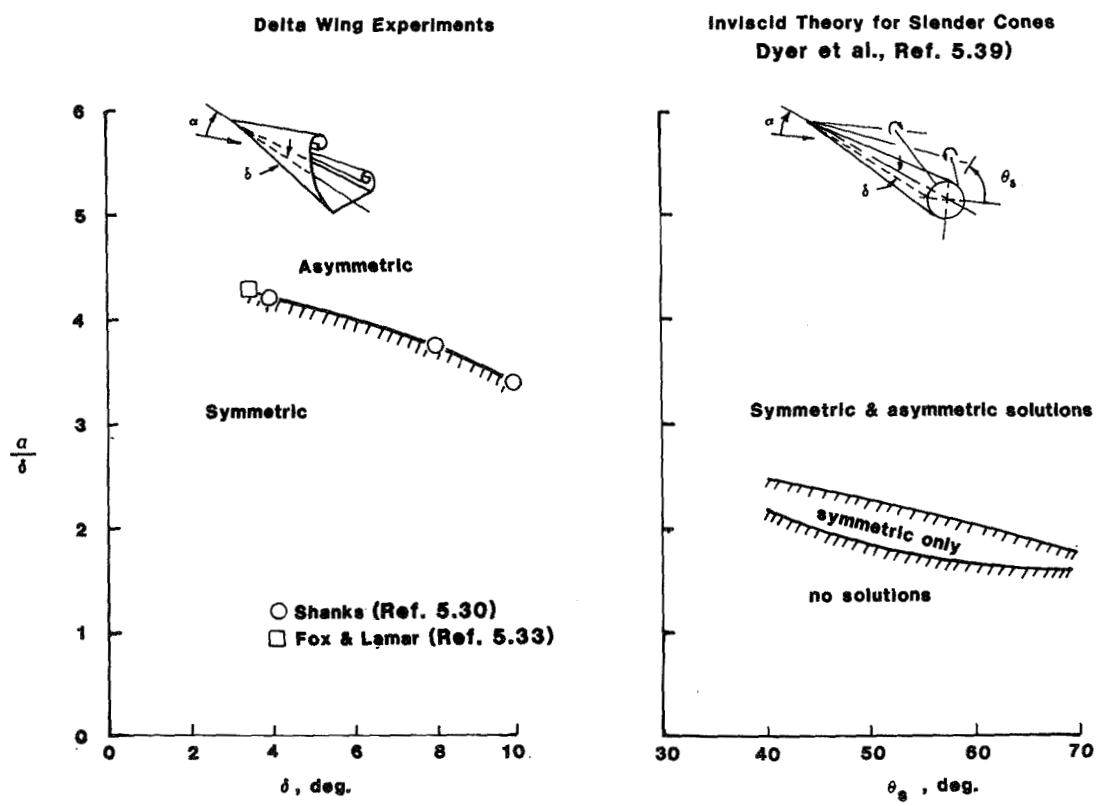

Figure 5.2 Examples of hydrodynamic instability of vortex pairs shed from symmetrical separation lines.

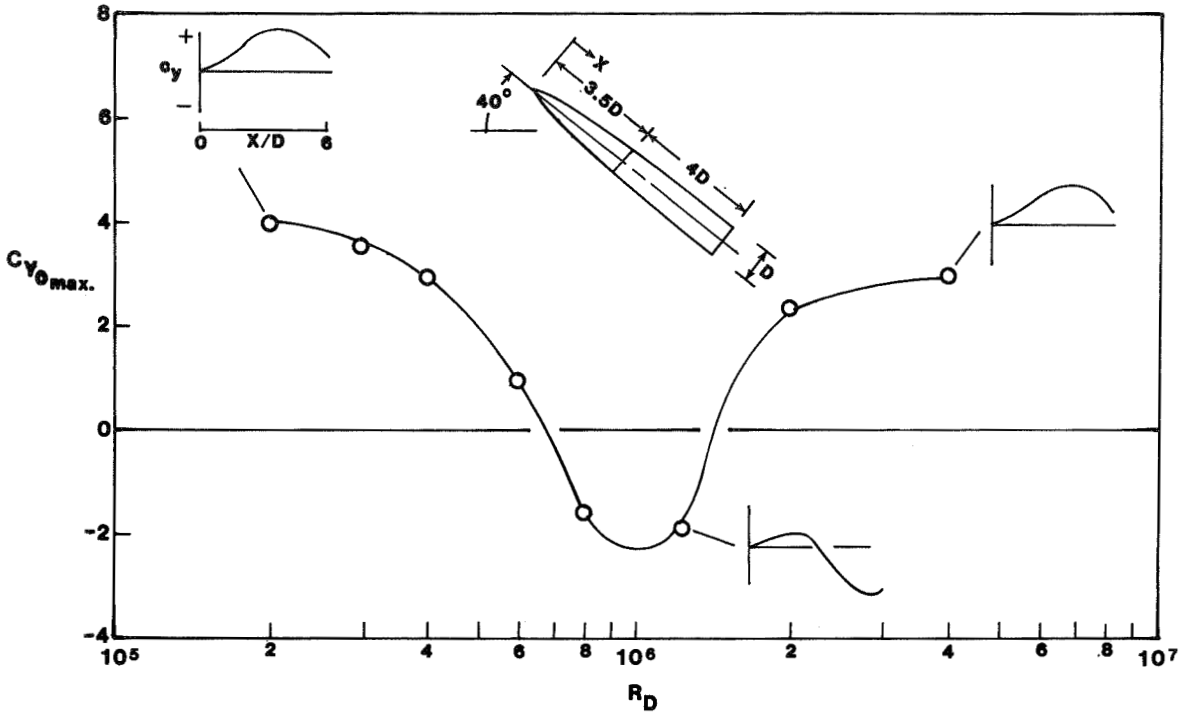

Figure 5.3 Variation of local and integrated maximum out-of-plane force coefficient for an ogive-cylinder. Data from Lamont (reference 5.57).

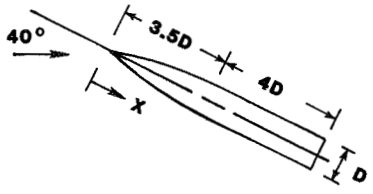

R_D x10^{-6}	Separation	S
0.2	laminar	0.20
0.6	transitional	0.32
1.25	fully turbulent	0.46
4.0	fully turbulent	0.26

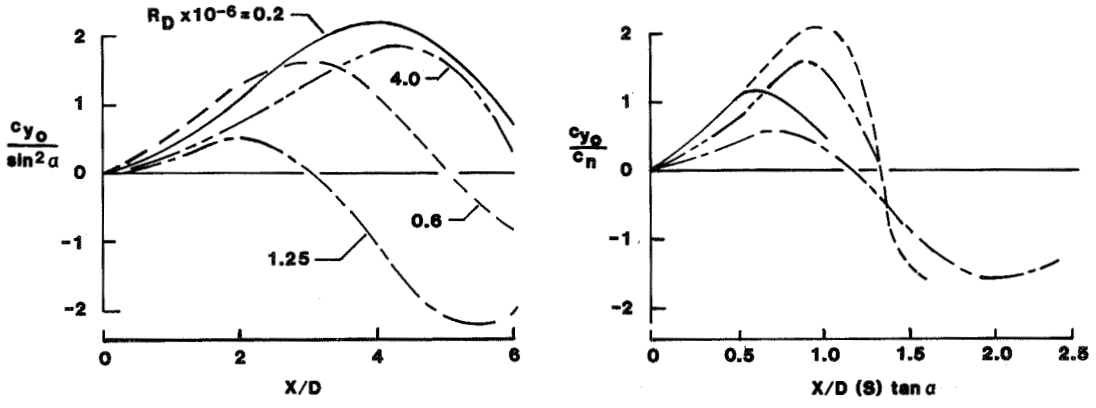

Figure 5.4 Application of impulsive flow analogy to the out-of-plane force variation along body length. Basic data from Lamont (reference 5.57).

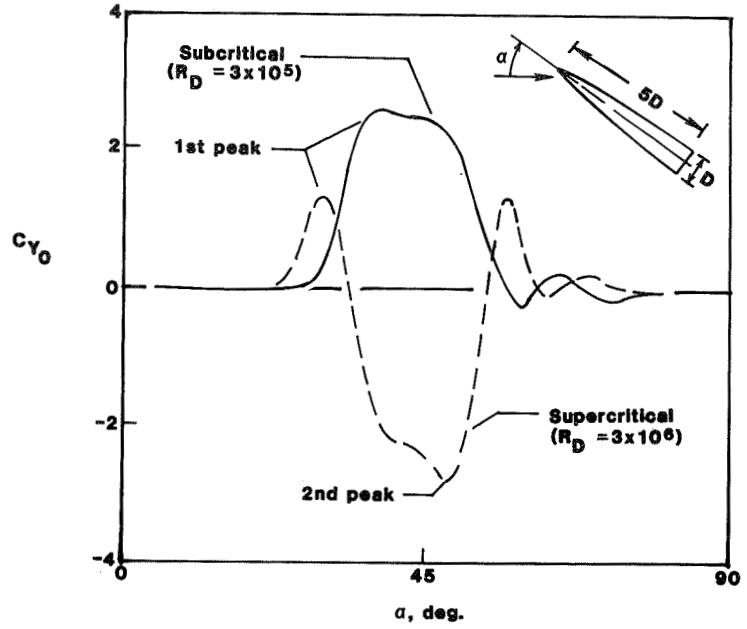

Figure 5.5 Illustration of first and second peaks in out-of-plane force variation with angle of attack. Data from Keener et. al. (reference 5.52).

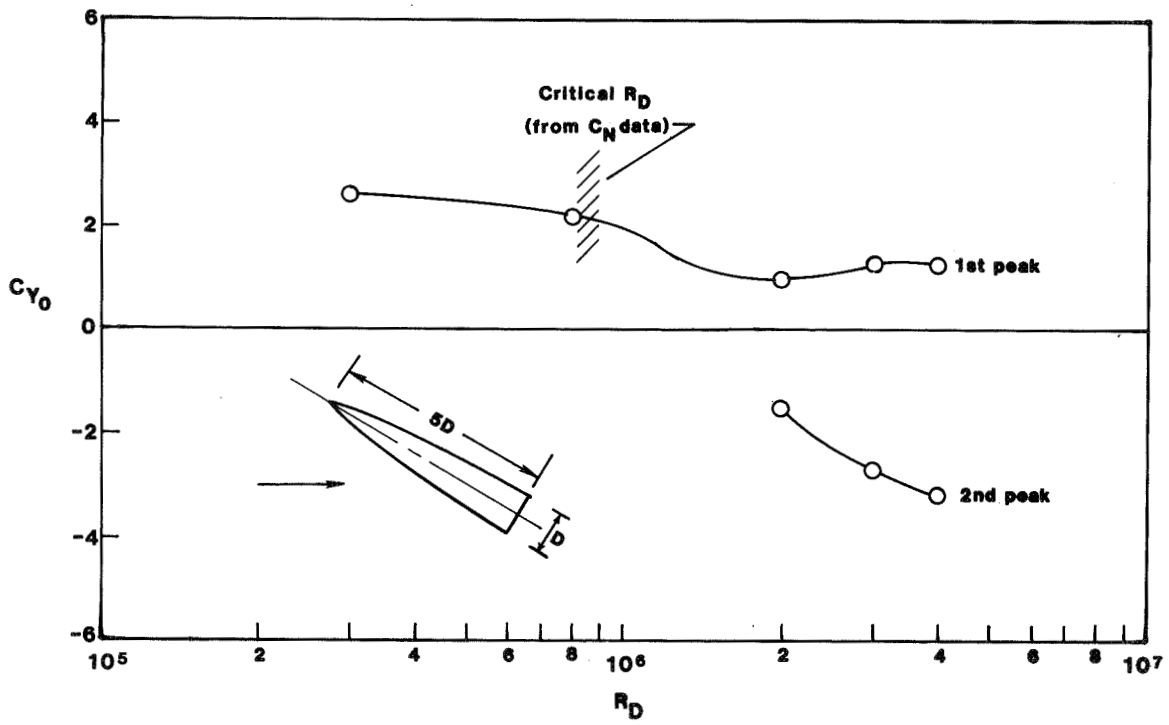

Figure 5.6 Variation of first and second out-of-plane force peaks. Data from Keener et. al. (reference 5.52).

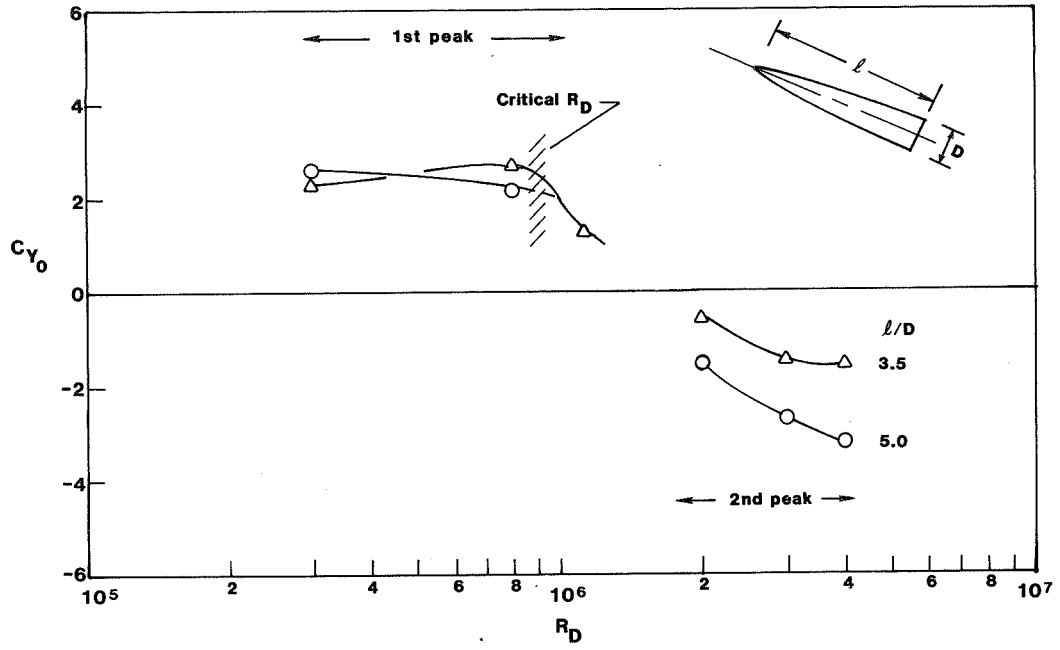

Figure 5.7 Effect of fineness ratio on out-of-plane force characteristics. Data from Keener et. al. (references 5.51 and 5.52).

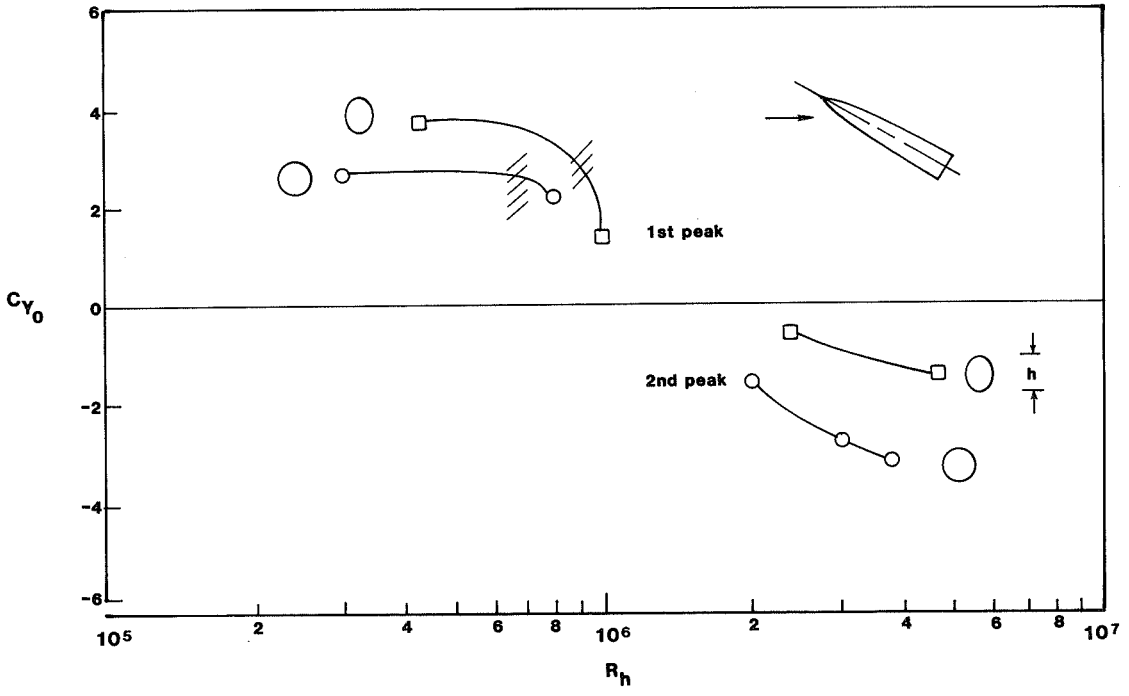

Figure 5.8 Effect of cross section on out-of-plane force characteristics for fineness ratio 5 forebody. Data from Keener et.al. (reference 5.52).

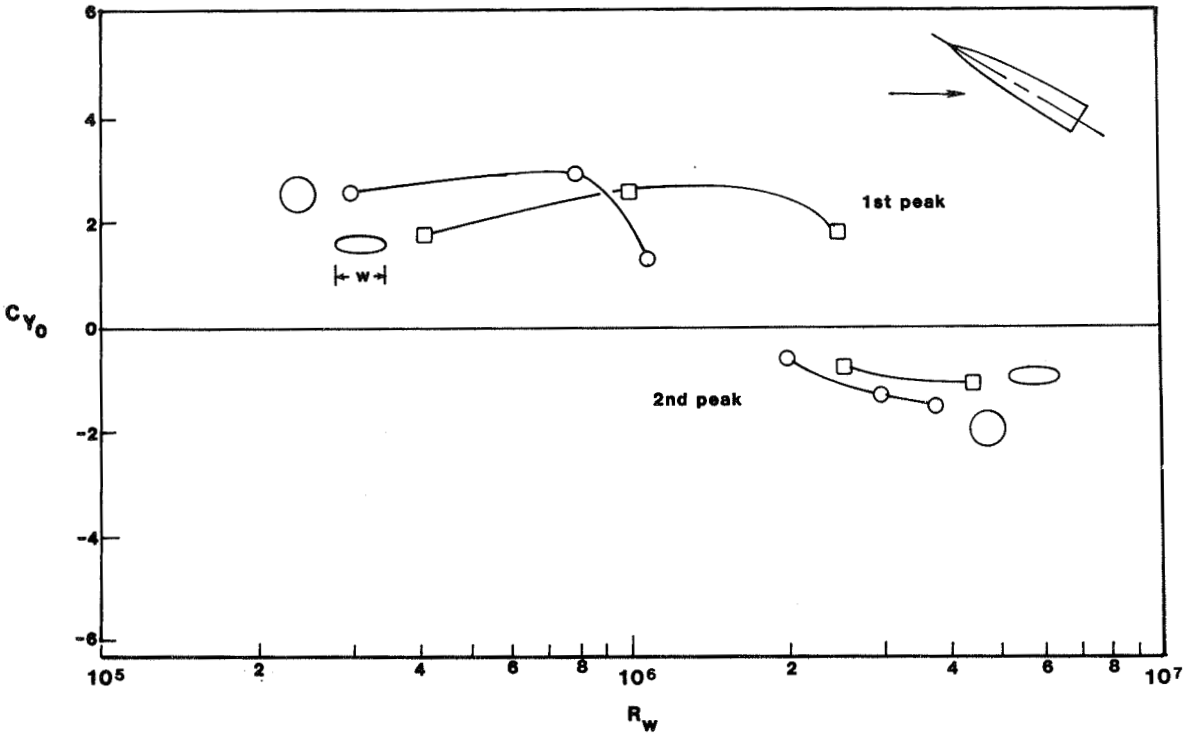

Figure 5.9 Effect of cross section on out-of-plane force characteristics for fineness ratio 3.5 forebody. Data from Keener et. al. (reference 5.51).

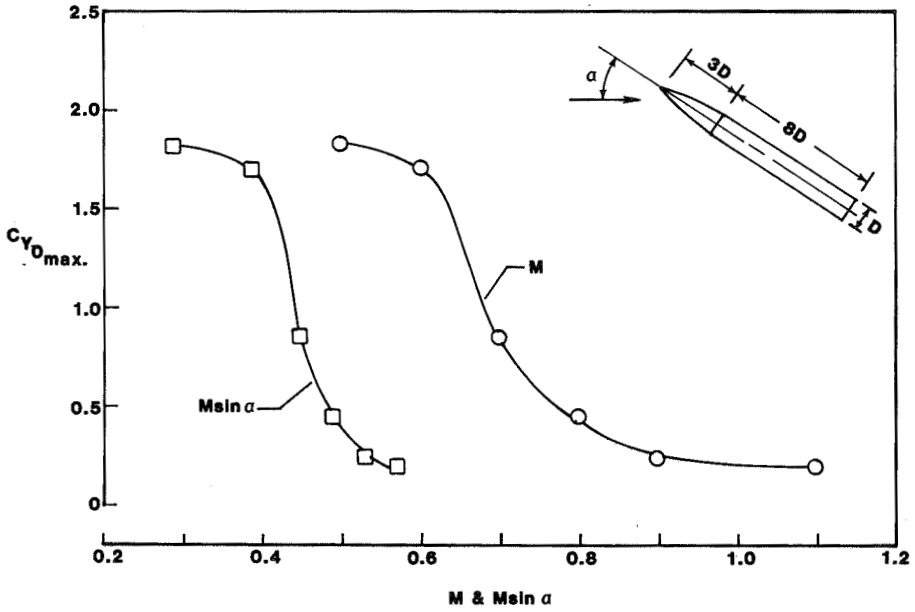

Figure 5.10 Variation of maximum out-of-plane force with Mach number at subcritical Reynolds number. Data from Pick (reference 5.42).

1. Report No.	2. Government Accession No.	3. Recipient's Catalog No.
NASA CR-3809		

4. Title and Subtitle	5. Report Date
A REVIEW OF SOME REYNOLDS NUMBER EFFECTS RELATED TO BODIES AT HIGH ANGLES OF ATTACK	August 1984
	6. Performing Organization Code
7. Author(s)	8. Performing Organization Report No.
Edward C. Polhamus	
	10. Work Unit No.
9. Performing Organization Name and Address	
Virginia Associated Research Campus 12070 Jefferson Avenue Newport News, VA 23606	11. Contract or Grant No. NAG1-261
	13. Type of Report and Period Covered
12. Sponsoring Agency Name and Address	Contractor Report
National Aeronautics and Space Administration Washington, DC 20546	14. Sponsoring Agency Code 505-31-53-08

15. Supplementary Notes

Langley Technical Monitor: Richard W. Barnwell
Final Report

16. Abstract

This report presents a review of some effects of Reynolds number on selected aerodynamic characteristics of two- and three-dimensional bodies of various cross sections in relation to fuselages at high angles of attack at subsonic and transonic speeds. Emphasis is placed on the Reynolds number ranges above the subcritical and angles of attack where lee side vortex flow or unsteady wake type flows predominate. Lists of references, arranged in subject categories, are presented with emphasis on those which include data over a reasonable Reynolds number range. Selected Reynolds number data representative of various aerodynamic flows around bodies are presented and analyzed and some effects of these flows on fuselage aerodynamic parameters are discussed.

17. Key Words (Suggested by Author(s))	18. Distribution Statement
Aerodynamics of bodies High angle of attack Reynolds number effects Mach number effects	Unclassified - Unlimited Subject Category 02

19. Security Classif. (of this report)	20. Security Classif. (of this page)	21. No. of Pages	22. Price
Unclassified	Unclassified	124	A06

For sale by the National Technical Information Service, Springfield, Virginia 22161 NASA-Langley, 1984